

Department of
Chemistry

Lancaster
University



MSc Chemistry (by Research)

Thesis

Mathew John Haskew

Supervisor: Dr John George Hardy

**Thermo-responsive and electroconductive shape-memory polymer
composites for useful applications**

Declaration

This thesis has been composed solely by myself and the work submitted is my own, except where corresponding references or acknowledgements state otherwise. No portion of the work referred to this thesis has been submitted in support of an application for another degree qualification for this or any other university or institute of learning.

Acknowledgments

I would like to thank Dr John George Hardy for his greatly appreciated supervision throughout my research project.

In addition, I would like to thank Dr Sara Baldock who helped me during my project, especially when using the Photonic Nanoscribe.

Finally, I wish to thank my family and friends for their support and encouragement throughout my studies.

List of figures	7
List of tables	9
Table of abbreviations	10
Abstract	12
1 Introduction	13
- 1.1 Background.....	13
- 1.2 How SMPs work.....	14
- 1.3 Examples of stimuli inducing the SME of SMPs.....	18
- 1.3.1 Thermally-induced SMP.....	18
- 1.3.2 Light-induced SMP.....	19
- 1.3.3 Electrically-induced SMP.....	21
- 1.3.4 Water-induced SMP.....	23
- 1.3.5 pH-induced SMP.....	26
- 1.4 Classification of SMPs.....	29
- 1.4.1 Thermoplastic SMPs.....	31
- 1.4.2 Thermoset SMPs.....	31
- 1.4.3 Shape-memory functionality.....	32
- 1.5 Characterisation of the SMPs.....	35
- 1.5.1 FTIR spectroscopy.....	35
- 1.5.2 UV-Vis spectroscopy.....	35
- 1.5.3 NMR spectroscopy.....	36
- 1.5.4 SEC/GPC.....	36
- 1.5.5 Morphology detection.....	37
- 1.5.6 Electrical conductivity measurement.....	37
- 1.5.7 TGA.....	37
- 1.5.8 DSC.....	38
- 1.5.9 DMA.....	38
- 1.5.10 Mechanical properties evaluation.....	39

- 1.6 Focus of the thesis.....	39
- 1.6.1 Direct laser writing or multiphoton fabrication using a Photonic Nanoscribe.....	40
- 1.6.2 TSMPI.....	41
- 1.6.3 Innovative application for TSMPI.....	42
- 1.6.4 OCL-ODX SMP.....	45
- 1.6.5 Innovative application for OCL-ODX SMP.....	46
2 Experimental.....	49
- 2.1 Synthesis of SMPs.....	49
- 2.1.1 TSMPI synthesis.....	49
- 2.1.2 OCL-ODX SMP synthesis.....	50
- 2.2 Modification of SMPs.....	51
- 2.2.1 TSMPI-PPy.....	51
- 2.3 Analysis of TSMPI.....	52
- 2.3.1 Thermal properties characterisation.....	52
- 2.3.2 Shape-memory characterisation.....	52
- 2.3.3 Optical properties characterisation.....	52
- 2.3.4 Molecular weight and structural characterisation.....	52
- 2.4 Analysis of TSMPI-PPy.....	54
- 2.4.1 Structural characterisation.....	54
- 2.4.2 Electrical conductivity characterisation.....	54
- 2.5 Analysis of OCL-ODX SMP.....	55
- 2.5.1 Thermal properties characterisation.....	55
- 2.5.2 Structural characterisation.....	55
3 Discussion of results.....	56
- 3.1 Abstract.....	56
- 3.2 Introduction.....	56
- 3.3 TSMPI.....	59
- 3.3.1 Thermal properties.....	59

- 3.3.2 Shape-memory.....	61
- 3.3.3 Optical properties.....	63
- 3.3.4 Molecular weight and structural information.....	66
- 3.4 TSMPI-PPy.....	76
- 3.4.1 2PP of pyrrole into/on TSMPI films using a Photonic Nanoscribe.....	76
- 3.4.2 Structural information.....	86
- 3.4.3 Electrical conductivity.....	88
- 3.5 OCL-ODX SMP.....	90
- 3.5.1 Thermal properties.....	90
- 3.5.2 Structural information.....	92
4 Future work.....	95
5 Conclusion.....	96
6 Bibliography.....	97
Appendix I.....	99
Appendix II.....	107
Appendix III.....	108
Appendix IV.....	117
Appendix V.....	118

List of figures

Figure 1: The general SME mechanism of SMPs.....	15
Figure 2: Molecular model of the thermally-induced SME mechanism of cross-linked SMPE.....	16
Figure 3: A general 3D plot of an SMP during a thermomechanical shape-memory cycle.....	17
Figure 4: The SME mechanism of a thermally-induced SMP.....	18
Figure 5: Schematic of the LASMPs SME mechanism.....	20
Figure 6: Representation of the electroactive SMPU and application.....	21
Figure 7: PPy-PEE composite film SME mechanism and application.....	24
Figure 8: Representation of the pH-responsive SMP composite SME mechanism.....	27
Figure 9: Schematic of the typical primary cross-links of a polymer network and during the shape recovery process.....	30
Figure 10: Schematic of the TSMPI-PPy composite and used as a negative switch.....	43
Figure 11: Schematic of the OCL-ODX-PPy composite and used as a biomedical device rejuvenating damaged nerves.....	47
Figure 12: DSC results of the synthesised TSMPI.....	59
Figure 13: Timeline of the shape recovery process of synthesised TSMPI at 40 °C above its T_g	61
Figure 14: UV-Vis transmittance spectrum of synthesised TSMPI films.....	63
Figure 15: UV-Vis transmittance spectrum of “PI 16” before and after shape recovery cycles.....	64
Figure 16: 3D molecular structure of a structural unit comprising TSMPI.....	65
Scheme 1: Reaction scheme for TSMPI.....	66
Figure 17: FITR spectrum of the synthesised TSMPI.....	67

Figure 18: 1D ^{13}C NMR theoretical spectrum of TSMPIs structural unit and the solid-state 1D ^{13}C NMR experimental spectrum of the synthesised TSMPI.....	68
Figure 19: GPC results of the synthesised TSMPI.....	70
Figure 20: XRD spectrum of the synthesised TSMPI film.....	75
Figure 21: Schematic of the 2PP process using a Photonic Nanoscribe.....	76
Figure 22: Picture from DeScribe software of a simple structure used to observe the initial 2PP of pyrrole into/on the TSMPI film.....	80
Figure 23: Picture of the TSMPI-PPy composite taken with an x10 optical microscope.....	80
Figure 24: Pictures from DeScribe software of the new structures that would be used for subsequent 2PP of pyrrole into/on the TSMPI film.....	82
Figure 25: Picture of the TSMPI-PPy composite taken with LUCUM software and an x10Primo Star plan achromat ZEISS lens.....	83
Figure 26: Pictures of the TSMPI-PPy composites.....	85
Scheme 2: Chemical structure of PPy and TSMPI.....	86
Figure 27: FTIR spectrum of the synthesised TSMPI film compared to TSMPI-PPy composite.....	87
Figure 28: Pictures taken using an x10 optical microscope during electrical conductivity tests on the TSMPI-PPy composite and the synthesised TSMPI film.....	88
Figure 29: DSC results of the synthesised OCL-ODX.....	90
Scheme 3: Reaction scheme for OCL-ODX.....	92
Figure 30: FTIR spectrum of the synthesised OCL-ODX.....	93
Figure 31: XRD spectrum of the synthesised OCL-ODX.....	94

List of tables

Table 1: Table of the varying shape-memory functionality of SMPs.....	33
Table 2: A table giving insight on classifying SMPs based on composition and structure, stimulus triggers, and the possible type of shape-memory functions.....	34
Table 3: A table listing the TRLs.....	57
Table 4: Values used to generate Figure 19a).....	71
Table 5: Values used to generate Figure 19b).....	71
Table 6: Stability test of the monomers with water, methanol and ethanol, which will be used to formulate the ink used during 2PP using a Photonic Nanoscribe to produce the TSMPI composite.....	78
Table 7: TSMPI-PPy production using Irgacure D-2959 5:95 pyrrole and ethanol ink.....	79
Table 8: TSMPI-PPy production using Darocur TPO 5:95 pyrrole and ethanol ink, and Dr Blading the administrated PAA to produce TSMPI films with an average film thickness of 30 to 40 μm	84

Table of abbreviations

Abbreviation	Explanation
3D	Three-dimensional
AFM	Atomic force microscopy
Ag NW(s)	Silver nanowire(s)
BAB	Flexible 1,3-bis(3-aminophenoxy) benzene
BPADA	Flexible bis-phenol A dianhydride
CAD	Computer-aided design
CAM	Chorioallantoic membrane
CNC(s)	Cellulose nanocrystal(s)
COSY	Correlation spectroscopy
CP(s)	Electroconductive polymer(s)
CTC	Charge transfer complex
DBTO	Dibutyltin oxide
DMA	Dynamic mechanical analysis
DMAc	N,N-dimethylacetamide
DMF	Dimethylformamide
DMSO-d6	Deuterated dimethyl sulfoxide
DSC	Differential scanning calorimetry
DTG	Differential gravitational analysis
EDOT	3,4-ethylenedioxythiophene
EG	Ethylene glycol
FTIR	Fourier transform infrared
GPC	Gel permeation chromatography
HBr	Hydrobromic acid
HSQC	Heteronuclear single quantum correlation
LASMP(s)	Light-activated shape-memory polymer(s)
LED	Light emitting diode
M _n	Number average molecular weight
M _w	Weight average molecular weight
NMR	Nuclear magnetic resonance
OCL-ODX	Oligo(ϵ -caprolactone) diol-oligo(<i>p</i> -dioxanone) diol
PAA	Poly(amic) acid
PDI	Polydispersity index
PE	Polyethylene

PECU	Poly(ethylene glycol)-poly(ϵ -caprolactone) polyurethane
PEE	Polyol pentaerythritol ethoxylate
PEU	Polyester urethane
PI(s)	Polyimide(s)
PPDO-diol	α , ω -dihydroxyoligo(<i>p</i> -dioxanone)
PPy	Polypyrrole
PS	Polystyrene
PTFE	Polytetrafluoroethylene
PU	Polyurethane
PVDF	Polyvinylidene fluoride
R _f	Strain fixity rate
RI	Refractive index
R _r	Strain recovery rate
SEC	Size-exclusion chromatography
SEM	Scanning electron microscopy
SI	Supplementary information
SMA(s)	Shape-memory alloy(s)
SME(s)	Shape-memory effect(s)
SMP(s)	Shape-memory polymer(s)
SMPE	Shape-memory polyethylene
SMPU	Shape-memory polyurethane
TEM	Transmission electron microscopy
TEMPO	2,2,6,6-tetramethyl-1-piperidinyloxy
T _g	Glass temperature transition
TGA	Thermogravimetric analysis
T _m	Melting temperature transition
TMDI	2,2(4),4-trimethylhexanediisocyanate
TME(s)	Temperature-memory effect(s)
TRL(s)	Technology readiness level(s)
TSMPI(s)	Transparent shape-memory polyimide(s)
T _{trans}	An SMP undergoing a transition due to an external stimulus
UV	Ultraviolet
UV-Vis	Ultraviolet visible
XRD	X-ray diffraction
<i>p</i> DO	1,4-dioxene-2one

Abstract

Shape-memory polymers (SMPs) are stimuli-responsive materials with the ability to undergo a large recoverable deformation upon the application of an external stimulus. International research interest into the shape-memory effects (SMEs) of these polymers is rapidly growing. Unique polymer composites combining the properties of existing SMPs with electroconductive polymers (CPs) have been produced via direct laser writing or multiphoton fabrication (using a Photonic Nanoscribe). The modified SMPs will be reported for the first time, in addition, their properties are investigated and prove insightful for potential applications of these materials.

1 Introduction

1.1 Background

SMPs are polymer-based materials which memorise a deformed state (a temporary shape) and possess the ability to revert to their original state (the SMPs fabricated original/permanent shape) upon exposure to a stimulus, such as a temperature change. They have been widely researched since the 1980s because of the abundance of potential applications imparted by their interesting properties (e.g. stimuli-responsiveness and shape-changing), which can lead to technological innovation.

The reversible transformation of SMPs function by primary cross-linking net points (hard segments) memorising and determining the permanent shape, and secondary switching segments (soft segments) with a transition (T_{trans}) to reduce strain stress and hold the temporary shape. Below the T_{trans} , the material will be in its permanent shape and be much stiffer compared to when T_{trans} is achieved and the SMPs will then be more malleable which can be deformed into a desired shape, usually by applying an external force. The deformed state will be maintained after the external force has been removed and the system is no longer at or above T_{trans} conditions. SMPs revert to their original state once the T_{trans} conditions are met. While most traditional SMPs can hold a permanent shape and a temporary shape, recent advances in technology have allowed the introduction of triple-shaped-memory materials. These polymers will switch from one temporary shape to another at the first T_{trans} , and then back to the permanent shape at another, higher activation temperature.¹ This is usually achieved when combining two dual shape-memory polymers with different glass transition temperatures (T_g).¹ SMPs have a large range of properties from stable to biodegradable, elastic to rigid, and soft to hard, depending on the structural units that constitute the SMP. Hence, SMPs do not only respond to temperature and magnetism like shape-memory alloys (SMAs), but also to moisture, electricity, light, and chemical stimulus (e.g. a pH change), etc.² Unlike SMAs, SMPs can be biodegradable, have much lower processing conditions (<200 °C, low pressure), have a greater extent of deformation (strain up to more than 200 % for most materials), but cost significantly less to produce i.e. cheap starting materials and inexpensive synthetic procedure.³ As the term “shape-memory” was first proposed by Vernon in 1941,⁴ the significance of SMPs was not fully realised until the 1960s, when cross-linked polyethylene (PE) was used for making heat-shrinkable tubes and films. More effort into the development of SMPs began in the 1980s and significant progress has been made in the last 5 to 10 years. With the rapid development and wide investigation of SMPs, their features are more and more prominent, particularly compared to SMAs.⁵

1.2 How SMPs work

To describe SMEs, two important quantities that is used are strain recover rate (R_r) and strain fixity rate (R_f). R_r describes the ability of a material to memorise its permanent shape, while R_f describes the ability of switching segments to fix the mechanical deformation. R_r is calculated using equation (1)

$$R_r(N) = \frac{\varepsilon_m(N) - \varepsilon_p(N)}{\varepsilon_m(N) - \varepsilon_p(N-1)} \times 100\% \quad (1)$$

where N is the cycle number, ε_m is the maximum strain imposed on the material, and ε_p is the strain of the sample after recovery. R_f is calculated using equation (2)

$$R_f(N) = \frac{\varepsilon_u(N)}{\varepsilon_m(N)} \times 100\% \quad (2)$$

where ε_u is the strain in the fixed temporary shape. SMPs can respond to specific stimuli through changes in macroscopic properties, (e.g. shape).² The polymer network underlying active movement involve a dual system, one that is highly elastic and another that can reduce the stiffness upon application of a certain stimulus. The latter system can be either molecular switches or stimulus sensitive domains.² Their shape-memory feature is a result from the combination of the polymers architecture, and a programming procedure that enables the formation of a temporary shape. Net points consist of covalent bonds or intermolecular interactions and the SMPs hard segments form the net points that link the soft segments, acting as a fixed phase, and the soft segments work as the molecular switches, acting as a reversible phase. The fixed phase prevents free flow of the surrounding polymer chains upon the application of stress. The reversible phase, on the other hand, undergoes deformation in a shape-memory cycle and is responsible for elasticity. For example, if the T_{trans} is T_g , the micro-Brownian motion of the network chains is fixed/frozen at low temperature (below T_g) and will be switched back on at high temperature (above T_g) recovering its original state. When T_{trans} is the crystal melting temperature (T_m), the switching segments crystallize at low temperature (below T_m), and then recover their original state at high temperature (above T_m). In addition, T_g normally extends over a broader temperature range compared to T_m , which tend to have relatively sharper transitions in most cases.² Moreover, after the exposure to a specific stimulus and the T_{trans} is achieved, the strain energy in the deformed state is released, consequently resulting in the shape recovery phenomenon. The general process of this SME for SMPs is depicted in **Figure 1**, wherein, the polymer network structure is either chemically or physically-cross-linked and the switching units are made from a semi-crystalline or amorphous phase.

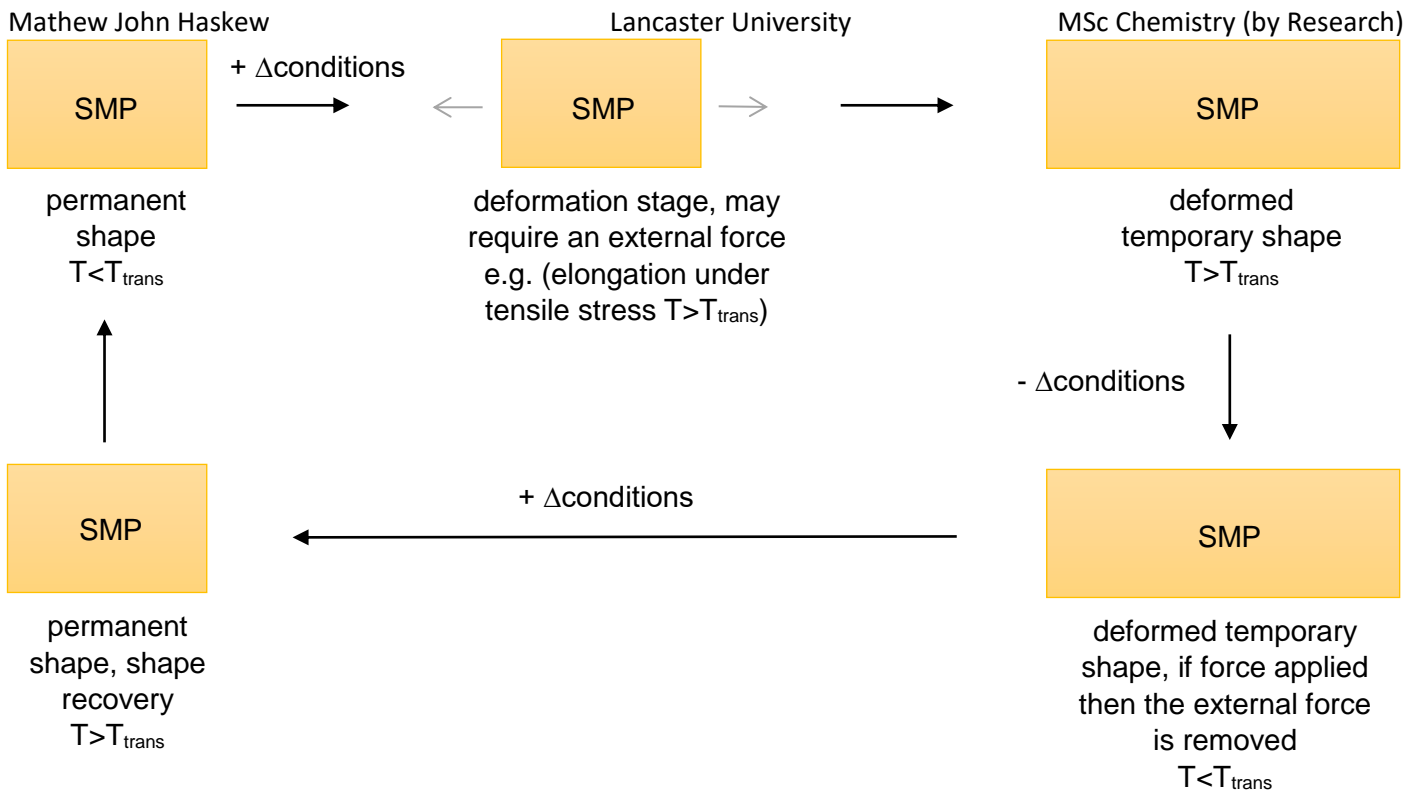


Figure 1. The general SME mechanism of SMPs. T represents the current state of the polymer and T_{trans} represents the state of the polymer with a stimulus (e.g. a temperature change) allowing transition of hard to soft segments, a permanent shape to be deformed into a temporary shape: Δ conditions represent the parameters needed for T_{trans} to be achieved, the “+” and “-” depict whether the parameters are at or above T_{trans} or below it respectively.

Shape-memory behaviour can be demonstrated in various polymer systems that are significantly different in molecular structure and morphology. SME mechanisms should be applied accordingly to the SMP; the mechanisms may share similarities but can differ. For instance, the SME mechanism of the chemically-cross-linked semi-crystalline PE SMP. The crystalline phase, with a T_{trans} being T_m , is used as the molecular switching unit providing shape fixity. The chemically-cross-linked PE network memorises the permanent shape after deformation upon heating.⁶ A molecular mechanism of the thermally-induced shape-memory PE (SMPE) in **Figure 2** is given.

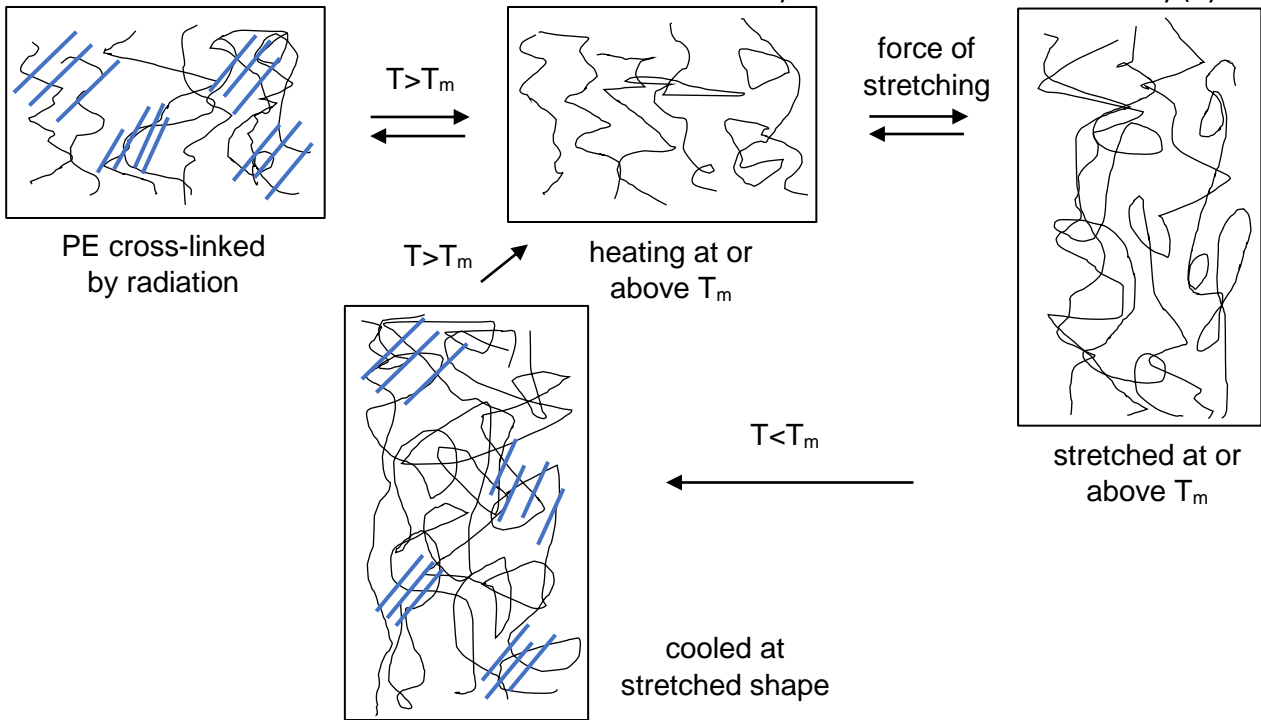


Figure 2. Molecular model of the thermally-induced SME mechanism of cross-linked SMPE.

Blue striated lines are the chemical cross-links in SMPE. When T is at or above T_m the polymer switches segment unit, from hard to soft, because of this the polymer can be stretched into the new shape. The chemically-cross-linked SMPE network memorise the shape once T is below T_m . Hereby, the temporary shape is maintained, until T is at or above T_m . When at or above T_m , the deformed polymer reverts to its original permanent shape.

The associated modulus of elasticity is dictated by configurational entropy reduction that occurs with deformation of the constituent chains and is therefore often termed entropy elasticity. For $T > T_{trans}$ (T_g , T_m or other), polymer networks exhibit super-elasticity wherein the polymer chain segments between cross-link points can deform quite freely and are prone to being twisted randomly, via rotations about backbone bonds, maintaining a maximum entropy ($S = k_B \ln \Omega$, k_B being the Boltzmann's constant and Ω being the number of configurations) and minimum internal energy as macroscopic deformation occurs.⁷ The classic predication from rubber elastic theory is that the resulting elastic shear modulus, G , is proportional to both cross-link density and temperature or (3):

$$G = \nu K_B T = \frac{pRT}{M_c} \quad (3)$$

where ν is the number density of network chains, p the mass density, R the universal gas constant, and M_c the molecular weight between cross-links.

From a macroscopic viewpoint, the SME in SMPs can be graphically represented in three-dimensions (3D), tensile strain vs. temperature and tensile stress (e.g. elongation) is demonstrated in **Figure 3**.

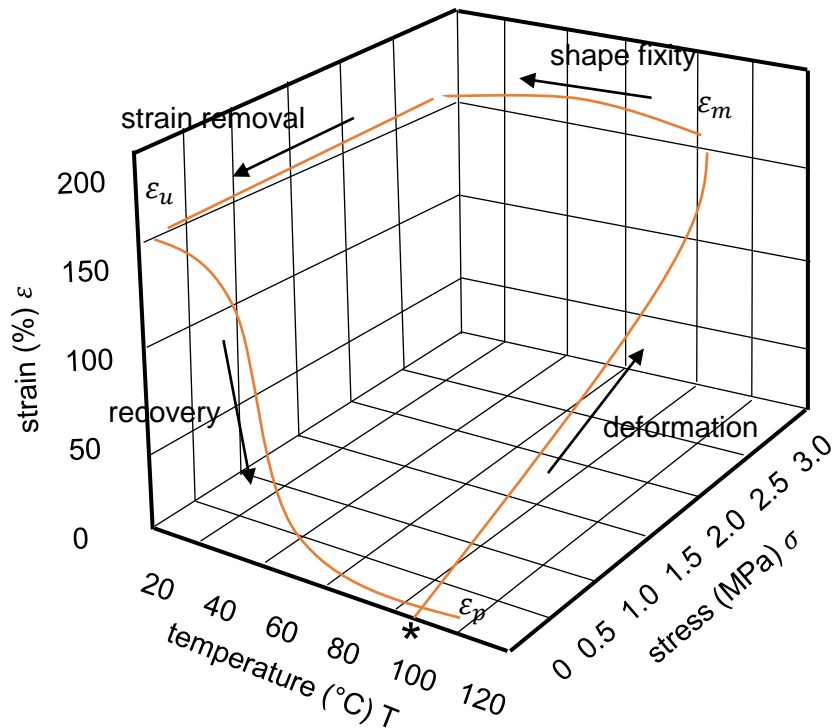


Figure 3. A general 3D plot of an SMP during a thermomechanical shape-memory cycle. The “asterisk” determines the starting point of the process. ϵ_m the maximum strain on the material, ϵ_u the strain in the fixed temporary shape, and ϵ_p the strain of the sample after shape recovery.

Using the shape-memory strain-temperature-stress relationship description in **Figure 3**, the features of SMPs that allow for good shape-memory behaviour include: a sharp transition that can be used to quickly fix the temporary shape at low temperature, and the ability to trigger shape recovery at high temperature; super-elasticity above T_{trans} that leads to the eventual shape recovery and avoids residual strain (permanent deformation); and complete and rapid fixing of the temporary shape by immobilising the polymeric chains without creep thereafter.⁷ Thus far, the SME models describing how SMPs recover their original state prominently involve thermal-responsive SMPs. However, careful design of the polymers allows the opportunity for SMPs to possess different stimuli responses and applications.⁶

1.3 Examples of stimuli inducing the SME of SMPs

1.3.1 Thermally-induced SMP

As previously discussed the SME of SMPs can be thermally-induced, and these SMPs are the most common.² Unlike **Figure 1** depicting a general overview of the SME mechanism of SMPs, and **Figure 2** showing a specific example of the SME mechanism for SMPE with the T_{trans} being T_m . In **Figure 4** a schematic of the SME mechanism for general thermally-induced SMPs with T_g (amorphous cases) and T_m (crystalline cases) is presented.

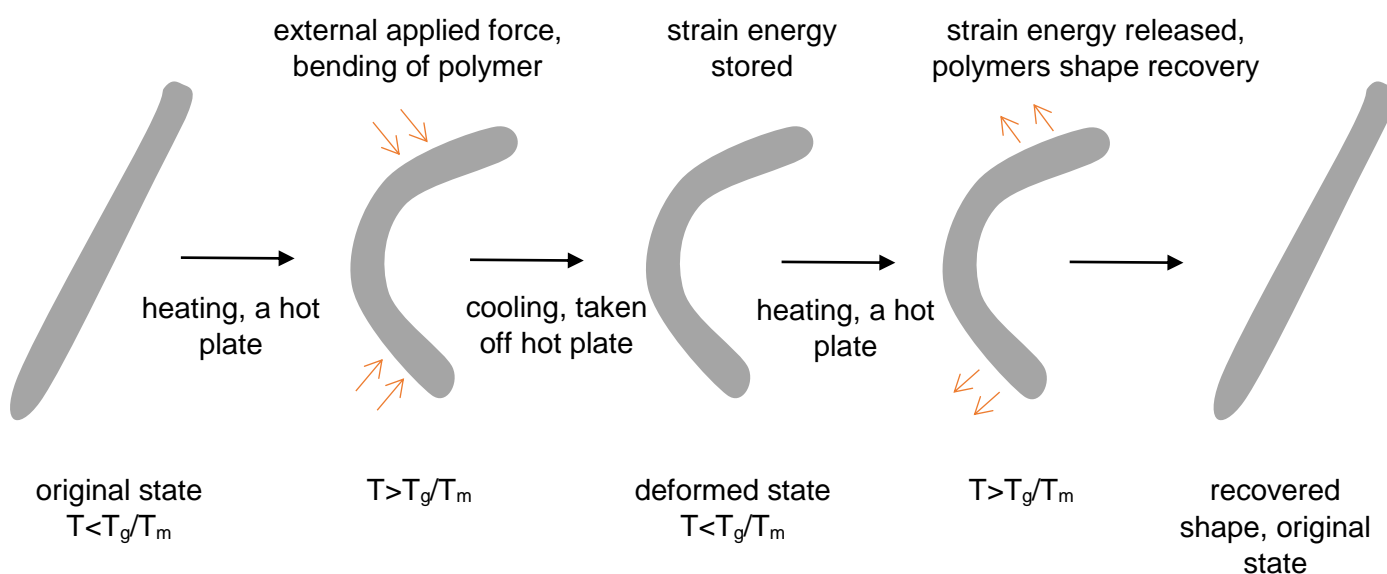


Figure 4. The SME mechanism of a thermally-induced SMP. Orange arrows show the SMPs direction of movement. Grey shaded shape depicts the SMP (e.g. in a film shape).

Over the course of SMP research, advanced thermomechanical constitutive models have been used to study the materials behaviour (e.g. the strain-temperature-stress development with time) in a very accurate way. Combining these models with SME mechanisms, and the detailed characterisation of the polymer (e.g. cross-links, interactions of compounds forming the polymer backbone) a deeper understanding of the SME of SMPs is achieved, which has proven beneficial for the development of new SMPs and their proposed applications.

1.3.2 Light-induced SMP

Light-activated shape-memory polymers (LASMPs) use the processes of photo-cross-linking or photo-cleavage to alter T_g . With LASMPs, the polymer network underlying active movement incorporates light sensitive domains possessing the ability to lower T_g . Therefore, LASMPs can reduce the cycle time of shape recovery and increase the responsiveness of the SMP. Previous studies have been successful at improving the response time of SMPs (e.g. by increasing the thermal conductivity with various conductive additives).⁸ However, the heating and cooling of polymers with substantial thickness takes time. Whereas, LASMPs introduce photo-cross-linking to eliminate the thermal dependency of SMPs because of a light-activated process. This process is achieved by using one wavelength of light, inducing photo-cross-linking, while a second wavelength of light reversibly cleaves photo-cross-linked bonds. This results in a material that can be reversibly switched between an elastomer and a rigid polymer. **Figure 5** depicts the process of LASMPs shape recoverability.

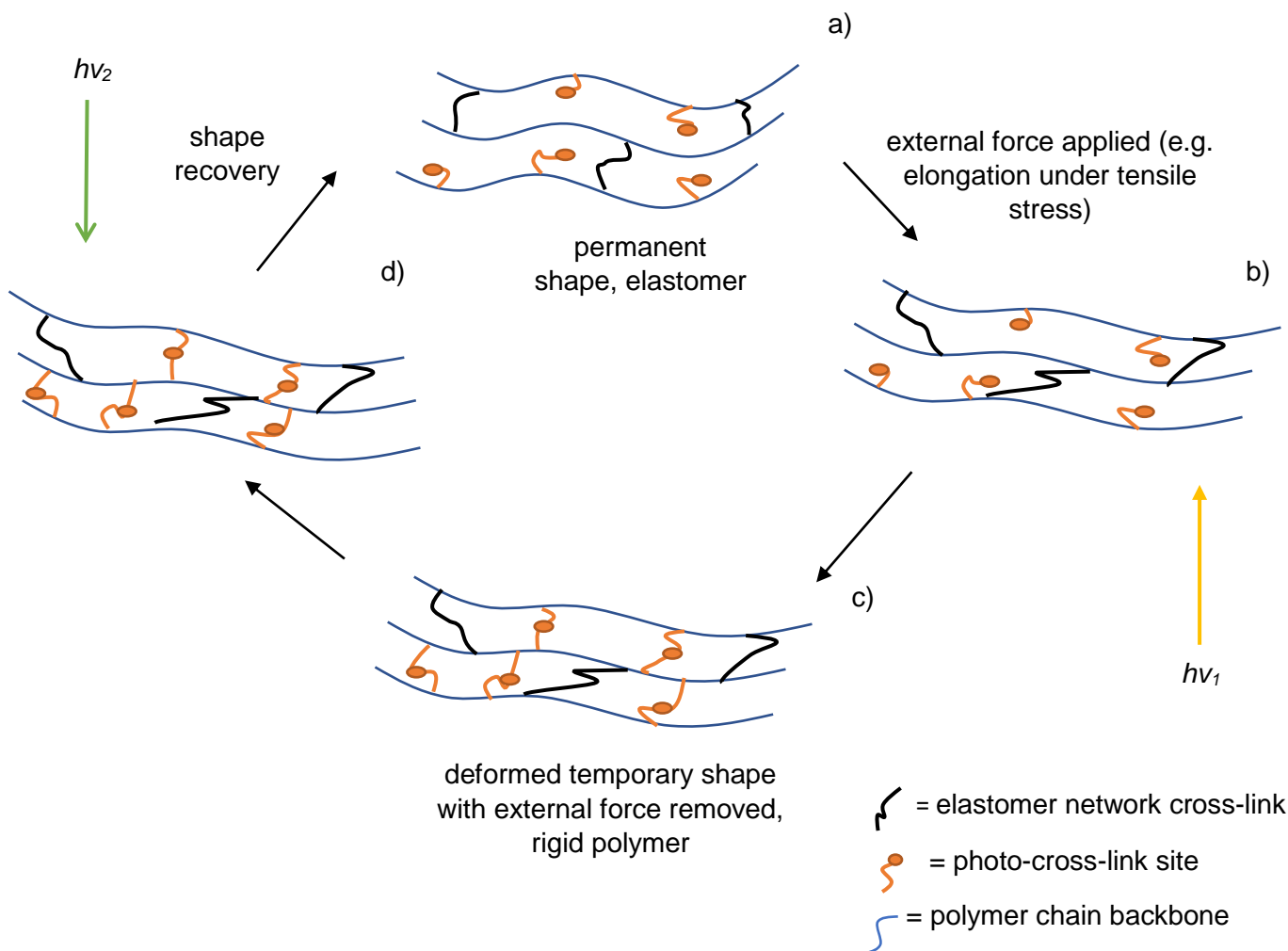


Figure 5. Schematic of the LASMPs SME mechanism. a) Low photo-cross-link density elastomer with a low T_g . b) Deformed state from a strain loaded sample (e.g. elongated and exposed to ultraviolet [UV] light). c) Temporary shape, high density photo-cross-link network with a higher T_g (temporary shape maintained, external force removed). d) Exposure to a UV light of different wavelength reversibly cleaves photo-cross-linked bonds and the sample reverts to its original state.

Light does not change the temperature of the material, only the cross-linking density within the material.⁸ It has been reported that polymers containing cinnamic groups can be fixed into pre-determined shapes utilising UV light illumination (>260 nm), and then recover their original state when exposed to UV light at a different wavelength (<260 nm).⁸

1.3.3 Electrically-induced SMP

Silver nanowire (Ag NW) shape-memory polyurethane (SMPU) composites in a bilayer structure have been fabricated which exhibit flexibility and superior electrical conductivity.⁹ The chemistry involved with this material combines the shape-memory characteristics of SMPs with electroconductive Ag NWs. Thus, Ag NW-SMPU composites were extended in applications of capacitive sensors, healable transparent conductors and potentially wearable electronics.⁹ Ag NWs are randomly distributed on the surface layer of the composites to form a conductive percolating network. These composites retained conductivity after a 12 % elongation, however, continual increase in elongation causes a dramatic increase to the composites resistance value and the eventual loss of electrical conductivity.⁹ A schematic of the composite is shown in **Figure 6**. When the material (deformed or in its original state), is connected to a typical circuit, a low voltage of 1.5 V was enough to activate a light-emitting diode (LED).⁹

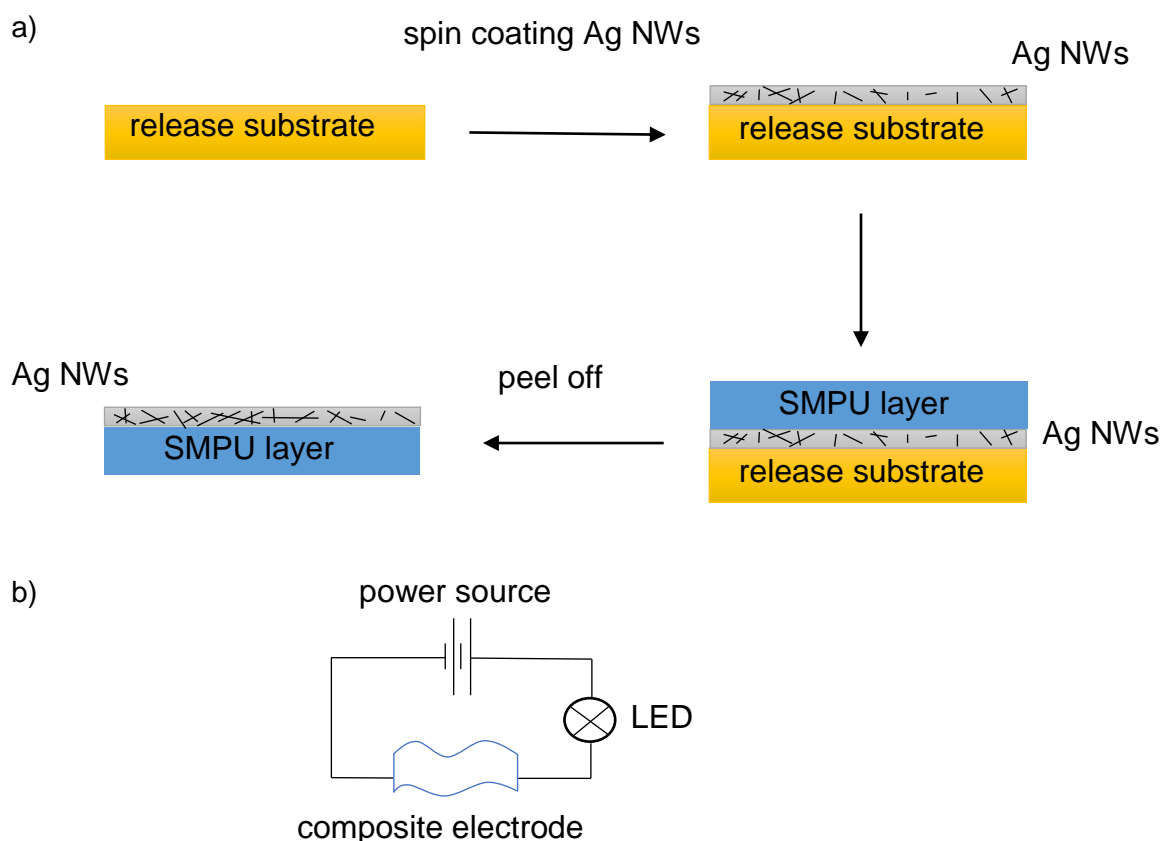


Figure 6. Representation of the electroactive SMPU and application. a) Demonstrating the fabrication of electroactive SMPU. b) A simple circuit to visualise how the electroactive SMPU can be utilised to activate an LED.

The composites possessing a higher Ag NW content exhibited a higher recovery ratio and reach the maximum recovery speed quicker.⁹ It was assumed that all the heat from electrical (Joule) heating was absorbed by the sample, i.e. no convective loss.⁹ Therefore, the composites with higher Ag NW content had a lower resistance value and the heating effectiveness was promoted. Heat initiates the thermal T_{trans} of the SMPU leading to an improved shape recovery. Voltages as low as 5 V reverted bent composites to their original state within 3 s.⁹ This is a good example of a multi-functional SMP and demonstrates the potential of SMP designs driving technological innovation. Unlike the SME mechanisms depicted in **Figure 1** and **2**, the thermal heating, in this case, is derived from electricity.

1.3.4 Water-induced SMP

The dynamic combination of rigid matrix polypyrrole (PPy) and a flexible interpenetrating polyol-borate network, strong and flexible films have been developed that can exchange water with the environment to induce film expansion and contraction.¹⁰ The free-standing composite polymer film was synthesised by electropolymerisation of pyrrole in the presence of polyol-borate complex. The polyol was pentaerythritol ethoxylate (PEE) which can coordinate with boron (III) species to form the dynamic polymer network.¹⁰ The polymer composite system features an interpenetrating network of a rigid polymer with a soft, solvent sensitive polymer that can perform water-gradient-induced displacement, converting chemical potential energy in water gradients to mechanical work.¹⁰ This polymer system adapts its architecture in response to an environmental condition change (sorption and desorption of water). Therefore, the SME process is driven by water stimulus sensitive domains, in **Figure 7** the SME mechanism of the water-responsive SMP and its application is presented.

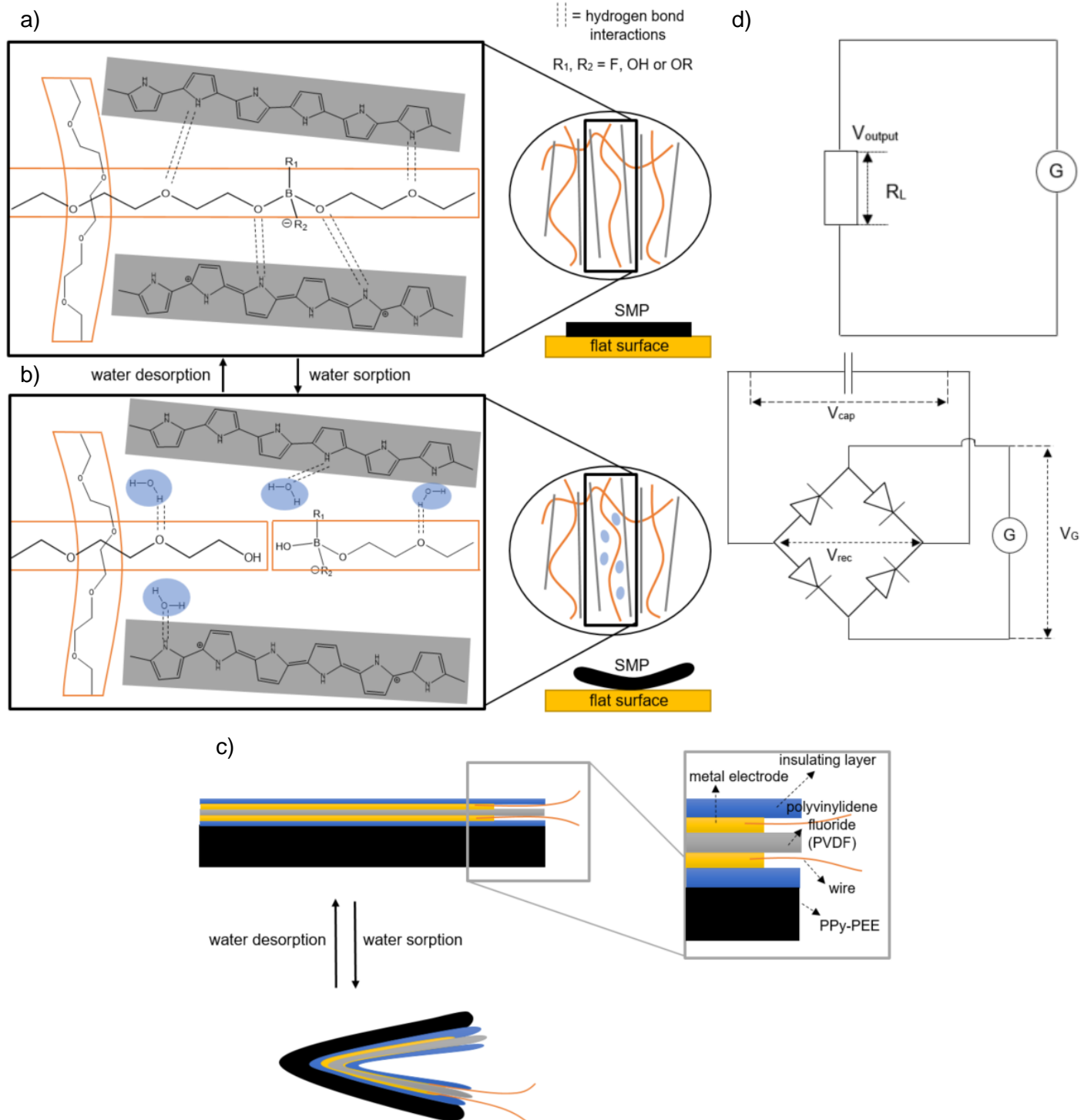


Figure 7. PPy-PEE composite film SME mechanism and application. a) Water desorption composite film, hydrogen bond interactions between the PPy chains (grey shading/lines) and PEE-borate (orange box/lines), and visual shape of the SMP film. b) Water sorption composite film, water molecules (blue dots) form new hydrogen bond interactions between the polymer chains, and a new deformed state of the SMP film. c) The assembly of a piezoelectric PVDF element with a PPy-PEE actuator to form the generator. d) Connection of the generator with a 10-mega ohm resistor as load and the configuration of the rectifying circuit and charge storage capacitor.

The hydrogen bonding interactions of the water sorption and desorption state is a reversible process. Since this SMP composition can exchange water with the environment to induce film expansion and contraction, a controlled, rapid and continuous locomotion can be produced. The unique design of the water-responsive PPy-PEE composite have been creatively applied to act as an actuator and generator driven by water gradients. The film actuator can generate contractile stress up to 27 megapascals, lift objects 380 times heavier than itself, and transport cargo 10 times heavier than itself.¹⁰ An assembled generator associating the actuator with a piezoelectric element driven by water gradients, outputs alternating electricity at ~ 0.3 Hz, with a peak voltage of ~ 1 V.¹⁰ The electrical energy can be stored in capacitors which could power micro and nanoelectronic devices.¹⁰ This is made possible because PPy is a CP enabling electropolymerisation, and the polyol-borate network is sensitive to water by means of hydrolysis and reforming of the borate ester cross-linking hub upon water sorption and desorption, which changes mechanical properties of the composite.¹⁰ This material is not only an example of another multi-functional SMP, but an SMP which responds to a different stimulus via water sensitive domains within the molecular architecture of the polymer. The SME mechanism for this SMP differs to that of **Figure 1** and **2**, utilising water as the shape-memory trigger for T_{trans} , and the original and deformed state interchange automatically via water sorption and desorption states. However, the shape-memory phenomenon remains the same, further demonstrating the brilliant potential of SMP designs driving technological innovation.

1.3.5 pH-induced SMP

SMP nanocomposites that are pH-responsive have been fabricated by blending poly(ethylene glycol)-poly(ϵ -caprolactone)-based polyurethane (PECU) with functionalised cellulose nanocrystals (CNCs). The functionalised CNCs possessed pyridine moieties (CNC-C₆H₄NO₂) through hydroxyl substitution of CNCs with pyridine-4-carbonyl chloride and with carboxyl groups (CNC-CO₂H) via 2,2,6,6-tetramethyl-1-piperidinyloxy (TEMPO) mediated surface oxidation, respectively.¹¹ At a high pH value, the CNC-C₆H₄NO₂ had attractive interactions from the hydrogen bonding between pyridine groups and hydroxyl moieties; at a low pH value, the interactions reduced or disappeared due to the protonation of pyridine groups, which are a Lewis base.¹¹ On the other hand, the CNC-CO₂H responded to pH variation in an opposite manner.¹¹ The hydrogen bonding interactions of both CNC-C₆H₄NO₂ and CNC-CO₂H can be readily disassociated by altering the pH values, endowing the pH-responsiveness of CNCs.¹¹ When the functionalised CNCs were combined with PECU polymer matrix to form a nanocomposite network, the mechanical properties of PECU were improved along with the pH-responsiveness of CNCs. The pH-sensitive CNC percolation network in the polymer matrix served as the switching units for shape-memory. Furthermore, the modified CNC percolation network and polymer molecular chains also had strong hydrogen bonding interactions among hydroxyl, carboxyl, pyridine moieties, and isocyanate groups, which could be formed or disrupted through changing pH value.¹¹ In **Figure 8** the SME process of this material is given.

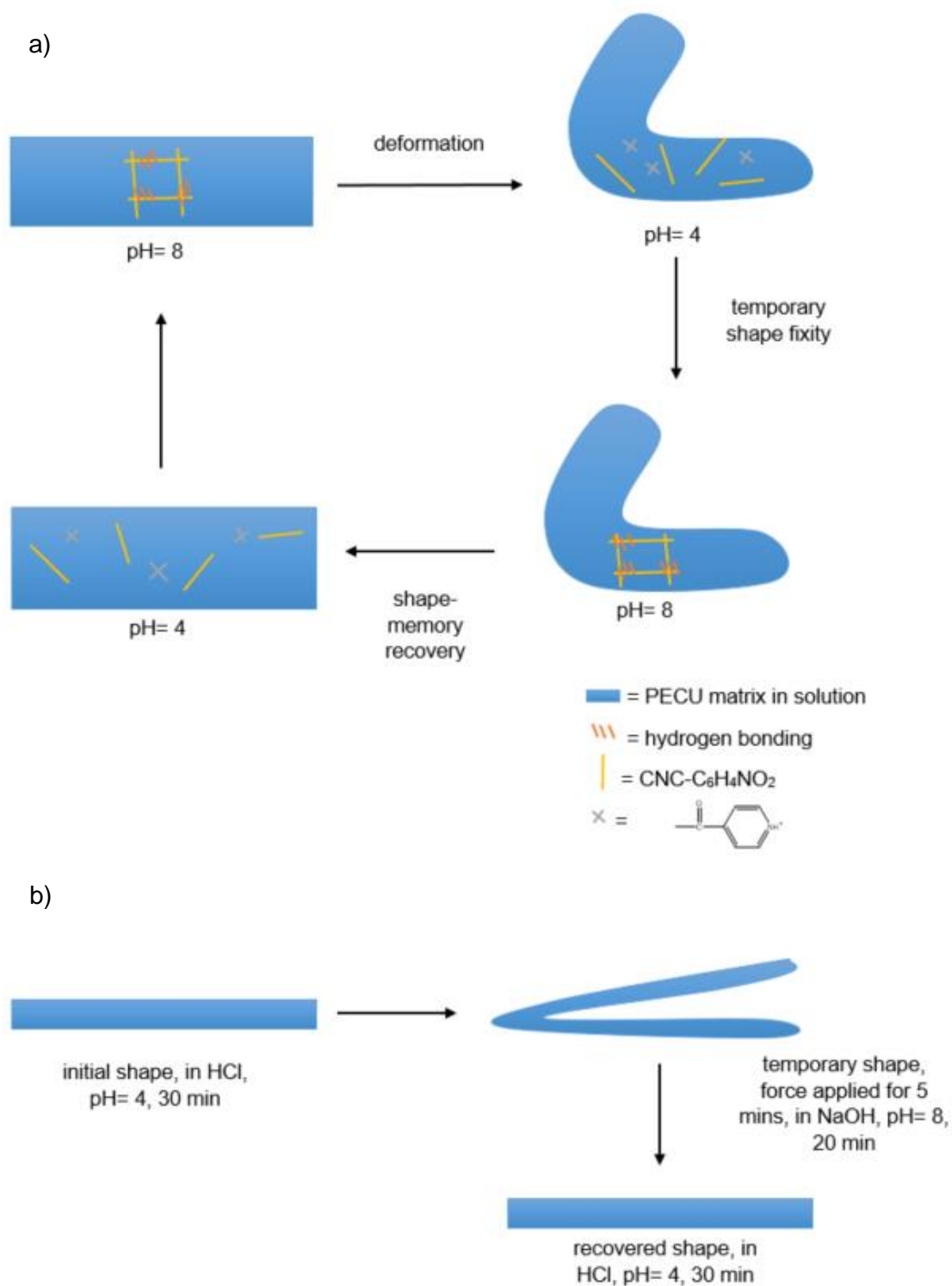


Figure 8. Representation of the pH-responsive SMP composite SME mechanism. a) Depicting the shape-memory materials involved with the SME relying on hydrogen bonding switches between CNC-C₆H₄NO₂ (CNC-CO₂H works similarly but the pH value for triggering SME are opposite), within the polymer matrix upon immersion in HCl (pH = 4) and NaOH (pH = 8). b) Conditions at each step of the process to induce the shape-memory recovery behaviour of the pH-responsive SMP.

The CNC percolation network serves as the switching unit of the SMP; both the PECU physical cross-linking and microphase separation act as the net point.¹¹ In acidic or alkali solutions, the primary condition to realise the pH-responsive SME based on hydrogen bonding interaction is that the material possesses good hydrophilicity, enabling H⁺ or OH⁻ ions to diffuse into material matrix accompanying with H₂O molecules. There are significant differences between spectra in the acid and spectra in the base.¹¹ In acid, the pyridine on the surface of CNC-C₆H₄NO₂ was protonated, leading to the damage of hydrogen bonding interactions of isocyanate groups of PECU and pyridine of CNC-C₆H₄NO₂. The vibration peak of the pyridine ring at 1598 cm⁻¹ disappeared in acid.¹¹ In base, the pyridine on the surface of CNC-C₆H₄NO₂ was deprotonated, causing the formation of hydrogen bonding interactions among nanocrystals and polymer matrix. Additionally, the hydrogen bonding interactions between the carboxyl groups on the surface of CNC-CO₂H and isocyanate groups of PECU were also confirmed by Fourier transform infrared (FTIR) spectroscopy.¹¹ As the SME of the nanocomposite networks were dependent on the pH variation of the environment, the effect can be readily controlled through changing hydrogen bonding interactions via altering the pH of the environment. Therefore, the pH-responsive shape-memory nanocomposites could be promising candidates in designing biomaterials for biomedical applications.¹¹ This is because different areas of the body have variations in physiological pH values. In particular pathological conditions, the physiological pH of biological systems generally appear as a sharp gradient.¹¹ A material with shape-memory capabilities, triggered by a pH change, could be very well suited for drug delivery applications. Again, the shape-memory phenomenon remains the same but here the SME mechanism for PECU/CNC-(C₆H₄NO₂, CO₂H) differentiates itself from **Figure 1** and **2** by possessing a sensitivity to a pH change.

1.4 Classification of SMPs

SMP materials are diverse, with many responding to different external stimuli such as, temperature, light, electricity, water and pH. There are different ways SMPs can achieve their SME utilising different SME mechanisms. Therefore, the classification of SMPs can be difficult, as organising these polymeric smart materials into one or two simple categories, would be a huge oversimplification of their abilities and characteristics. Although, SMPs can be classified based on their composition and structure, stimulus, and shape-memory function. To begin, SMPs are considered to consist of net points and molecular switches or stimuli sensitive domains. These net points can be achieved by covalent bonds (chemically-cross-linked) or intermolecular interactions (physically-cross-linked). Chemically-cross-linked SMPs involve suitable cross-linking chemistry and are referred to as thermosets.¹² Physically-cross-linked SMPs involve a polymer morphology consisting of at least two segregated domains and are referred to as thermoplastics.¹² The network chains of the SMP can be either amorphous or crystalline and therefore, the T_{trans} is either a T_g or T_m . The network architectures are thought to be constructed through cross-linking net points, with polymer segments connecting adjacent net points.¹² The strongly cross-linked architectures ensure the polymer can maintain a stable shape on the macroscopic level. Thermoplastic polymers exhibit a more reversible nature, meaning the physical cross-linked net points can be disrupted and reformed with relative ease. The interconnection of the individual polymer chains in a physically-cross-linked network is achieved by the formation of crystalline or glassy phases. For thermoset polymers, the individual polymer chains are connected by covalent bonds and are therefore more stable than physically-cross-linking networks, and show an irreversible nature.¹² A further basic requirement of an SMP is the formation of strong reversible interactions (secondary cross-links) between the polymer segments so that a macroscopic shape deformation can be fixed.¹² **Figure 9** donates the physical and chemical cross-linking networks, as well as, the secondary cross-links during a SME process.

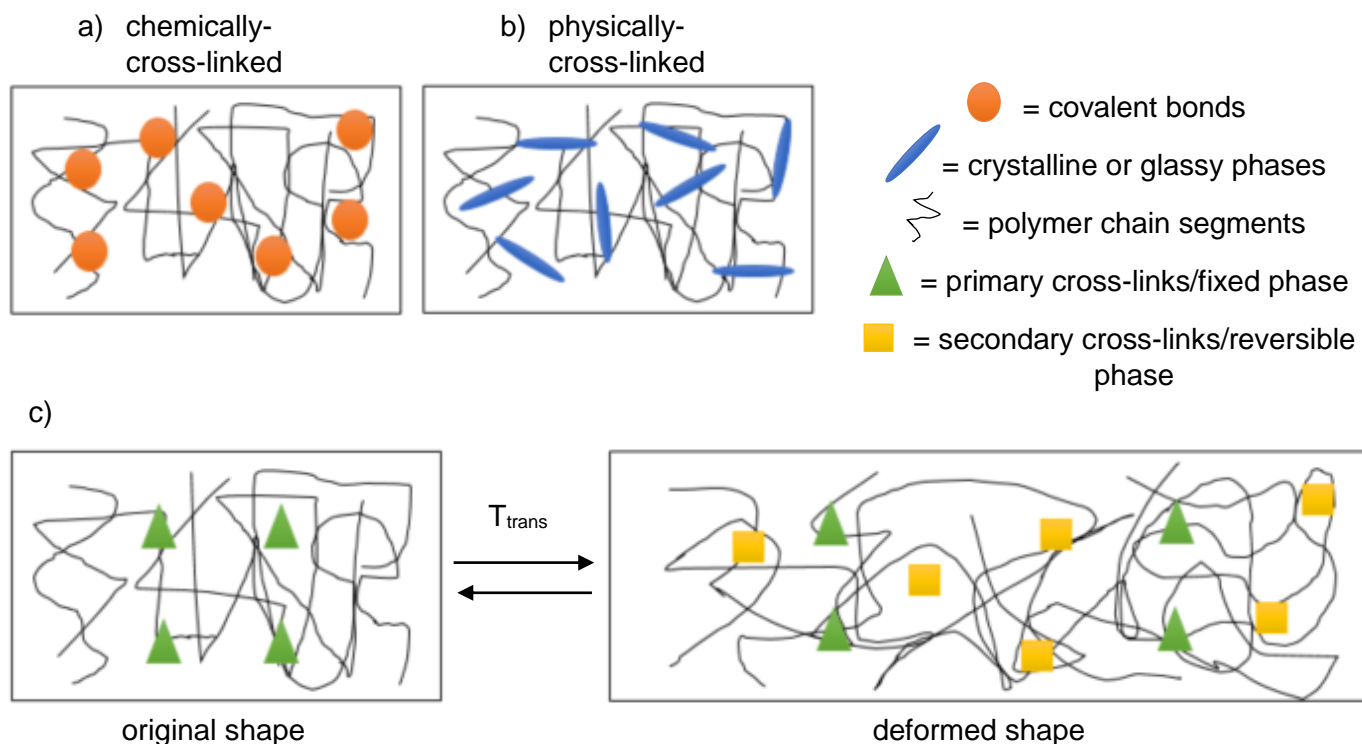


Figure 9. Schematic of the typical primary cross-links of a polymer network and during the shape recovery process. a) Chemically-cross-linked associated with thermoset polymers b) Physically-cross-linked associated with thermoplastic polymers. c) Polymer networks during shape recovery showing the switching between fixed phase (hard segments/primary cross-links) and reversible phase (soft segments/secondary cross-links). The primary cross-links being either chemically-cross-linked i.e. covalent bonds or physically-cross-linked i.e. intermolecular interactions, crystalline or glassy phases. The secondary cross-links being either crystalline or glassy phases.

Regarding thermo-responsive SMPs, they can be classified according to the nature of their permanent net points and the T_{trans} related to the switching domains into four different categories: (I) physically-cross-linked thermoplastics, $T_{trans} = T_g$; (II) physically-cross-linked thermoplastics, $T_{trans} = T_m$.¹² (III) chemically-cross-linked amorphous polymers, $T_{trans} = T_g$; (IV) chemically-cross-linked semi-crystalline polymer networks $T_{trans} = T_m$.¹²

1.4.1 Thermoplastic SMPs

For the physically-cross-linked SMPs, the formation of a phase-segregated morphology is the fundamental mechanism behind the thermally induced SME of these materials.¹² One phase provides the physical cross-links while the other acts as a molecular switch. They can be further classified into linear polymers, branched polymers or a polymer complex. Linear SMPs may consist of block copolymers and high molecular weight polymers, the typical physically-cross-linked SMP is linear block copolymers, such as polyurethanes (PU). In polyesterurethanes (PEU), oligourethane segments are the hard-elastic segments, while polyester serves as the switching segment.¹²

1.4.2 Thermoset SMPs

For chemically-cross-linked SMPs, two methods are commonly used to synthesise covalently cross-linked networks. (I) Addition of a multi-functional cross-linker during polymerisation. The chemical, thermal and mechanical properties of the network can be adjusted by the choice of monomers, their functionality, and cross-linker content.¹² (II) The subsequent cross-linking of a linear or branched polymer. The networks are formed based on many different polymer backbones.¹² Covalently cross-linked SMPs possess chemically interconnected structures determining the original macroscopic shape. The switching segments of these materials are generally the network chains between net points, and a T_{trans} of the polymer segments is used as the shape-memory switch.¹² The chemical, thermal, mechanical and shape-memory properties are determined by the reaction conditions, curing times, the type and length of the network chains, and the cross-linking density.¹² Comparing physically-cross-linked SMPs with chemically-cross-linked SMPs, the chemically-cross-linked SMPs often show less creep, thus, any irreversible deformation of the polymer during shape recovery is less. This is because covalent cross-linked networks are more stable than physical cross-linked networks. As a result, chemically-cross-linked SMPs usually show better chemical, thermal, mechanical and shape-memory properties than physically-cross-linked SMPs. For example, the shape recovery ratio of thermoplastic SMPU is usually in the range of 90 to 95 % within 20 shape recovery cycles, and the elastic modulus being between 0.5 and 2.5 GPa at room temperature.¹² Additionally, when exposed to air, it is sensitive to moisture and therefore shows unstable mechanical properties. In contrast, an epoxy SMP shows better overall performance as a shape-memory material.¹² The shape recovery ratio reaching 98-100 %, the elastic modulus was between 2 and 4.5 GPa, and they were stable in the presence of moisture.¹² Due to the relatively poor thermal and mechanical properties of thermoplastic SMPs (e.g. SMPU) are mostly researched and used as functional materials at a small scale, such as for biomaterials and SMP textiles.¹² However, the thermosetting SMPs (e.g. styrene-based and epoxy SMPs) are generally used for structural materials, such as space deployable structures and automobile actuators.¹²

1.4.3 Shape-memory functionality

The approaches to designing different shape-memory functions become more abundant as scientists and engineers better understand the SME mechanism of SMPs. One-way SMEs, two-way (such as, dual shape PPy-PEE discussed in **Figure 7**), triple, multiple SMEs and even temperature-memory effects (TMEs) have been widely investigated in SMPs.¹³ As the type of SMP materials increasingly diversify, two and even three different types of shape-memory functions can be achieved simultaneously in the same SMP material.¹³ These types of materials can be usually achieved when combining different SMPs possessing different properties. A schematic of one-way, two-way, dual shape and triple shape functionality SMPs in **Table 1** is given.

	one-way SME	two-way SME
dual shape	<p>original shape</p> <p>deformed shape maintained</p>	<p>original shape</p> <p>deformed shape</p>
triple shape	<p>original shape</p> <p>deformed shape¹ maintained</p> <p>deformed shape² maintained</p>	<p>original shape</p> <p>deformed shape¹</p> <p>deformed shape²</p>

Table 1. Table of the varying shape-memory functionality of SMPs. In one-way, once the T_{trans} conditions are no longer met, the deformed temporary shape is retained until T_{trans} conditions are met again, and the original shape will be recovered. In two-way, the original shape is recovered once T_{trans} conditions are no longer met. In triple shape, more than one T_{trans} is possible and the material can possess multiple temporary shapes.

As the composition and structure, different stimuli inducing the SME mechanism, and the shape-memory functionality of SMPs have now been discussed, an integrated insight into the classification of SMPs is shown in **Table 2**.



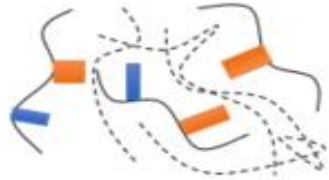

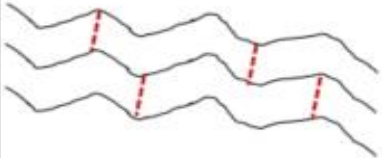

composition and structure	stimulus	shape-memory function type
block copolymer  	TEMPERATURE } ELECTRICITY } MAGNETIC	ONE-WAY SME TWO-WAY SME
supramolecular polymer 	} WATER SENSITIVE }	TRIPLE SHAPE SME
polymer blend/composites  e.g. PPy-PEE discussed in Figure 7	} OXIDATION- REDUCTION }	MULTI-SHAPE SME
cross-linked homopolymer 	} LIGHT/RADIATION }	MULTI-FUNCTIONALITY
polymer IPN/semi-IPN 		

Table 2. A table giving insight on classifying SMPs based on composition and structure, stimulus triggers, and the possible type of shape-memory functions. The table represents an overview at categorising SMPs but does not encompass the entirety of SMPs. Instead, aims to highlight the diversity of SMPs and the possible shape-memory functions, reinforcing their increasingly prominent features and their abundant potential applications.

1.5 Characterisation of the SMPs

To holistically understand SMPs and optimally utilise their unique features for innovative applications, not only how they work and how they are classified, but also how they are characterised empirically is vital. The main characterisation techniques and the corresponding chemical, optical, structural, thermal, and mechanical parameters of SMPs will consequently be discussed.

1.5.1 FTIR spectroscopy

FTIR spectroscopy is a technique used to obtain an infrared spectrum of absorption or emission of a solid, liquid or gas. It is a very useful tool to identify different chemical bonds i.e. functional groups present within a sample. The wavelength of light absorbed is characteristic of the chemical bond, which can be distinguished in the spectrum. By interpreting the infrared absorption spectrum, the functional groups present in the molecule can be ascertained (in combination with other data confirming their presence). FTIR spectrometry is often used to investigate the difference in structure of the networks in a molecule during the synthesis of an SMP.¹⁴ In addition, Raman spectroscopy and X-ray diffraction (XRD) are generally used to determine the corresponding chemical structures of SMPs.¹⁴

1.5.2 UV-Vis spectroscopy

Ultraviolet-visible (UV-Vis) spectroscopy/spectrophotometry refers to absorption spectroscopy or reflectance spectroscopy in the UV-Vis spectral region. The absorption or reflectance in the visible range directly affects the perceived colour of the samples involved. In this region of the electromagnetic spectrum, atoms and molecules undergo electronic transitions. Absorption spectroscopy is complementary to fluorescence spectroscopy, in that fluorescence deals with transitions from the excited state to the ground state, while absorption measures transitions from the ground state to the excited state.¹⁵ Although, UV-Vis spectroscopy is routinely used in analytical chemistry for the quantitative determination of different analytes, such as transition metal ions, highly conjugated organic compounds, and biological macromolecules. This method could provide information on the characterisation of light-induced SMPs and assist characterisation of optically transparent SMPs by evaluating their optical properties.

1.5.3 NMR spectroscopy

Nuclear magnetic resonance (NMR) spectroscopy is a spectroscopic technique to observe local magnetic fields around atomic nuclei. The sample is placed in a magnetic field and the NMR signal is produced by excitation of the nuclei sample with radio waves into nuclear magnetic resonance, which is detected with sensitive radio receivers. The intramolecular magnetic field around an atom in a molecule changes the resonance frequency, thus, giving access to details of the electronic structure of a molecule and its individual functional groups. As the fields are unique or highly characteristic to individual compounds, in modern organic chemistry practice, NMR spectroscopy is the definitive method to identify monomolecular organic compounds. Similarly, biochemists use NMR to identify proteins and other complex molecules. Besides identification, NMR spectroscopy provides detailed information about the structure, dynamics, reaction state, and chemical environment of molecules. The most common types of NMR are ^1H and ^{13}C NMR spectroscopy, but there are also: solid-state, correlation spectroscopy (COSY) and heteronuclear single quantum correlation (HSQC), all applicable to any kind of sample that contains nuclei possessing spin. NMR spectra is unique, well-resolved, analytically tractable and often highly predictable for small molecules. Different functional groups are clearly distinguishable, and identical functional groups with differing neighbouring substituents still give distinguishable signals.¹⁶ Utilising NMR spectroscopic methods to characterise SMPs may not yield definitive data i.e. identifying the exact structure of the polymer. However, the addition of the information provided could reinforce other data (e.g. FTIR data on the present functional groups), thus enabling SMPs chemical and structural characteristics to be more clearly justified.

1.5.4 SEC/GPC

Size-exclusion chromatography (SEC) or gel-permeation chromatography (GPC) are chromatographic methods in which molecules in solution are separated by their size and molecular weight. SEC is a widely used polymer characterisation method because of its ability to provide good molecular mass distribution results for polymers. SEC can be used as a measure of both the size and the polydispersity index (PDI) of a synthesised polymer, that is, the ability to find the distribution of the sizes of polymer molecules. If standards of a known size are run previously, then a calibration curve can be created to determine the sizes of SMP molecules of interest in the solvent chosen for analysis.¹⁷

1.5.5 Morphology detection

XRD, optical microscopy, scanning electron microscopy (SEM) and transmission electron microscopy (TEM) can be used to observe a polymers morphological structure and the surface morphology of SMPs or SMP composites.¹⁴ X-ray crystallography is a technique used for determining the atomic and molecular structure of a sample, in which the morphology of the sample may cause a beam of incident X-rays to diffract into many specific directions (e.g. determining whether a polymer is amorphous or semi-crystalline). An optical microscope is a type of microscope that uses visible light and a system of lenses to magnify images of small samples; the resulting resolution is often at the micron level.¹⁴ A SEM uses scattered electrons inspecting the topographies of samples at high magnifications, producing an image with a depth of field that is typically 300 to 600 times better than that of an optical microscope.¹⁴ A TEM is a microscopy technique whereby a beam of electrons is transmitted through an ultra-thin specimen, interacting with the specimen as it passes through, which is analogous to optical microscopy.¹⁴ However, under favourable conditions TEM can resolve detail at the magnitude of about 1 nm.¹⁴

1.5.6 Electrical conductivity measurement

Electroconductive substances can be incorporated into SMPs producing electroactive SMP composites, such as Ag NW-SMPU shown in **Figure 6**. CPs can conduct electricity if they are appropriately conjugated (e.g. PPy). To evaluate the electrical properties, a variety of methods are employed to measure the electrical conductivity.¹⁴ If the electrical resistance ranges from 10^8 to 10^{11} Ohms (Ω), a digital high resistivity determiner could be employed.¹⁴ The four-point probes measurement, which eliminates the lead resistance, may also be used to determine the conductivity.¹⁴ During resistive heating, an infrared camera can be employed to investigate the temperature distribution of the SMPs during the shape recovery process.¹⁴

1.5.7 TGA

Thermogravimetric analysis (TGA) is used to investigate thermal stability by evaluating the change in mass as a function of temperature. During the shape recovery process, the highest temperature should be lower than the onset temperature point of decomposition of SMPs. TGA or differential gravitational analysis (DTG) is used to determine the critical temperature during the decomposition process of SMPs or SMP composites. TGA is a very useful tool for a first, simple and fast evaluation of the thermal stability properties before studying the materials SME.¹⁴

1.5.8 DSC

Differential scanning calorimetry (DSC) is used in many different industries, its application in the plastics industry is widely accepted. It is used to characterise materials for T_g , T_m and other material reaction characteristics such as specific heat, percent crystallinity, and reaction kinetics.¹⁸ For SMP use, in most cases, DSC is used to determine the T_g during the transition process.

1.5.9 DMA

Dynamic mechanical analysis (DMA) is used to monitor the thermal and dynamic mechanical properties of the SMPs and their composites. In this technique, a strain or stress is applied to a sample at a set frequency and the response analysed to obtain phase angle and deformation data. The data allows for the calculation of the complex modulus in equation (4) (e.g. storage modulus and loss modulus), damping or tan delta (δ) as well as viscosity data.¹⁴ The dynamic mechanical properties of a polymer are described in terms of a complex dynamic modulus¹⁹

$$E^* = E' + iE'' \quad (4)$$

where E' is the storage modulus and is a measurement of the recoverable strain energy; when deformation is small, it is approximately equal to the Young's modulus. E'' denotes the loss modulus and is related to the hysteresis energy dissipation. The phase angle (δ) is given by (5)

$$\tan \delta = \frac{E''}{E'} \quad (5)$$

DMA allows the rapid scanning of the modulus and viscosity of an SMP as a function of temperature or frequency.²⁰ In addition, DMA is very sensitive to the motions of polymer chains and, therefore, they are powerful tools for measuring the T_g in SMPs.¹⁴

1.5.10 Mechanical properties evaluation

The mechanical properties of SMPs under varying temperature conditions are important parameters to evaluate the thermal, mechanical and shape-memory performance. The relevant tests include uniaxial tension tests, compression tests, three-point bending tests, relaxation tests, creep tests, and nanoscale indentations by atomic force microscopy (AFM).¹⁴ Yang et al. studied nanoscale indentation on polymer surfaces using AFM. With increasing molecular weight of cross-linker and decreasing cross-linker concentration, the contact pressures decreased at a fixed maximum load. The results provided insight into the nanoscale response of these novel materials.^{14, 21} The typical programming of a thermo-responsive SMPs shape recovery process has been introduced in **Figure 3**. A cyclical thermomechanical test is a standard approach to characterise the mechanical and shape-memory properties of SMPs. At an elevated temperature $T > T_{trans}$, the SMP sample is deformed to a pre-determined maximum strain ϵ_m at a constant strain rate ($\dot{\epsilon}$) under the external force loading. The sample is held at ϵ_m and then cooled below T_g to a new temperature $T < T_{trans}$. After the constraint is released at $T < T_{trans}$, the stress is reduced to zero, and a very small elastic strain is recovered (shape fixity) where ϵ_u is defined as the pre-deformed remaining strain after the applied stress is fully removed. The sample is reheated from $T < T_{trans}$ to $T > T_{trans}$ at a constant heating rate (\dot{T}) without applying any external force loading ($\sigma = 0$). The pre-deformed strain ϵ_u is recovered with only a very small irreversible strain ϵ_p left after shape recovery at $T > T_{trans}$. Thus, describing the shape recovery phenomenon, and the thermomechanical cycle SME quantities, R_r and R_f , can be deduced using equations (1) and (2) respectively.

1.6 Focus of the thesis

The thesis focuses on innovations involving the work described on an optically transparent shape-memory polyimide (TSMPI) and a linear, phase-segregated multi-block copolymer oligo(ϵ -caprolactone) diol-oligo(*p*-dioxanone) diol (OCL-ODX) SMP. By utilising a relatively new technique of multiphoton fabrication (using a Photonic Nanoscribe) to photopolymerise a CP (e.g. PPy) into/on the surface of TSMPI and OCL-ODX SMP, the objective is to produce and evaluate the properties of these novel materials. The combination of the SMP and CP can lead to unique and technologically innovative applications.

1.6.1 Direct laser writing or multiphoton fabrication using a Photonic Nanoscribe

This technique provides a platform for two-photon polymerisation (2PP) of microstructures into/on samples by using a high-sensitivity microscope camera, 3D laser lithography system, and a suitable ink with photoinitiator to initiate the photopolymerisation process. The laser beam is focused into the sample and 2PP is triggered only in the focal spot volume (a voxel); direct laser writing is achieved using x, y and z movement stages to create the required structures. Earlier work can be found using this laser writing technique in 2006, where photoresist templates for 3D–2D–3D photonic crystal heterostructures were fabricated.²² The microscope lens must observe through the sample i.e. photoresist, and dependent on the configuration the supporting substrate (e.g. a glass coverslip) and measure a refractive index (RI) matching fluid before writing can take place. The internal calibration will therefore allow 2PP at different detected interfaces (working distance is dependent on the objective lens magnification), between the index matching fluid, microscope lens and laser. Furthermore, computer-aided design (CAD) generated structures can be easily imported via STL file formats. Thus, highly customised microstructures can potentially be written into/on sample substrates.

1.6.2 TSMPI

Polyimides (PIs) are normally derived from a dianhydride and a diamine or a dianhydride and a diisocyanate. They can be of aliphatic, semi-aromatic or aromatic nature, and aromatic PIs are normally more common due to their thermostability. PI materials are lightweight, flexible, resistance to heat and chemicals. Therefore, they can have many possible applications (e.g. they have been utilised in the electronics industry for flexible cables and as an insulating film on magnet wire).²³ Regarding the PI with shape-memory and optically transparent properties, TSMPI has been fabricated with a reported T_g of between 171 °C and 191 °C, a curved TSMPI film recovered its original state in roughly 30 s.²⁴ Additionally, the polymer possesses a high thermostability character, with major thermal decomposition beginning at 540 °C, and excellent thermomechanical properties and shape-memory performance, retaining a high optical transparency after many shape-memory cycles.²⁴ A 120 μm thick film of TSMPI exhibits a transmittance higher than 81 % in 450 to 800 nm.²⁴ The high optical transparency mainly originates from suppressed intra/intermolecular charge transfer complex (CTC) interactions caused by the special structure of the PI.²⁴ The TSMPI was fabricated by employing flexible bis-phenol A dianhydride (BPADA) as dianhydride and flexible 1,3-bis(3-aminophenoxy)benzene (BAB) as diamine.²⁴ The thermoplastic amorphous polymer contains hydrogen bond interactions between polymer network chains, responsible for the reversible phase and the shape-memory process. At $T > T_g$ the hydrogen bonds are disrupted i.e. switched off and the flexibility of the polymer is achieved. Reverting to the original state or allowing deformation into a temporary shape. At $T < T_g$ hydrogen bond interactions between polymer network chains can reform and the hard segments, being the rigid polymer backbone, form the net points and re-link the soft segments (reversible hydrogen bonds) inhibiting elasticity. It was observed via DMA (the peak of the loss factor $\tan \delta$ obtained by DMA is often taken as T_g of rigid-chain polymers), TSMPI exhibits a T_g of 171 °C which is higher than those of other transparent SMPs, but lower than those of other shape-memory PIs. It has been proven that the relative flexibility of the polymer backbone can affect dynamics through the glass transition, which have great influence on the T_g of polymers. Many SMPs composed of polymers with flexible main chains possess T_g lower than 110 °C, while high temperature SMPs, such as TSMPI, are composed of rigid main chains comprising phenyl rings and flexible linkages. The isopropylidene and ether linkages within the backbone, together with the *meta*-substitute structure provide flexibility to the rigid PI molecule, and the molecular chains act as a reversible phase of the shape-memory process. The report concluded an efficient way to obtain optically clear TSMPIs with vast potential in controlling the chemical structure and the molecular weight. In addition, a T_g of 171 °C, higher than those of other optically transparent SMPs.²⁴

1.6.3 Innovative application for TSMPI

A unique SMP composite utilising TSMPI and PPy was conceived. The concept involves pyrrole being photopolymerised via multiphoton fabrication into and on the surface of thin films of TSMPI. As a result, a TSMPI and PPy composite is produced; **Figure 10** demonstrates the materials use.

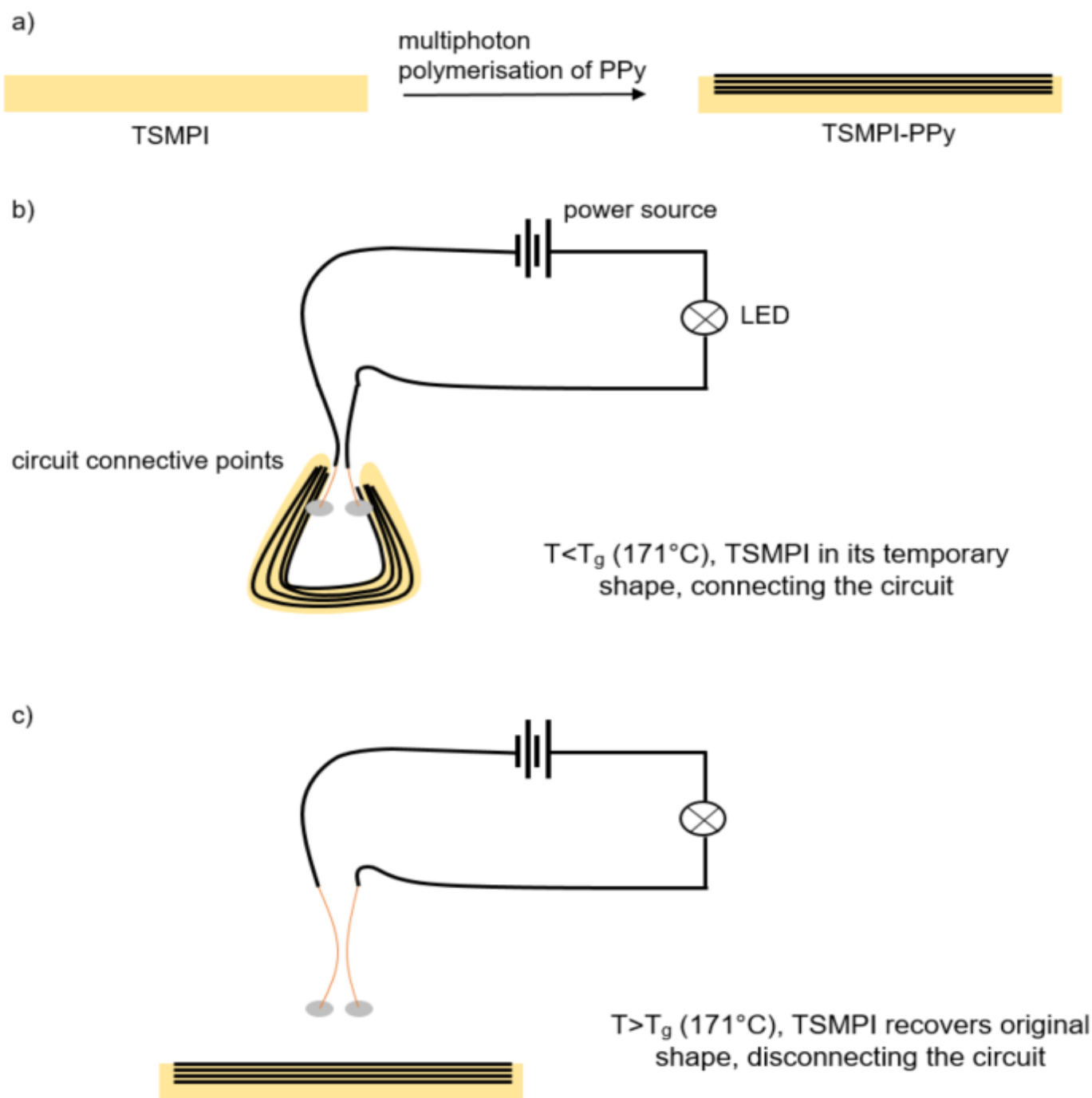


Figure 10. Schematic of the TSMPI-PPy composite and used as a negative switch. a) Simple route showing the fabrication of the TSMPI-PPy composite, combining the features of each polymer. The black lines depict PPy, photopolymerised into and on the surface of TSMPI. b) A basic circuit with a power source and LED output is used to depict how this material could be useful. The deformed temporary shape of the TSMPI-PPy is in contact with two connective plates, thus, completing the circuit and the LED is lit. c) Above the T_g of TSMPI, the SME process occurs and therefore disconnects the circuit, the two connective plates are no longer in contact with PPy, resulting in the LED being switched off.

Due to TSMPIs high T_g , this negative switch application can be suitable for any high thermal systems and could act as the critical temperature failsafe. The concept would provide a relatively cheap, reliable and sensitive negative switch disconnecting systems to prevent overheating that can cause damage. Although, this materials shape-memory function is one-way, heating followed by the deformation into the desired temporary shape is required after one cycle of the shape recovery process. It would be suggested to utilise this concept simultaneously with other safety parameters in case a whole system failure was to occur, the TSMPI-PPy composite can be relied upon to disconnect the circuit preventing damage. This is because the composite only requires temperature to work. However, further investigations could lead to a similar design with a two-way shape-memory functionality, eliminating the need to deform the TSMPI back into shape and the material can continue to work independently.

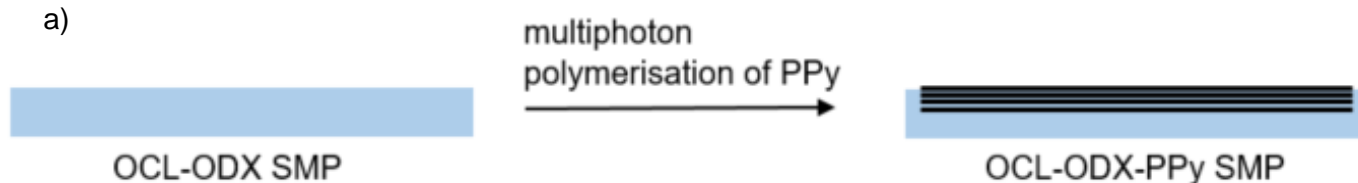
1.6.4 OCL-ODX SMP

Diols are a chemical compound containing two hydroxyl groups. This pairing of functional groups is pervasive, and many subcategories have been identified.²⁵ They react as alcohols by esterification and ether formation, and diols (e.g. ethylene glycol [EG]) are commonly used as co-monomers in polymerisation reactions. In the first step of the OCL-ODX SMP synthesis, macrodiols with different thermal characteristics are synthesized through ring-opening polymerisation of cyclic diesters or lactones, with a low-molecular-weight diol as initiator, and purified.²⁶ OCL was chosen as the precursor for the switching segments having a T_m , while crystallisable ODX with a higher T_m than OCL was chosen as a hard segment to provide the physical cross-links.²⁷ The T_m of the latter macrodiols is determined by the average chain length, which can be tailored by the monomer/initiator ratio. In the second step, the two macrodiols are coupled with 2,2(4),4-trimethylhexanediisocyanate (TMDI). The thermoplastic linear multi-block copolymer contains a phase-segregated system, of which, the polymer architecture can be tailored in macroscopic properties by variation of molecular parameters.²⁸ The SMP enables temporary shapes of up to 400 % deformation and a T_{trans} recorded at 40 °C (fastest shape change was recorded at this temperature).²⁸ Hydrolysable ester bonds were introduced into the polymers so that they would cleave under physiological conditions. The degradation kinetics can be controlled through the composition and relative mass content of the precursor macrodiols. An increase in the ODX content leads to faster loss in mass, because the concentration of rapidly hydrolysable ODX-ester bonds in the amorphous phase increased.²⁸ Furthermore, as the purpose of this SMP was for suturing wounds, degradation products could have been an issue. Hence, the tissue compatibility of the SMP was also investigated with chorioallantoic membrane (CAM) tests, which are a sensitive method of evaluating toxicity.²⁸ Nine separate experiments were carried out and all tests showed good tissue compatibility when graded according to Folkman.²⁸ There were no detectable changes in the number or shape of blood vessels or damage under or near the polymer film. Hereby, the report concluded an SMP that was biodegradable and tissue compatible that when actuated (the T_{trans} through T_m is ~ 40 °C) in a loose suture shape, could tighten and close wounds quite effectively. The SME generated an actuating force of 1.6 N *in vitro* and during an animal experiment, 0.1 N could be detected in the surrounding tissue.²⁸

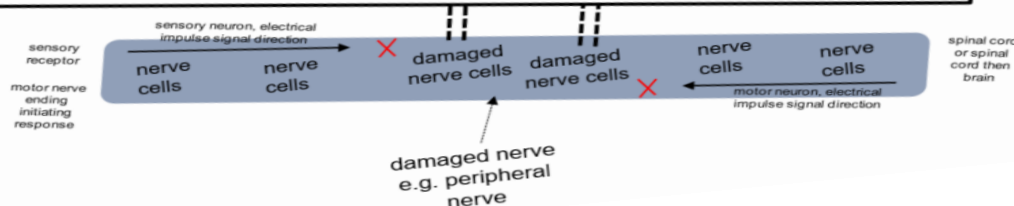
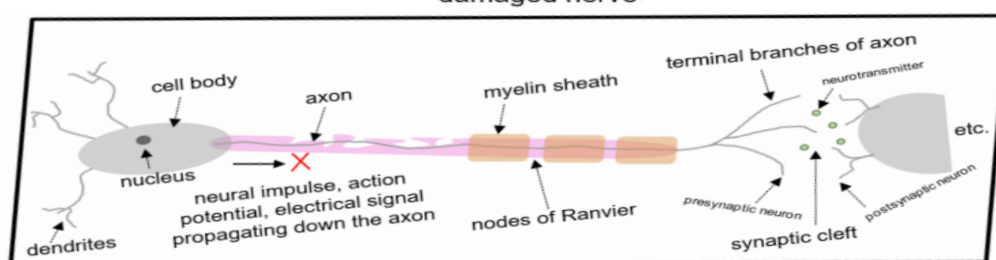
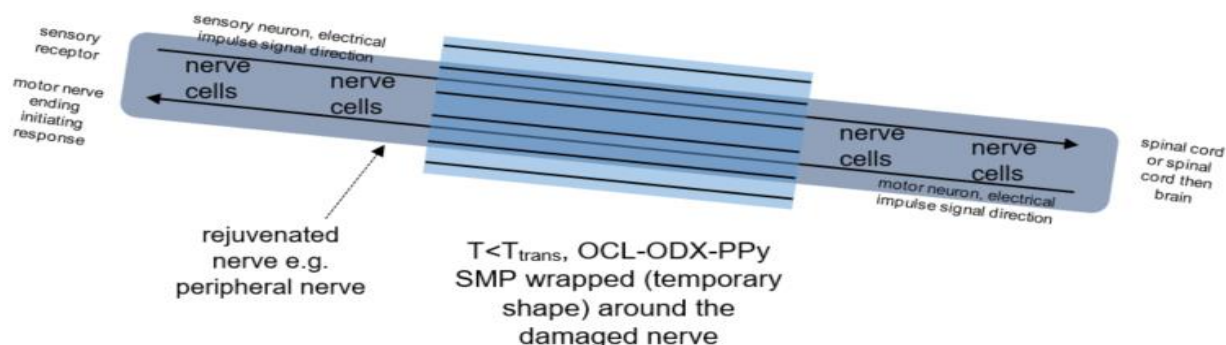
1.6.5 Innovative application for OCL-ODX SMP

TSMPI and OCL-ODX SMP similarly possess an excellent SME after many shape-memory cycles, but also possess different properties (e.g. T_{trans} and OCL-ODX SMPs tissue compatibility [TSMPIs tissue compatibility is not known, but since T_g is 171 °C, it is unlikely TSMPIs SME could be safely/effectively used *in vivo*]). Thus, employing the same concept first described in **Figure 10**, the OCL-ODX SMP and PPy composite leads to a different application; **Figure 11** demonstrates the materials use.

a)



b)



c)

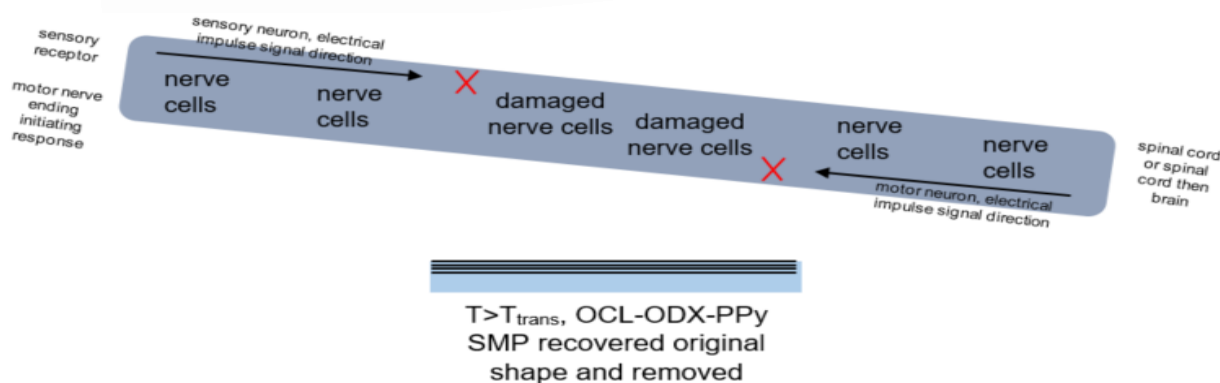


Figure 11. Schematic of the OCL-ODX-PPy composite and used as a biomedical device rejuvenating damaged nerves. a) Simple route showing the fabrication of the OCL-ODX-PPy composite, combining the features of each polymer. The black lines depict PPy, photopolymerised into and on the surface of OCL-ODX SMP. b) A diagram depicting the OCL-ODX-PPy composite wrapped around a damaged nerve allowing the electrical stimulation of cells (e.g. Schwann cells) to enhance the production of nerve growth factor and thereby restore normal nerve function. c) Above the T_{trans} of OCL-ODX SMP, the SME process occurs and therefore unwraps from the nerve.

The OCL-ODX-PPy composite proves to be an interesting biomedical application that could restore normal nerve functions. This is plausible due to OCL-ODX SMPs tissue compatibility and its reasonably low T_{trans} . Additionally, the OCL-ODX SMP is biodegradable under physiological conditions, thus, the composite would not necessarily require surgical removal after the repair of the damaged nerves as most of the composite would degrade, leaving behind a small amount of PPy which is biocompatible. Furthermore, this concept can be useful within the electronics industry acting as electroactive and thermo-responsive components (e.g. wires or coatings). The potential application for shape-memory materials appear vast, their attractive features seem to promise technological innovation. With further research and investigation, their benefits are increasingly realised.

2 Experimental

2.1 Synthesis of SMPs

2.1.1 TSMPI synthesis

N,N-dimethylacetamide (DMAc) purchased from Alfa Aesar and used as received. 4,4'-(4,4'-isopropylidenediphenoxy) bis (phthalic anhydride) (BPADA) >98 % and 1,3-bis (3-aminophenoxy) benzene (BAB) >96 % purchased from TCI and used as received.

4.55 mmol BAB was mixed into a 3-necked flask with 20 mL DMAc and stirred under dry nitrogen for 20 min. 5 mmol BPADA was added in batches within 1 h into the 3-necked flask at room temperature, with intense stirring under dry nitrogen for 22 h to form viscous poly(amic) acid (PAA). The flask was then transferred into a vacuum drying chamber at room temperature for 3 h to remove any air bubbles. An air-bubble level measurement ensured a glass substrate was horizontal on a hot plate. The PAA was then slowly transferred onto the glass substrate via micropipette, 500 μL gave an average film thickness of 112 μm and average mass of 73 mg. The film was not fully homogenous, and the thickness was determined using a micrometre screw gauge, finding the average after taking 3 different point measurements on the film. The glass substrate with the transferred PAA then underwent a step-wise imidization curing process at 80 °C/2 h, 110 °C/2 h, 160 °C/2 h, 190 °C/2 h and 230 °C/1 h. The TSMPI film was detached from the glass substrate by submerging in boiling deionized water for 1 h and carefully removed from the glass.

2.1.2 OCL-ODX SMP synthesis

62 % hydrobromic acid (HBr) was purchased and used as received from Honeywell (SLS). 2-(2-methoxyethoxy) acetic acid was purchased and used as received from Fluorochem. >99.5 % ethylene glycol (EG) was purchased and used as received from TCI. 98 % dibutyltin oxide (DBTO) was purchased and used as received from Alfa Aesar. 95 % n-hexane/hexane was purchased and used as received from Fischer Chemical. 99.8 % 1,2-dichloroethane, sodium bicarbonate, OCL M_n 2000 g mol^{-1} , and 2,2(4),4-trimethylhexanediisocyanate (TMDI) was purchased and used as received from Sigma-Aldrich.

Step 1: Synthesis of 1,4-dioxane-2-one (*p*DO)

In a 500 mL flask with dropping funnel and reflux condenser, 22.64 mL (0.3 mol) 62 % HBr was added to 26.8 g (0.2 mol) of 2-(2-methoxyethoxy) acetic acid while the reaction mixture was held at 0 °C. Afterwards, the mixture was stirred at room temperature for 3 h, heated to 150 °C within 2 h, and refluxed at this temperature for an additional 3 h. After cooling to room temperature, sodium bicarbonate was added until the reaction mixture's pH was 3. The crude product was purified by subsequent distillation (bp 76-81 °C) under vacuum. Characterisation was in line with the literature H. Grablowitz and A. Lendlein, *J. Mater. Chem*, **2007**, *17*, 4050–4056.

Step 2: Synthesis of α , ω -dihydroxyoligo(*p*-dioxanone) (ODX)

A general procedure is described for the polymerisation of *p*DO with DBTO as catalyst and EG as initiator. The monomer was polymerised in bulk to oligomeric products via ring-opening polymerisation. A mixture of 5 g (0.049 mol) *p*DO with 30.5 mg (0.25 % mol) DBTO was heated to 110 °C until the catalyst completely dissolves. After adding 0.124 g (2 mmol) EG the reaction was stirred for 3 h. Purification consisted of dissolving the crude product in 1,2-dichloroethane and precipitating in hexane and drying for 3 h under vacuum at room temperature.

Step 3: Synthesis of the co-polymer (OCL-ODX)

OCL with an M_n of 2000 g mol^{-1} was chosen as the precursor for the switching segments having a lower T_m than ODX. 67 % by weight of ODX was chosen as the hard segment to provide the physical cross-links. 0.6 mmol of OCL and 0.44 mmol ODX was dissolved in 1,2-dichloroethane and heated to 80°C. An equimolar amount of TMDI was added. The synthesis was carried out under exclusion of water, and solvents and monomers were dried by standard techniques. The crude product was precipitated in hexane.

2.2 Modification of SMPs

2.2.1 TSMPI-PPy

An Eppendorf contained an ink stock of 1 mL 5:95 volume ratio pyrrole (50 μ L, 0.7 mmol) and ethanol (950 μ L). 30 mg (~ 10 % mol of pyrrole) of photoinitiator (Darocur TPO) was dissolved and the ink was incubated in a fridge overnight, to limit the exposure to light the Eppendorf was covered with aluminium foil. 10 μ L of the ink was placed onto a TSMPI film (film thickness 30 to 60 μ m) before carrying out multiphoton fabrication using the Photonic Professional GT Nanoscribe. Using an x63 lens and index matching fluid (underneath a glass cover slip), various structures (e.g. 500 μ m x 100 μ m x 3 μ m [7 z-axis passes] stitched long bars) were fabricated into/on the TSMPI film with writing parameters of 80 % laser power at 10,000 μ m/s speeds. The composites were detached from the glass coverslip substrate by subsequent washing with ethanol.

2.3 Analysis of TSMPI

2.3.1 Thermal properties characterisation

DSC was used to characterise the thermal properties, specifically the T_g , of TSMPI at a heating and cooling rate of $10\text{ }^\circ\text{C min}^{-1}$ using the Mettler Toledo DSC1, equipped with a Julabo FT900 Intracooler.

2.3.2 Shape-memory characterisation

The TSMPI film shape recovery was characterized using a hot plate and a glass substrate. The hot plate was set to $191\text{ }^\circ\text{C}$ ($T_g + 40\text{ }^\circ\text{C}$) and the sample was bent on the glass substrate from both sides to achieve a deformed “tent” shape. The temporary shape was set by removing the glass substrate with the sample from the hot plate and allowed to cool to room temperature. Once replaced back onto the hot plate at $191\text{ }^\circ\text{C}$ ($T_g + 40\text{ }^\circ\text{C}$), the sample recovered to its original film shape and the process was repeated an additional two times. The SMEs were recorded using a Samsung S7 edge smartphone.

2.3.3 Optical properties characterisation

The UV-Vis transmittance of the TSMPI films was executed using Agilent Technologies Cary 60 UV-Vis spectrometer from 250 to 800 nm at a resolution of 1 nm. The optical properties of the TSMPI film were taken before and after SME cycles and three tests were conducted for each TSMPI film at a UV-Vis scan rate of 600 nm min^{-1} and exhibited consistent results.

2.3.4 Molecular weight and structural characterisation

The transmittance FTIR spectra of BAB, BPADA, PAA and TSMPI samples were registered on Agilent Technologies Cary 630 FTIR from 500 to 4000 cm^{-1} , at a resolution of 4 cm^{-1} . Lint free tissue with methanol, purchased and used as received from Sigma-Aldrich, was used to clean the crystal lens before each sample test.

Fitted with a 5 mm ^1H -X broadband observe (BBO, 109Ag-19F) RT probe, the 1D ^1H and 1D ^{13}C NMR spectra of 0.05 mmol BAB and BPADA dissolved in 650 μL deuterated dimethyl sulfoxide (DMSO- d_6), and 650 μL PAA were carried out on the solution state NMR Bruker AVANCE III 400. The instrument was controlled using TopSpin 3.5pl7. A TSMPI film prepared for solid-state 1D ^{13}C NMR had a mass of 73 mg and an average thickness of 108 μm . The film was broken into smaller fragments \sim 0.5 to 2 mm in length and were carefully loaded into the rotor. The solid-state 1D ^{13}C NMR spectra were carried out on the Bruker AVANCE III HD 400 WB, using double res mode, a 3.2 mm HFX Y probe, ^{13}C on the X channel and MAS 12.5 kHz. The instrument was controlled using TopSpin 3.5pl7.

The number average molecular weight (M_n) and the weight average molecular weight (M_w) was determined by GPC using a Shimadzu Prominence HPLC system, equipped with a RID-20A refractive index detector. The instrument was also equipped with a Wyatt Technologies mini-DAWN Treos MALS detector and a Viscostar II viscometer. 1 mg TSMPI samples were dissolved with 1 mL dimethylformamide (DMF) in glass vials and left overnight to ensure the TSMPI samples were fully dissolved in DMF. The solution was then filtered into GPC silicone septum glass vials, using Fischer 0.22 μm pore polytetrafluoroethylene (PTFE) filters. The system was run at 40 $^\circ\text{C}$ with a flow rate of 1 mL min^{-1} using a Phenomenex Phenogel Linear (2) column with DMF as the eluent. The M_n and M_w values were obtained by utilising a calibration curve using Agilent Technologies polystyrene (PS) standards.

The XRD of TSMPI films were carried out on SmartLab Studio Rigaku under Cu $\text{K}\alpha_1$ radiation. A 1D silicon detection strip was used and the accelerating voltage and emission current were at 45 kV and 200 mA, respectively.

2.4 Analysis of TSMPI-PPy

2.4.1 Structural characterisation

The transmittance FTIR spectra were measured on Agilent Technologies Cary 630 FTIR from 500 to 4000 cm^{-1} , at a resolution of 4 cm^{-1} . Lint free tissue with methanol, purchased and used as received from Sigma-Aldrich, was used to clean the crystal lens before each sample test.

2.4.2 Electrical conductivity characterisation

A modified Micromanipulator miBot from Imina Technologies was used to observe the difference in resistance (Ω) of the TSMPI-PPy composite compared to TSMPI film. The measured region of the black structures had a 14 to 18 μm gap between the micro-electric probes, with the cameras field of view at 100 μm .

2.5 Analysis of OCL-ODX SMP

2.5.1 Thermal properties characterisation

DSC was used to characterise the thermal properties, specifically the T_m , of OCL, ODX and the subsequent OCL-ODX at a heating and cooling rate of $2\text{ }^\circ\text{C min}^{-1}$ using the Mettler Toledo DSC1, equipped with a Julabo FT900 Intracooler.

2.5.2 Structural characterisation

The transmittance FTIR spectra of OCL, ODX and OCL-ODX samples were registered on Agilent Technologies Cary 630 FTIR from 500 to 4000 cm^{-1} , at a resolution of 4 cm^{-1} . Lint free tissue with methanol, purchased and used as received from Sigma-Aldrich, was used to clean the crystal lens before each sample test.

The XRD of OCL-ODX samples were carried out on SmartLab Studio Rigaku under $\text{Cu K}\alpha_1$ radiation. A 1D silicon detection strip was used and the accelerating voltage and emission current were at 45 kV and 200 mA , respectively.

3 Discussion of results

3.1 Abstract

The synthesis of TSMPI and OCL-ODX SMP reported in literature was reproduced and characterised. Here, the modification of TSMPI by photopolymerising PPy into/on the SMP using a Photonic Nanoscribe is reported for the first time. The structural and electrical properties of the TSMPI-PPy composite was investigated to elucidate how these materials can be utilised for the applications proposed in **Figure 10** and **11**.

3.2 Introduction

Previously discussed, as the understanding of SMPs continually develops among the scientific and engineering community, the design of new and potentially innovative SMPs will be more apparent. **Figure 6** demonstrates the feasibility of combining SMPs with electroconductive substances (e.g. Ag NWs), the results of which allow an LED to be lit. In addition, these composites retained an electrical conductivity threshold of 12 % elongation. Comparing the potential deformation range of SMPs, strain up to more than 200 % are normal for most materials, 12 % is considerably low. However, for research purposes, the Ag NW-SMPU composite provides insightful information to inspire the design of new SMP composites. In this thesis, novel and innovative applications are proposed and the production of two unprecedented SMP composites, TSMPI-PPy and OCL-ODX-PPy is reported. Furthermore, their feasibility towards the applications are investigated, in accordance with technology readiness levels (TRLs) portrayed in **Table 3**.²⁹

TRL scale	Explanation
1	Idea: Unproven concept
2	Basic research: Principles postulated, but no experimental proof
3	Technology formulation: Concept and application formulated
4	Applied research: Laboratory tests completed and proof of concept
5	Small scale prototype: Initial prototype for laboratory environment
6	Large scale prototype: Tested at the intended environment
7	Prototype successful: Results from TRL 6 close to or meet expected outcome
8	Demonstration system: Operation at intended environment pre-commercial scale
9	Optimising commercial system: Resolving manufacturing issues
10	Full commercial application: Technology available

Table 3: A table listing the TRLs. Green shading represents the preliminary research. Blue is the research conducted to prove feasibility (e.g. academic research). Yellow is the development of the technology (e.g. optimisation). Orange is the demonstration of the technology at intended environment. Red is the commissioning of the technology.

Thus, by referring to **Table 3** with the aim to reach TRL 3/4, provides insight into the research and development journey and demonstrates the significance of the experiments conducted. It was hypothesised that the introduction of a CP (such as PPy) on and near the surface of the chosen SMPs, would enable the generation of flexible CP materials. This is supported by previous work on electroconductive polymeric composite materials based on PPy by Ilicheva et al.³⁰ Oxidative polymerisation of pyrrole was carried out in aqueous solution in the presence of a PE film hydrophilized with grafted polyacrylic acid, with repeated polymerisation of the pyrrole to increase PPy content in the composite.³⁰ The electrical conductivity and physical and mechanical properties of the composites were investigated. It was reported that composites with 6.8 % PPy content possessed a conductivity of 1.62 ± 0.09 S/cm via four-point probe method.³⁰ Furthermore, it was established that increasing the pyrrole concentration in the reaction mixture by threefold increased the conductivity from 1.62 S/cm to 1.66 S/cm, whereas, repolymerisation of the pyrrole a second time increased the conductivity from 1.66 S/cm to 5.43 S/cm.³⁰ Moreover, the stress-strain curves obtained from the composites were the same as the PE-polyacrylic acid matrix. The mechanical tests did not show any signs of PPy peeling even at the composites break.³⁰ The PPy in the bulk of the PE-polyacrylic acid matrix formed a spatially continuous phase of rigid-chain polymer in the flexible substrate, “inheriting” its mechanical properties.³⁰ However, the formation of a separate phase of PPy in the matrix-substrate influences the mobility of the polyacrylic acid chains by lowering its T_g , confirmed via thermal analysis.³⁰ Ultimately, when the electrical conductivity was measured, it had stopped at 11 ± 1 % elongation.³⁰ It was stated that films of CPs are highly fragile and have extremely low elasticity, and that mechanical properties are a decisive criterion for identifying potential areas of composite material applications.³⁰ The report concluded that the new materials exhibited electrical conductivity with good mechanical properties, due to the presence of a PE film tightly bonded with PPy through polyacrylic acid.³⁰ However, an electrical conductivity working threshold of 11 ± 1 % is still low and comparable to other examples discussed thus far. Therefore, by utilising the method of 2PP using a Photonic Nanoscribe, and SMPs with their unique SMEs to “carry” PPy, will yield interesting information on the polymerisation processes into/on the matrix-substrate and the SMP composites properties i.e. how it may affect electrical conductivity and the shape recovery process. Potential results could be improved electrical conductivity, and/or inspiring future investigations to contribute to the understanding of these unique materials and their potential applications.

3.3 TSMPI

3.3.1 Thermal properties

The thermal properties of the synthesised TSMPI are analysed by DSC, as shown in **Figure 12**. It is observed that the measured T_g was ~ 20 °C lower than the literature value TSMPI.

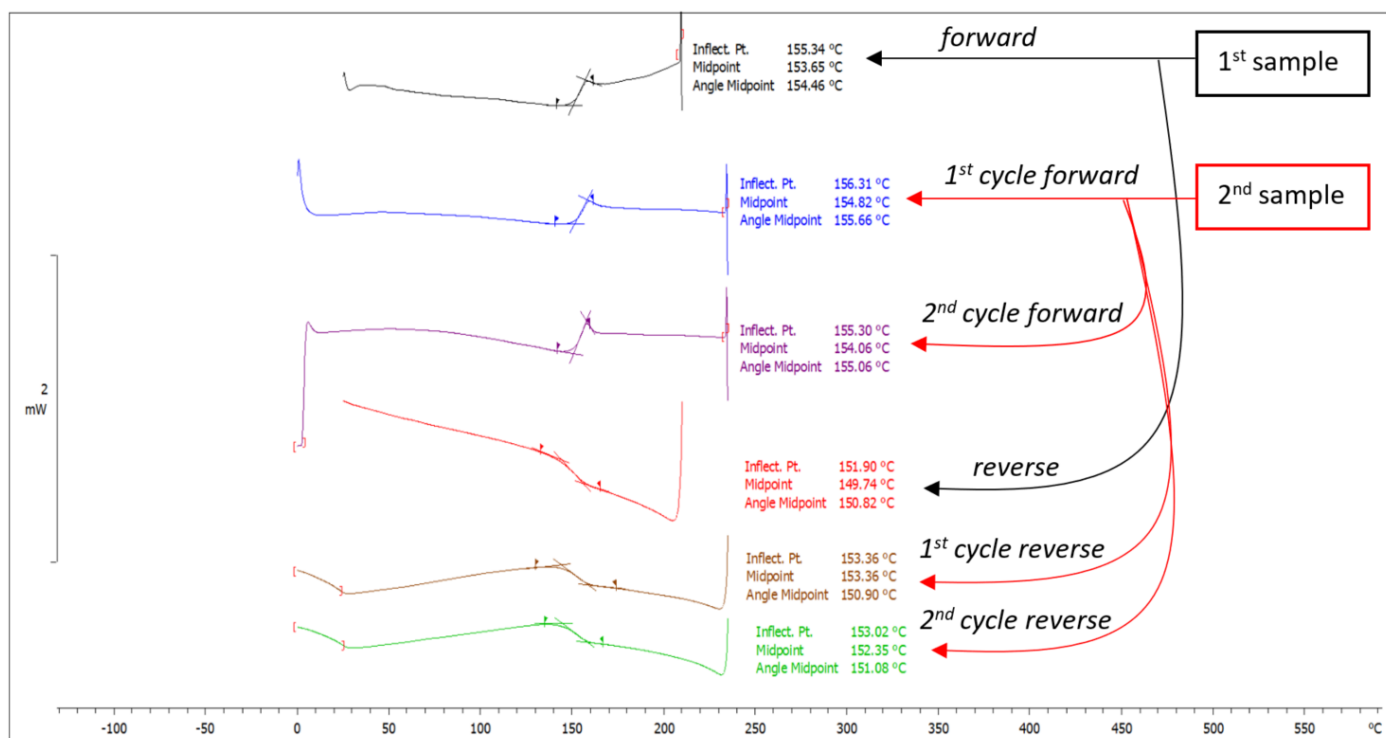


Figure 12. DSC results of the synthesised TSMPI. 1st sample consisted a range of 25 to 210 °C and heating/cooling rate of 10 °C min⁻¹. 2nd sample consisted a range of 0 to 235 °C and heating/cooling rate of 10 °C min⁻¹ with an additional heat/cool cycle.

By taking the average of the integrated peaks midpoint, the T_g of the synthesised TSMPI is 153 °C, 18 °C lower than that of the literature value TSMPI. This can be attributed to slightly different experimental conditions (e.g. different quantities of BAB and BPADA added in the reaction mixture), which ultimately affects polymer chain lengths within the polymer matrix. Shorter polymer chain lengths can lead to less entanglement of the network chains in the polymer matrix, reducing the possible intermolecular forces (e.g. hydrogen bond and Van der Waals' interactions) between the polymer chains, resulting in a lower T_g .

Normally, when conducting the characterisation of a polymers thermal properties TGA is carried out before DSC or DMA, because the information gathered from TGA could determine the working range for DSC or DMA. This is important when working with unknown polymer samples i.e. the thermal properties have yet to be documented. However, in the case for TSMPI, it has been reported thermally stable up to 485 °C (<5 % weight loss) with major decomposition beginning at 540 °C.²⁴ Therefore, conducting a DSC on the synthesised TSMPI was sensible and time efficient, because the thermostability and T_g of a similar polymer has been previously reported, thus, a working range can be fabricated. Hereby, through obtaining the specific T_g value, which is an essential property of the shape recovery process of the SMP, the SMEs to characterise the polymers shape-memory can be tested.

3.3.2 Shape-memory

A deployable heat and cool stage test, with deformation (e.g. bending) above its T_g , was conducted to observe the synthesised TSMPIs SME. **Figure 13** depicts the timeline of the shape recovery process of the synthesised TSMPI film from its deformed “tent” shape. Three cycles were conducted showing consistent results recovering its original shape within one minute, the average shape recovery time was ~ 40 s, the first cycle is shown for clarity.

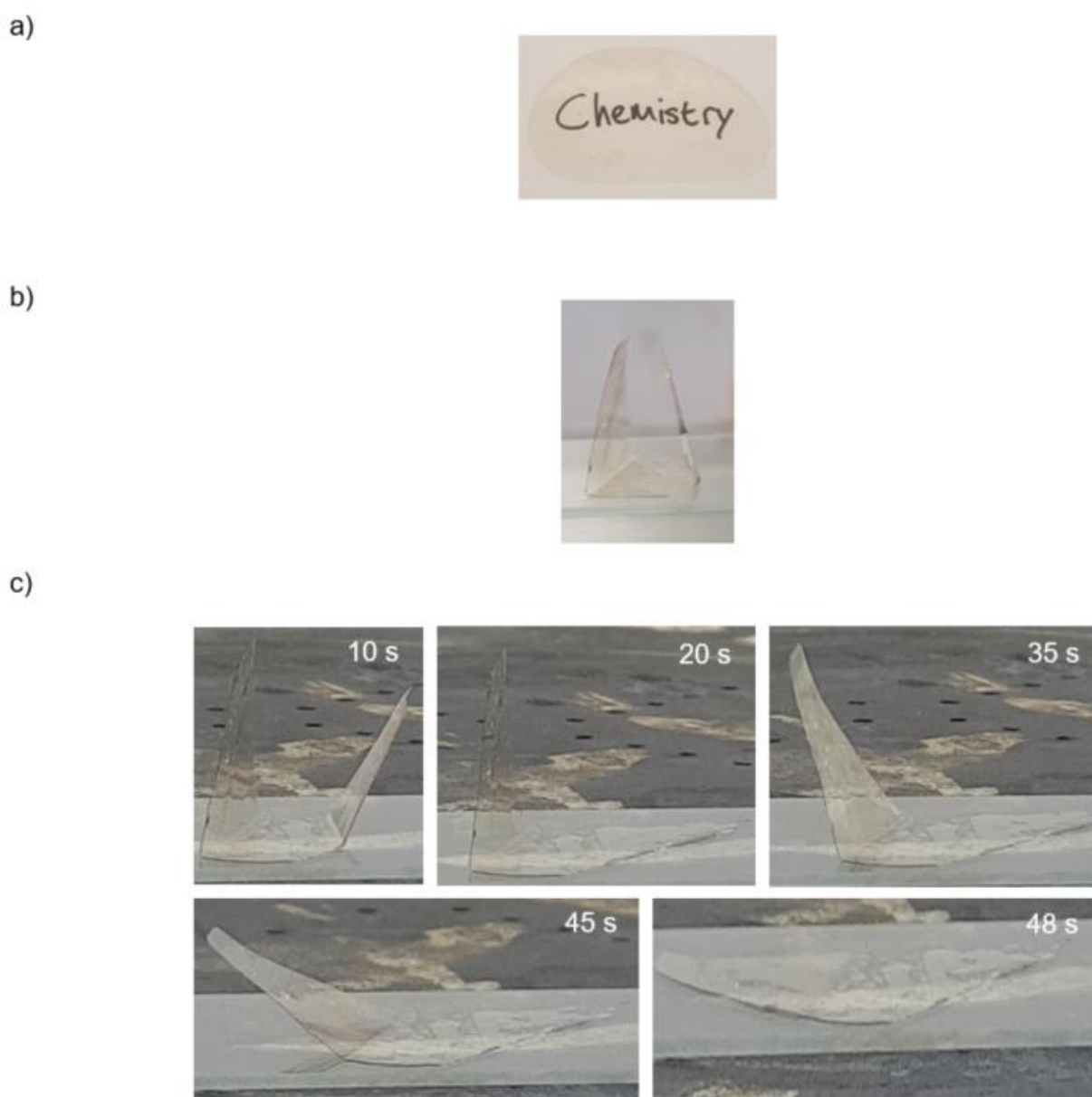


Figure 13. Timeline of the shape recovery process of synthesised TSMPI at 40 °C above its T_g . a) The TSMPI film in its original shape. b) TSMPI film in the deformed “tent” shape on a glass substrate, achieved by heating at 193 °C and bent into its deformed shape then cooled at room temperature. c) Timeline of the TSMPIs shape recovery process.

Various samples of the synthesised TSMPI were tested with the SMEs recorded, as shown in supplementary information (SI). Different deformed shapes were achieved and with varying times of shape recovery, which can be attributed to the degree of TSMPI film in contact with the heat source. More contact increases the heat transfer due to the larger surface of TSMPI available, resulting in a faster shape recovery process.

From **Figure 13c)** it is apparent that the synthesised TSMPI possesses SMEs, therefore, it can be distinguished as an SMP.

3.3.3 Optical properties

The optical transparency is a necessary property to successfully conduct 2PP of PPy into/on the surface of TSMPI using a Photonic Nanoscribe. Therefore, the UV-Vis transmittance was conducted, and the results are as shown in **Figure 14**.

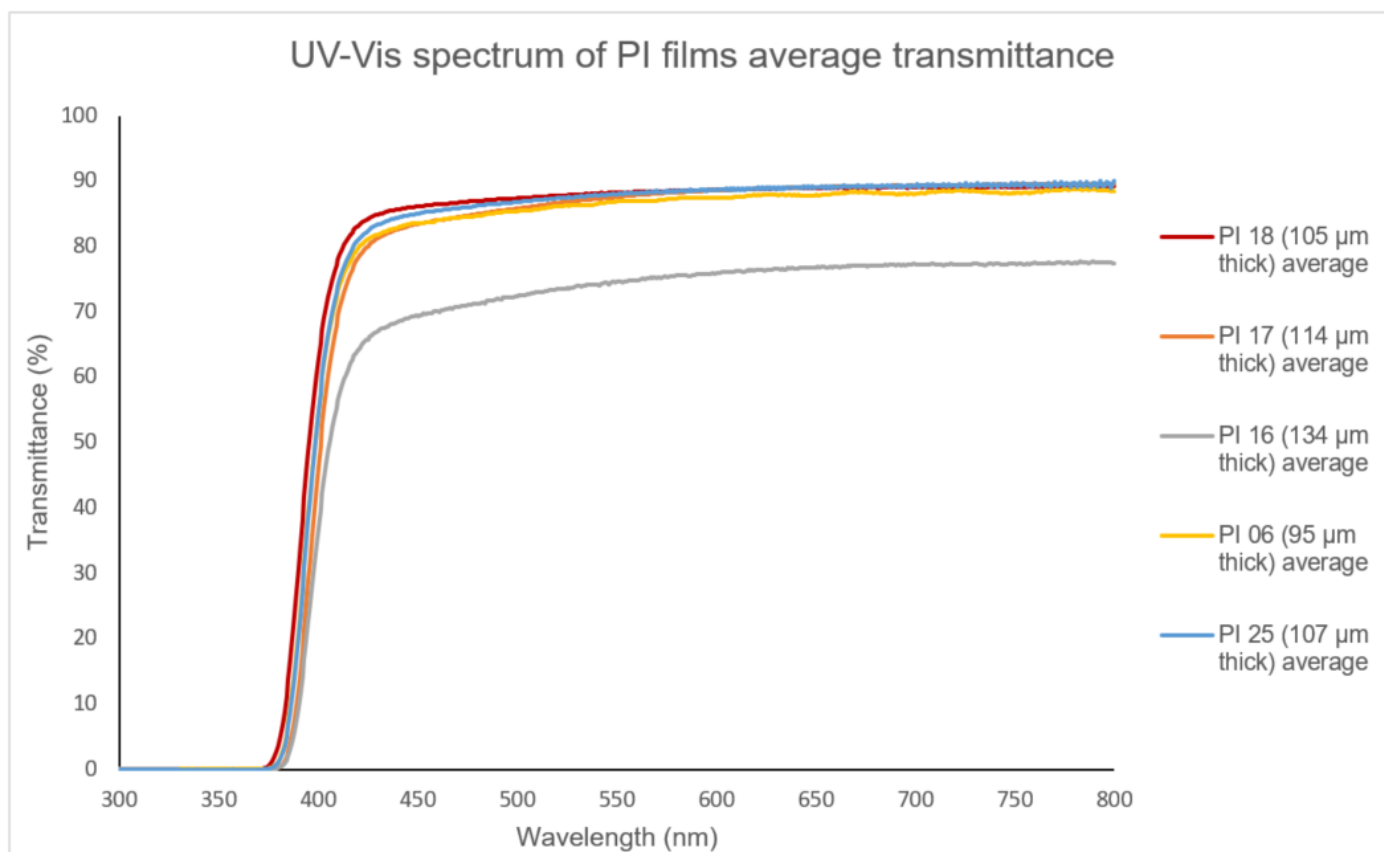


Figure 14. UV-Vis transmittance spectrum of synthesised TSMPI films. Consistent values were obtained for all samples. Furthermore, each sample follows the same character i.e. transmittance decreases sharply around 420 nm.

It can be seen from **Figure 13** that the synthesised TSMPI films are almost colourless, suggesting very good optical transparency, which can now be ascertained with the support of the UV-Vis transmittance results in **Figure 14**. The maximum transmittance observed is ~ 88 % at 800 nm which is consistent for samples with a thickness between 95 to 114 μm. However, sample “PI 16” with the thickness of 134 μm possessed a maximum transmittance of ~ 77 % at 800 nm, suggesting the thickness of the film can affect the optical transparency. Hereby, the results depicted in **Figure 14** detail that the synthesised TSMPI films with a thickness range of 95 to 134 μm, possesses a >64 % transmittance between 420 to 800 nm wavelength of light.

In addition to the synthesised TSMPI films UV-Vis transmittance results, the UV-Vis transmittance of the samples after shape recovery were also taken, the results are shown in **Figure 15**. The UV-Vis transmittance results of “PI 16” is shown for clarity.

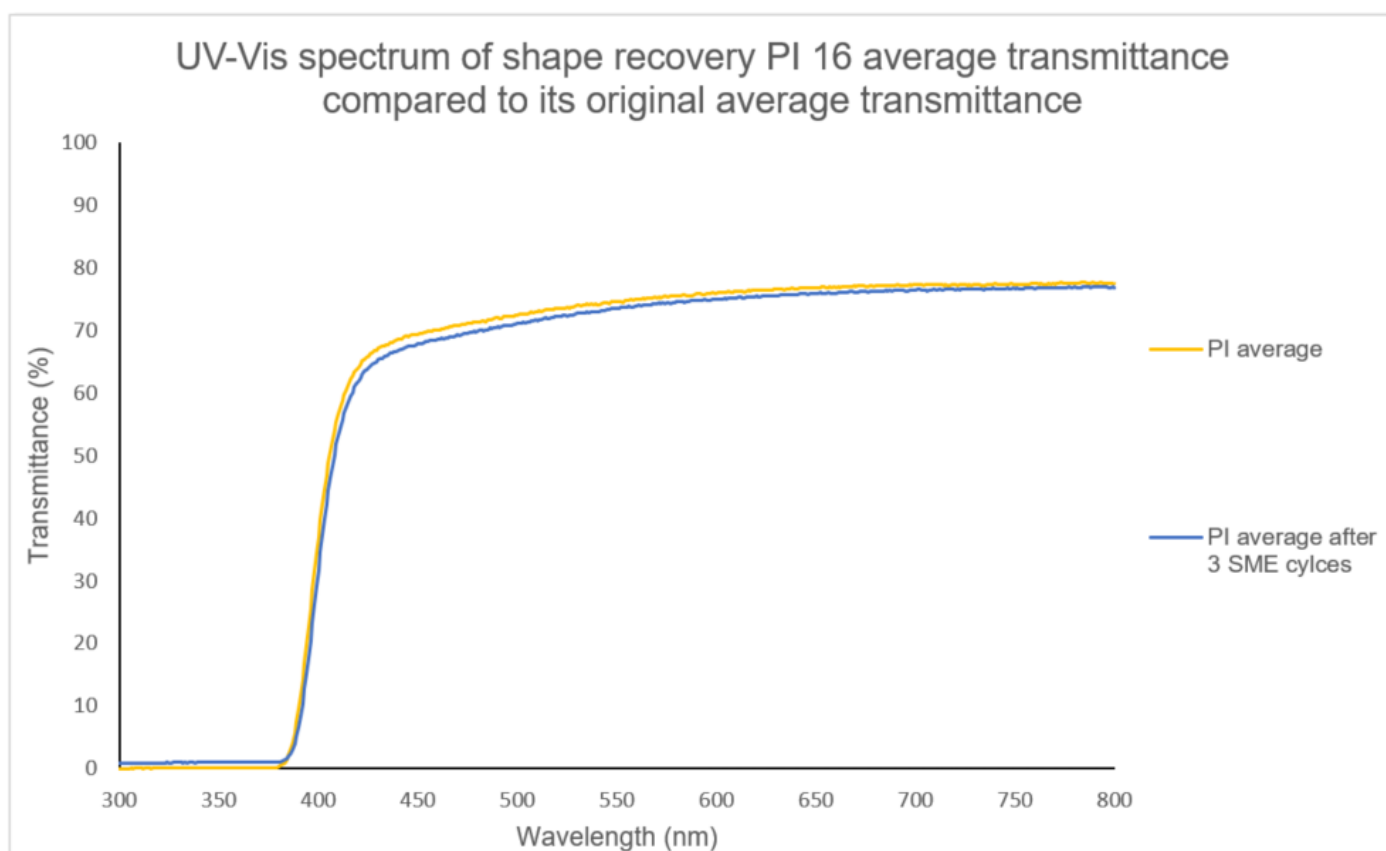


Figure 15. UV-Vis transmittance spectrum of “PI 16” before and after shape recovery cycles. Consistent results were obtained for each test. Yellow line is the UV-Vis transmittance before the SME cycle tests were conducted, and the blue line is the UV-Vis transmittance after three SME cycles and the TSMPI film recovered.

By comparing the before and after shape recovery UV-Vis transmittance of the synthesised TSMPI film, there is almost no discernible difference in the transmittance values. The UV-Vis transmittance of the shape recovery TSMPI film possessed 99 % of its original average maximum transmittance at 800 nm. Therefore, the synthesised TSMPI film maintains its very good optical transparency after multiple SME cycles.

It has been shown that the colouration of aromatic PIs is mainly caused by intra/intermolecular CTC formation between the alternating electron-acceptor (dianhydride) and electron-donor (diamine) groups, with higher CTC interactions resulting in deeper colours.²⁴ However, in the case for TSMPI, the high transparency originates from strongly suppressed CTC interactions due to its unique structure, a 3D molecular structure of TSMPIs structural unit is shown in **Figure 16**.

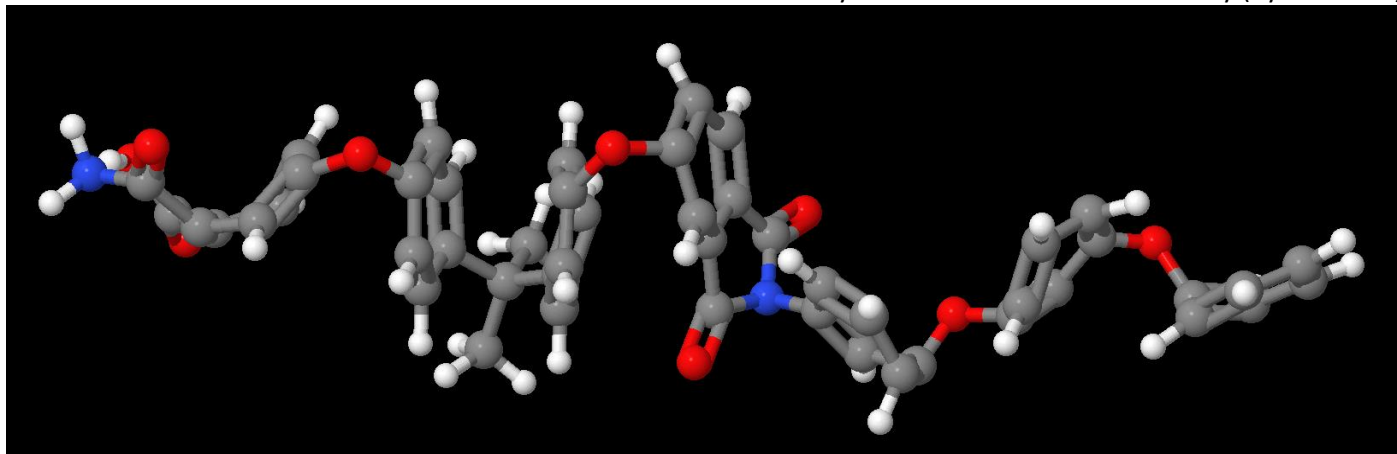
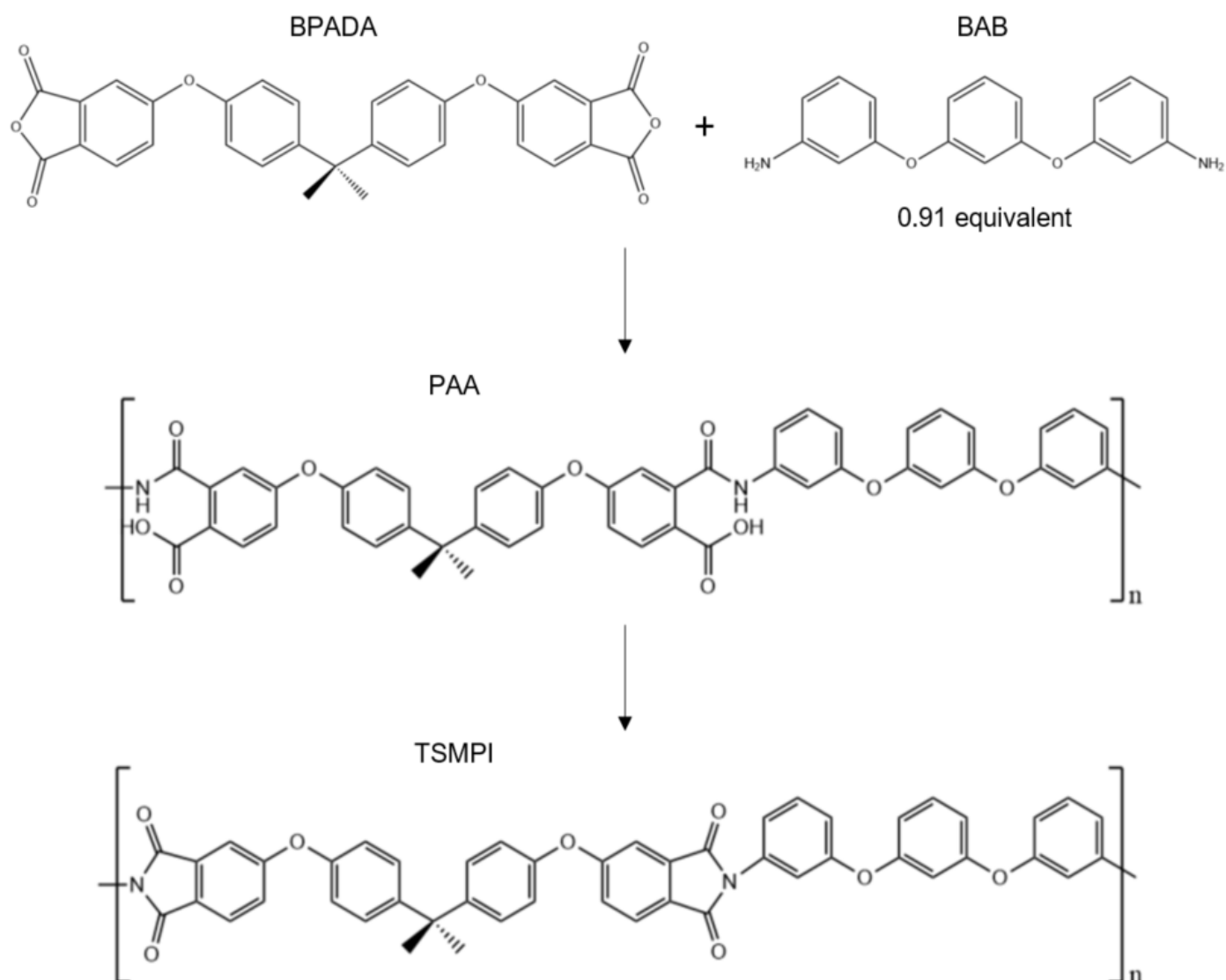


Figure 16. 3D molecular structure of a structural unit comprising TSMPI. Grey, white, red and blue are C, H, O and N atoms respectively.

Seen in **Figure 16**, the introduction of the large pendant isopropyl groups in the dianhydride, increases the free volume of each molecule and prevents compact stacking of molecular chains, thus, decreasing the intermolecular CTC interactions.²⁴ The isopropyl groups and flexible ether linkages in the dianhydride can limit the charge flow along the main chain, which will suppress intramolecular CTC interactions.²⁴ The molecular structure is folded when *meta*-substituted, and the intermolecular CTC interactions decrease. Both the *meta*-substituted structures and flexible ether linkages in the diamine can decrease charge flow, which will reduce the intramolecular CTC interactions.²⁴ Hereby, the formation of both intra/intermolecular CTC interactions are obstructed due to TSMPIs unique structure being derived from BAB and BPADA, as a result, very good optical transparency is observed.

3.3.4 Molecular weight and structural information

The reaction scheme for TSMPI via the polycondensation of PAA is shown in **Scheme 1**.



Scheme 1. Reaction scheme for TSMPI. Polycondensation reaction of TSMPI from starting reagents BAB and BPADA.

After the synthesis of TSMPI, its FTIR spectra were measured as it is a useful method to characterise functional groups present within a sample. In this case, to identify the formation of the PI from the PAA. The representative FTIR spectrum of the synthesised TSMPI is shown in **Figure 17**.

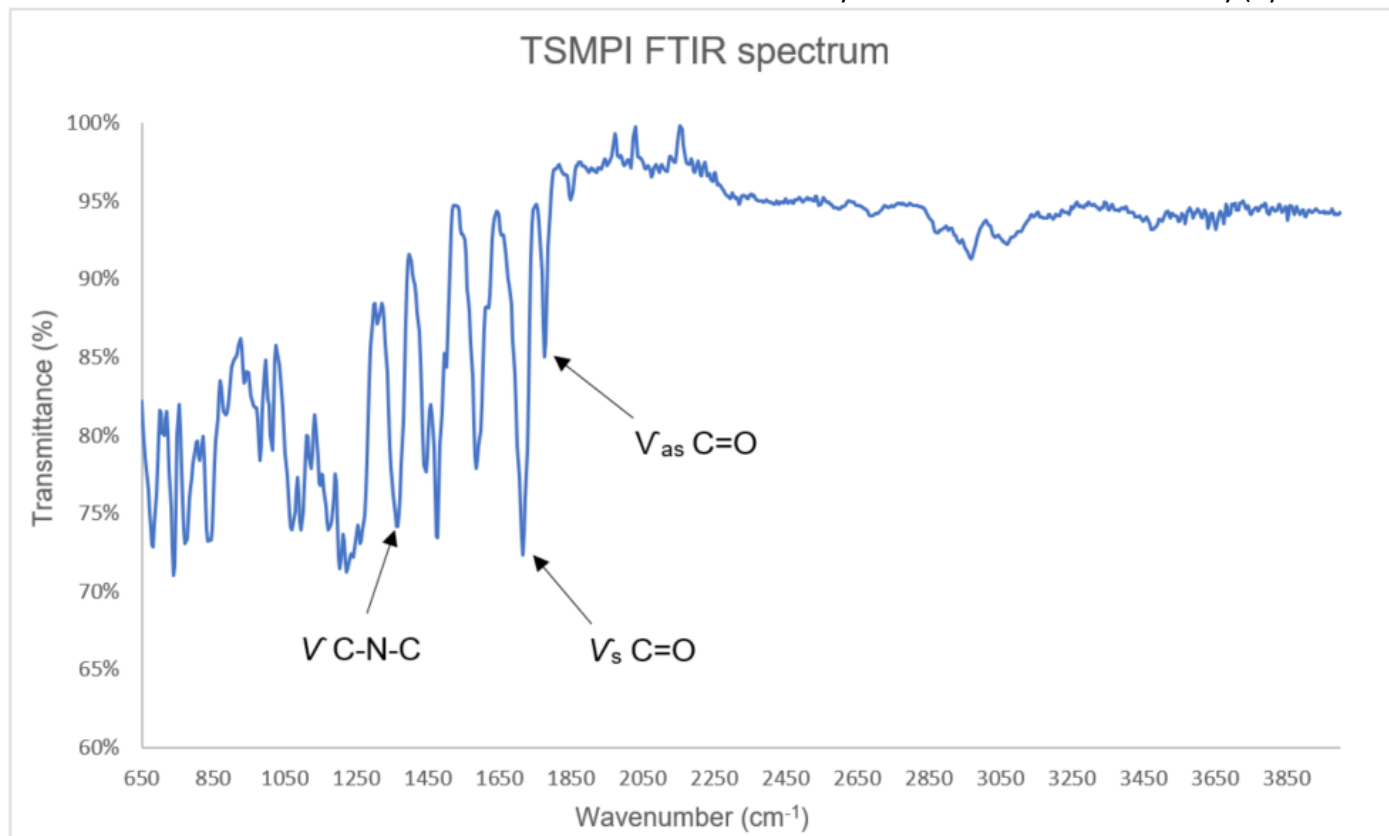


Figure 17. FTIR spectrum of the synthesised TSMPI. Peaks at 1369 cm^{-1} ($V\text{ C-N-C}$), 1715 cm^{-1} ($V_s\text{ C=O}$) and 1779 cm^{-1} ($V_{as}\text{ C=O}$) confirm the formation of the imide functional group.

The results from the FTIR spectrum in **Figure 17** demonstrate that the sample is fully imidized within the detection limit of IR. This is because the presence of carbonyl isoimide peaks (1795 to 1820 cm^{-1} or 921 to 934 cm^{-1}) are absent, and the carbonyl stretching in an intermolecular imide linkage near 1670 cm^{-1} is not observed either.²⁴ In addition, the typical characteristic peaks of the PAA are no longer present. The FTIR spectra of BAB, BPADA and PAA are shown in the SI.

The 1D solid-state ^{13}C NMR was conducted to further characterise and understand the structure of the synthesised TSMPI film, primarily to support the information derived from the FTIR spectrum in **Figure 17**. The NMR spectra for TSMPI has yet to be reported and therefore, no known literature values were used for the basis of comparison. Thus, using prediction NMR spin dynamics software (from nmrd.org)³¹, the 1D ^{13}C NMR theoretical spectrum of TSMPIs structural unit is given in **Figure 18**. This spectrum was used to compare the experimental spectrum obtained from the synthesised TSMPI film.

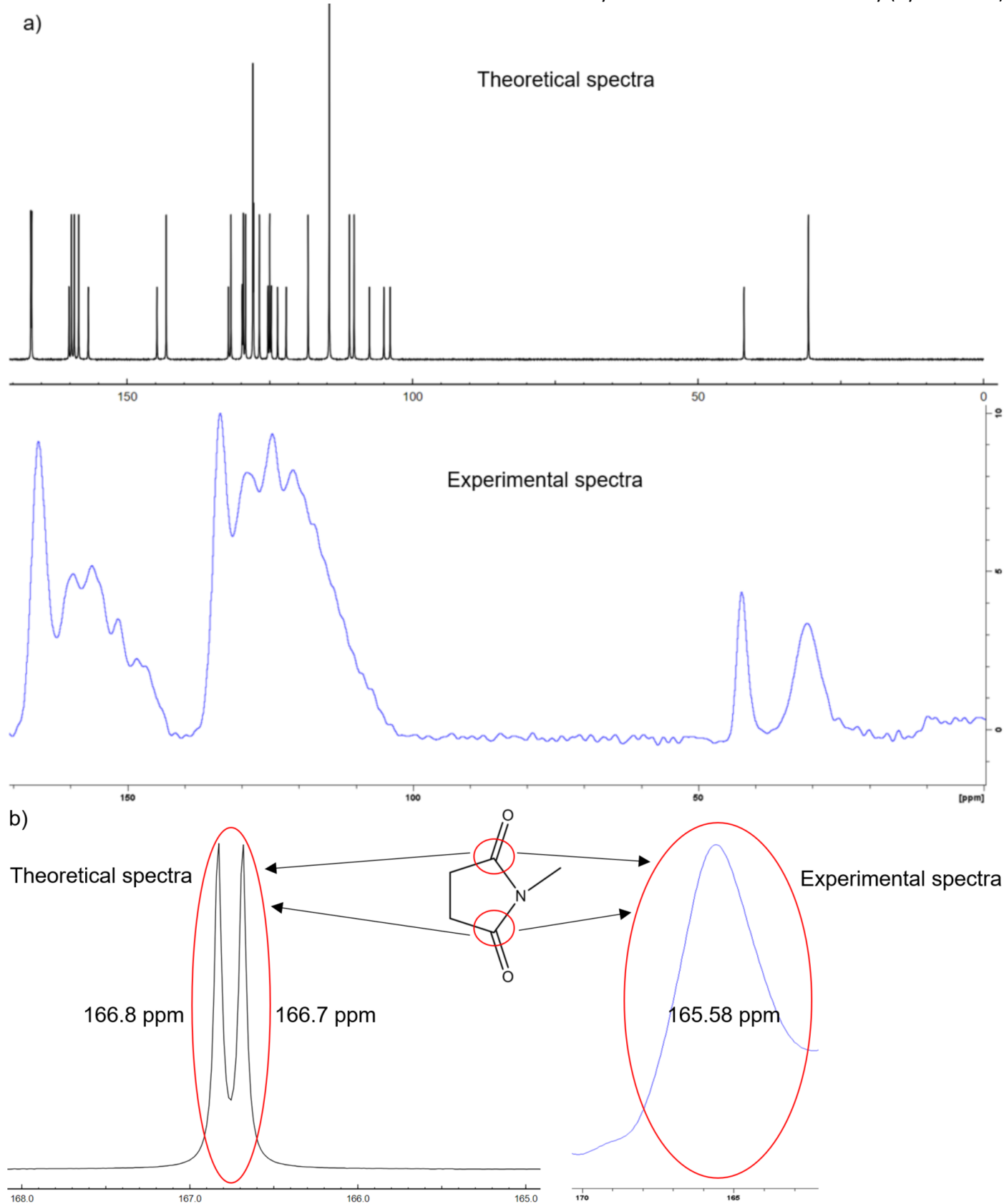


Figure 18.1 ^{13}C NMR theoretical spectrum of TSMPIs structural unit and the solid-state ^{13}C NMR experimental spectrum of the synthesised TSMPI. a) A comparison of the ^{13}C NMR spectra. b) Close inspection and comparison of the imide, specifically, the C-N-C functional group.

By comparing the spectra from **Figure 18a**), the synthesised TSMPI films solid-state 1D ^{13}C NMR spectrum possesses peaks in the same regions as the structural unit of TSMPIs 1D ^{13}C NMR spectrum. However, the experimental spectrum has broader peaks, which makes it difficult to confidently distinguish each peak when comparing it to the theoretical spectrum. The broadening of the peaks during solid-state NMR is a result of the full effects of anisotropic interactions being observed in the spectrum. Whereas, the theoretical spectrum was determined based on the structure that was uploaded and its anisotropic NMR interactions being averaged, thus, very sharp peaks are observed, and solvent peaks are absent.³¹ The solid-state ^1H NMR of the synthesised TSMPI film was not conducted, due to the broadening of the peaks, which make it more difficult to distinguish the peaks as the typical ^1H NMR range is 0 to 15 ppm. Therefore, results from a solid-state ^1H NMR spectra of large polymers, such as TSMPI, are more difficult to interpret compared to solid-state ^{13}C NMR.

Moreover, the theoretical spectrum appears to be a useful tool for initial comparison, because characteristic groups, such as sp^3 hybridised carbons $\text{CR}_2(\text{CH}_3)_2$ (R representing the rest of the polymers structural unit), are accurately represented. The peak for $(\text{CH}_3)_2$ was observed at 30.86 ppm from the experimental spectrum and at 30.6 ppm from the theoretical spectrum. The peak for $\text{CR}_2(\text{CH}_3)_2$ was observed at 42.37 ppm from the experimental spectrum and at 41.9 ppm from the theoretical spectrum. The presence of these sp^3 carbons were first observed in **Figure 17**, where the peak at 2967 cm^{-1} donates the stretching frequency of the sp^3 C-H group. Hereby, the results from ^{13}C NMR are complimented by the results from FTIR. Because the accuracy of the theoretical spectrum is relative to the experimental spectrum, it was sensible to compare the theoretically predicted C-N-C (imide functional group) peak with the experimentally obtained value. Therefore, as seen in **Figure 18b**), the theoretical and experimental values are in good agreement, at 166.8/166.7 and 165.58 ppm respectively.

Here, NMR is reported as a technique for characterising TSMPI, and the combination of FTIR and NMR provides a more in-depth analysis of the polymers structure, particularly the C-N-C region. The NMR spectra of BAB, BPADA and PAA were also conducted and shown in the SI.

The synthesised TSMPI possesses an M_n of 13572 g mol^{-1} (± 507.4), M_w of 39933 g mol^{-1} (± 1792.9) and a PDI of 2.95 (± 0.106). The M_n and M_w values were determined via GPC and by taking the average of seven synthesised TSMPI samples. In addition, the standard error for M_n , M_w and PDI were also calculated and incorporated into the graphs shown in **Figure 19**.

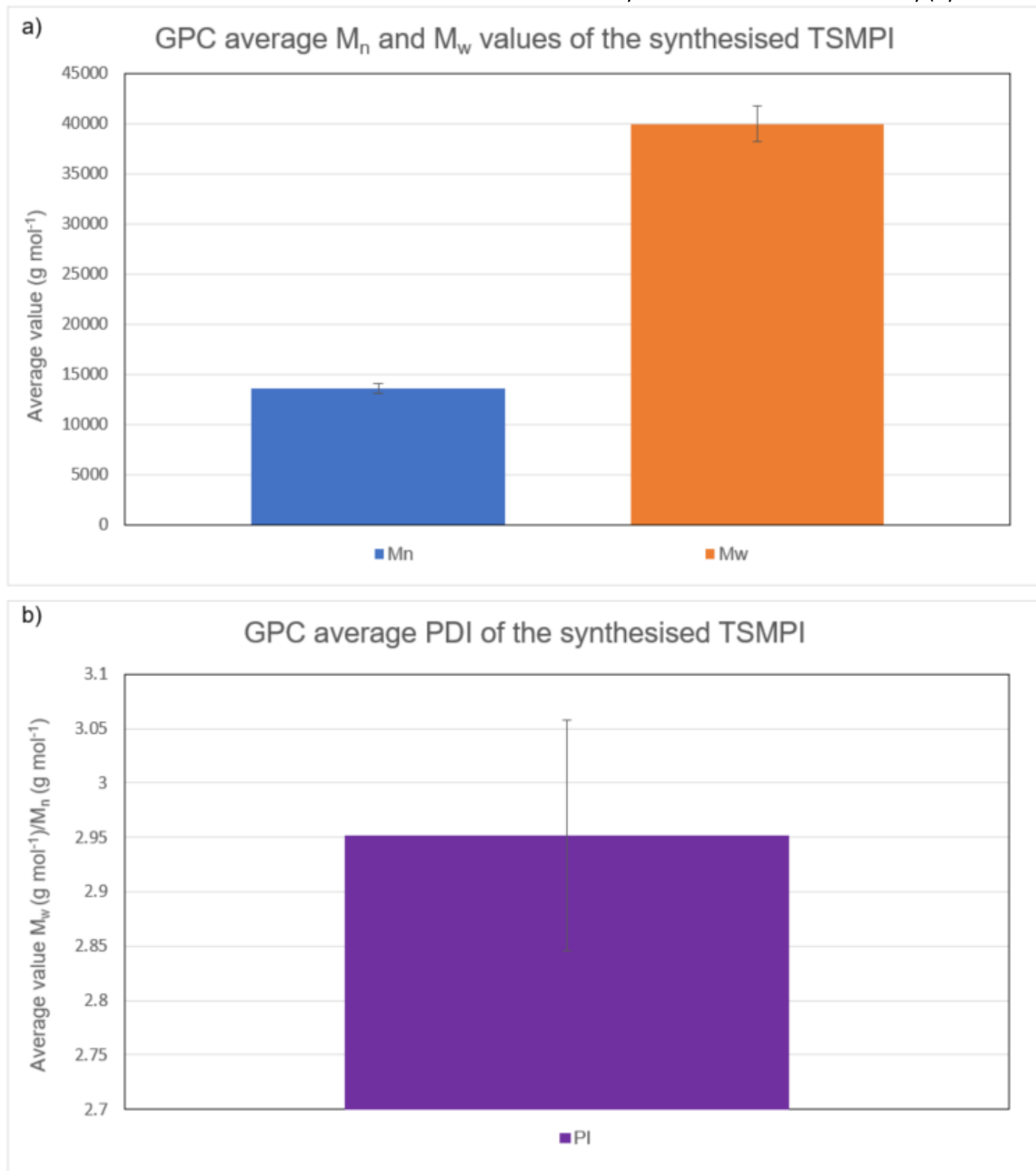


Figure 19. GPC results of the synthesised TSMPI. a) The average values of the seven synthesised TSMPI samples used for GPC, with the calculated standard error bars for M_n and M_w at 507.4 g mol^{-1} and $1792.9 \text{ g mol}^{-1}$ respectively. b) The average value M_w/M_n of the seven synthesised TSMPI samples used for GPC, with its calculated standard error bar at $0.106 M_w/M_n$.

The values used to generate **Figure 19a)** were determined by using **Table 4**. In addition, the values used to generate **Figure 19b)** were determined by using **Table 5**.

a)

Synthesised TSMPI sample	M_n	Average M_n	M_w	Average M_w
1	10848	13572	33681	39933
2	14531		34164	
3	13248		38752	
4	13773		39285	
5	14168		42441	
6	13004		43081	
7	15430		48127	

b)

TSMPI	Standard deviation	Standard error
M_n	1342.5	507.4
M_w	4743.8	1792.9

Table 4. Values used to generate Figure 19a). a) Values depicting the M_n and M_w . b) Values depicting the standard error for M_n and M_w .

a)

Synthesised TSMPI sample	M_w/M_n	Average M_w/M_n
1	3.10	2.95
2	2.35	
3	2.93	
4	2.85	
5	2.99	
6	3.31	
7	3.12	

b)

TSMPI	Standard deviation	Standard error
M_w/M_n	0.282	0.106

Table 5. Values used to generate Figure 19b). a) Values depicting the PDI. b) The value depicting the standard error for PDI.

The experimental values represented in **Table 4** and **5** were calculated using the following equations, (6), (7) and (8)

Average equation: (6)

$$(\Sigma M_n) \div 7$$

$$(\Sigma M_w) \div 7$$

$$(\Sigma M_w / M_n) \div 7$$

Standard deviation equation: (7)

$$\text{Step 1} = (M_n - \text{average}M_n)^2, \text{ Step 2} = \Sigma \text{Step 1} \div 7, \text{ Step 3} = \sqrt{\text{Step 2}}$$

$$\text{Step 1} = (M_w - \text{average}M_w)^2, \text{ Step 2} = \Sigma \text{Step 1} \div 7, \text{ Step 3} = \sqrt{\text{Step 2}}$$

$$\text{Step 1} = (M_w / M_n - \text{average}M_w / M_n)^2, \text{ Step 2} = \Sigma \text{Step 1} \div 7, \text{ Step 3} = \sqrt{\text{Step 2}}$$

Standard error equation: (8)

$$\text{Standard deviation } M_n \div \sqrt{7}$$

$$\text{Standard deviation } M_w \div \sqrt{7}$$

$$\text{Standard deviation } M_w / M_n \div \sqrt{7}$$

where *Step 1* and *Step 2* depicts that the answers obtained from the corresponding step are used.

The experimental values represented in **Table 4** and **5**, which was subsequently used to generate **Figure 19**, was possible due to the PS standards used to fabricate the working calibration curve, as shown in the SI.

Comparing the observed values in **Figure 19** to the literature values of TSMPI, the literature M_n was at 21700 g mol^{-1} , M_w was at 42500 g mol^{-1} and with a PDI of 1.96. Thus, the synthesised TSMPIs M_n and M_w values were lower and possessed a greater PDI. However, the literature TSMPI had an average film thickness of $120 \mu\text{m}$ compared to the synthesised TSMPI films average thickness of $112 \mu\text{m}$. With close examination of the experimental M_n and M_w values in **Table 4**, it was observed that the synthesised TSMPI sample 1 possessed the lowest M_w value, and an M_n value noticeably lower compared to the next lowest sample, at $\sim 2200 \text{ g mol}^{-1}$ lower. This sample refers to "PI 06", first observed in **Figure 14** with an average film thickness of $95 \mu\text{m}$. This TSMPI film was synthesised slightly different to all other documented synthesised TSMPI films. $410 \mu\text{L}$ of PAA was administered slowly via micropipette onto the glass substrate, whereas, the subsequent TSMPI films were synthesised using $500 \mu\text{L}$. This was so because thin films ($<100 \mu\text{m}$), were more difficult to process and successfully detach large films ($>70 \text{ mg}$), from the glass substrate after the thermal curing process. Because the synthesised TSMPI sample 1 for GPC possessed less PAA for its synthesis, explains why the lowest M_w and noticeably low M_n values were observed. Physically less polymer material was available during the synthesis of TSMPI from PAA, which affects the potential M_n and M_w values. If the synthesised TSMPI sample 1 values were ignored, the average M_n , M_w and PDI values would be 14026 g mol^{-1} , 40975 g mol^{-1} and 2.92 respectively, which are more like the literature values.

Hereby, the volume of PAA used and the processing conditions for the film (e.g. administration of PAA onto the glass substrate) affects the M_n , M_w , film thickness and optical transparency. It is well-known that the intermolecular force interactions between polymer chains will become weaker for samples with a lower M_n , thus, colours of the PI films will become lighter with the decrease of M_n .²⁴ This is supported by the synthesised TSMPI sample 7 possessing the highest M_n and M_w values, which also refers to "PI 16" that is observed in **Figure 14** with an average thickness of 134 μm . This TSMPI film possessed the lowest % transmittance, thus more colouration, compared to other synthesised TSMPI films depicted in **Figure 14**. As a result, the potential CTC interactions between polymer chains in "PI 16" are greater. Furthermore, using the GPC results in **Figure 19** and referring to the DSC results in **Figure 12**, could explain why the synthesised TSMPI film possesses an 18 °C lower T_g than the literature TSMPI. The lower M_n value obtained would mean that the total weight of all the polymer molecules in the sample, and/or the total number of polymer molecules in the sample is reduced. Therefore, shorter and/or fewer polymer chains are demonstrated in the synthesised TSMPI film. As a result, the potential intermolecular force interactions between polymer network chains is reduced, thus, a lower T_g is observed. In addition, this could suggest a difference in the SMEs, as the T_g is an essential property for the shape recovery process. Therefore, the different observed times for shape recovery mentioned previously, could be attributed to film thickness, M_n , and T_g properties, as well as, the degree of TSMPI film in contact with the heat source. This is supported when comparing the synthesised TSMPI films shape recovery taking ~ 40 s, whereas, the literature TSMPI films shape recovery took ~ 30 s.

To summarise, the M_n is vital for determining T_g and SMEs, and the film thickness for optical transparency. Ultimately, this information will prove important for producing the TSMPI-PPy composite via 2PP using a Photonic Nanoscribe for its proposed application.

To document the synthesised TSMPI films morphological structure, XRD was conducted and the results are shown in **Figure 20**.

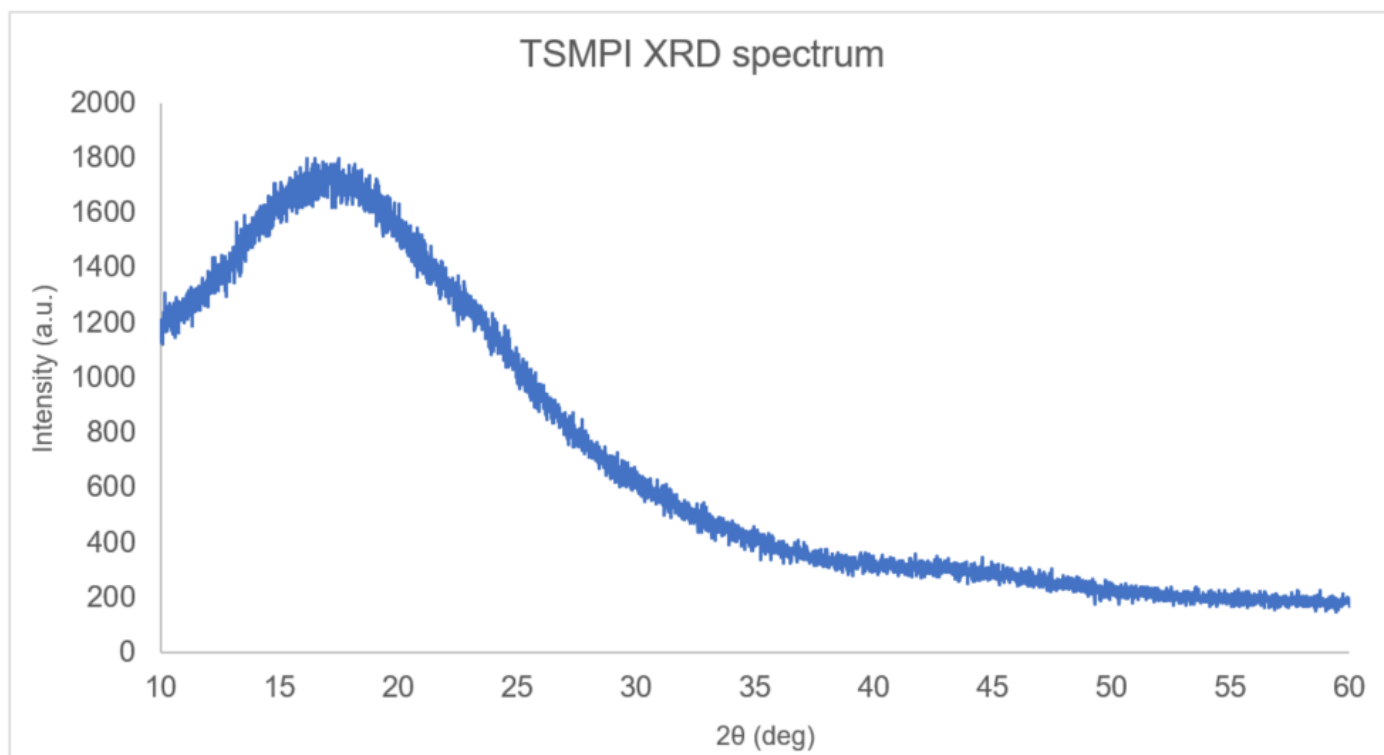


Figure 20. XRD spectrum of the synthesised TSMPI film. A broad peak is observed at 2θ 18° indicative of an amorphous polymer structure.

From **Figure 20**, the broad peak observed at 18° is due to the diffraction of intermolecular packing, characteristic of some regularity combined with amorphous halo.²⁴ Amorphous materials do not possess long periodicity, therefore, in amorphous polymeric materials, molecules are randomly distributed in 3D space and have order only in a few molecular dimensions. As a result, X-rays will be scattered in many different directions, yielding a broad peak or large 2θ range. Whereas, semi-crystalline polymers would yield high intensity narrow peaks, due to the degree of order present within the material.

The results from XRD manifest that the synthesised TSMPI film is amorphous in morphological structures, which can be attributed to loose chain packing and aggregation caused by its ether and isopropylidene linkages in dianhydride, as well as the *meta*-substituted ether linkages in the diamine units. Thus, the XRD analysis in addition to the results gathered from SME tests and GPC, the potential entanglement of TSMPIs network chains are essential for its shape-memory process.

3.4.1 2PP of pyrrole into/on TSMPI films using a Photonic Nanoscribe

2PP of monomers using a Photonic Nanoscribe is a relatively new technique, as a result, limited information was available to facilitate the production of the TSMPI-PPy composite. Therefore, a method development process was conducted to reliably produce TSMPI-PPy composites using this technique. The 2PP process using a Photonic Nanoscribe is shown in **Figure 21**.

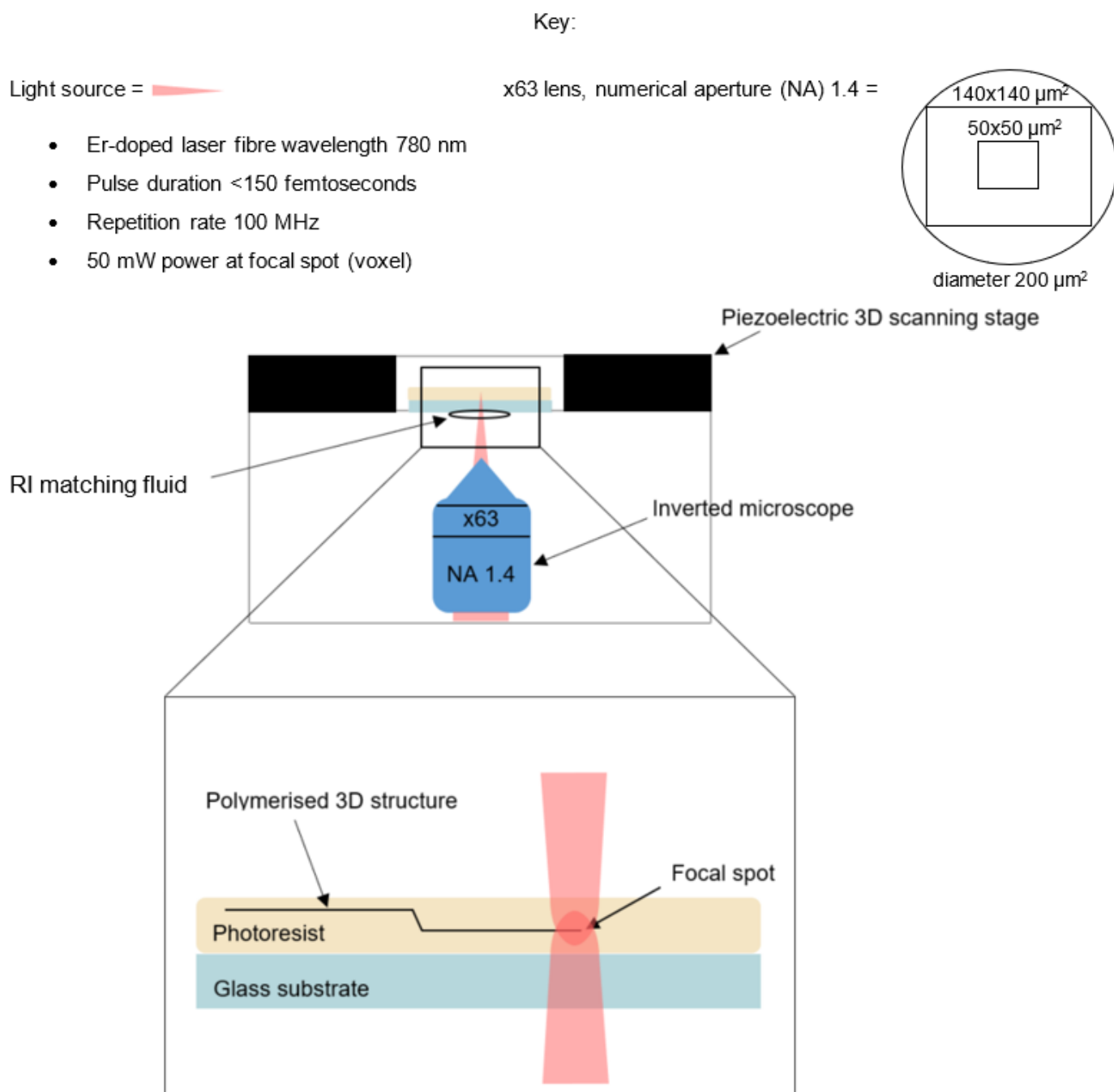


Figure 21. Schematic of the 2PP process using a Photonic Nanoscribe. This technique enables the fabrication of 3D microstructures into/on transparent materials.

The objective lens magnification is essential for determining the working distance and voxel, as seen from **Figure 21**, an x63 lens was depicted which enables the fabrication of high resolution microstructures into/on transparent materials. The approximate voxel ratio with an objective x63 lens is 2.5:1 (80 μm to 90 μm feature, 130 to 140 nm lateral resolution, <200 nm vertical feature, 1 μm vertical high) and the working distance range is 190 μm . Furthermore, the index matching fluid on the glass substrate detects any laser aberrations and focuses the laser accordingly, necessary for maintaining optimum resolution and enabling the fabrication of the microstructures.

Here, the 2PP process is achieved by nonlinear absorption of two photons simultaneously by a photoinitiator molecule, which will subsequently initiate the photopolymerisation process of a CP monomer (e.g. pyrrole). This is attributed to a high-power ultrashort pulse (femtoseconds) laser, with an intensity above a specific critical value that is dependent on both the material and pulse width. When a femtosecond laser beam is focused inside a transparent material with an adequate energy, nonlinear absorption can be confined to a region near the voxel inside the material where the laser intensity exceeds the critical value. In this way, internal modification of transparent materials (e.g. TSMPI) and the fabrication of structures (e.g. PPy) inside them can be performed.

Firstly, the stability of the synthesised TSMPI film was observed within the presence of the monomers of known CPs (e.g. pyrrole, 3,4-ethylenedioxythiophene [EDOT] and aniline), and it was observed that all synthesised TSMPI film fragments that were used dissolved within 1 h. However, synthesised TSMPI film fragments (of similar length and mass) were observed to be stable in water and alcohols (e.g. methanol and ethanol) within 1 h. Thus, the stability of the synthesised TSMPI films were measured in ratios consisting of the monomers with water, methanol and ethanol, as portrayed in **Table 6**. The mixture of the monomers with water, methanol and ethanol were regularly shaken/inverted to ensure the solution was homogenous, and the synthesised TSMPI film fragments were immersed for 1 h. The synthesised TSMPI film fragments used were weighed and measured (e.g. length) before and after the stability test. This was done because the TSMPI film must remain stable during the 2PP phase, to “carry” the polymerised CP structures into/on the synthesised TSMPI films.

a)

Monomer	Ratio of monomer with water in 1 mL					
	5:95	10:90	20:80	30:70	40:60	50:50
Aniline	x	-	-	-	-	-
EDOT	-	-	-	-	-	-
Pyrrrole	x	-	-	-	-	-

b)

Monomer	Ratio of monomer with methanol in 1 mL					
	5:95	10:90	20:80	30:70	40:60	50:50
Aniline	?	?	x	-	-	-
EDOT	?	?	x	-	-	-
Pyrrrole	?	?	x	-	-	-

c)

Monomer	Ratio of monomer with ethanol in 1 mL					
	5:95	10:90	20:80	30:70	40:60	50:50
Aniline	✓	?	x	-	-	-
EDOT	?	?	x	-	-	-
Pyrrrole	✓	?	?	-	-	-

Table 6. Stability test of the monomers with water, methanol and ethanol, which will be used to formulate the ink used during 2PP using a Photonic Nanoscribe to produce the TSMPI composite. a) Monomers mixed with water at varying ratios. b) Monomers mixed with methanol at varying ratios. c) Monomers mixed with ethanol at varying ratios. The green tick depicts the synthesised TSMPI film fragments that were completely recovered with no noticeable difference. Yellow question mark depicts the synthesised TSMPI film fragments that were recovered but with a noticeable difference (e.g. a decrease in mass, length, colour or integrity i.e. brittle). Red cross depicts the synthesised TSMPI film fragments that were recovered but were significantly damaged and no longer appear as a film. The dash depicts that the synthesised TSMPI film fragments were not recovered because they completely dissolved in the solution.

From the results in **Table 6c**), it is reported that the synthesised TSMPI film fragments immersed in 5:95 pyrrole and ethanol remained stable within 1 h, therefore, this was used for the ink. Furthermore, 5:95 aniline and ethanol was stable within 1 h but showed a lower stability at higher concentrations of aniline and, as a result, was not used for the ink. However, a 5:95 aniline and ethanol ink could be alternatively used.

The photoinitiator Irgacure D-2959 was dissolved in the 5:95 pyrrole and ethanol ink. Irgacure D-2959 is a highly efficient radical photoinitiator for UV curing of systems of unsaturated monomers (e.g. pyrrole), and at 0.1 % concentration in acetonitrile, exhibits an excitation spectrum upwards of 380 nm.³² To note, the Photonic Professional GT Nanoscribe possesses an Er-doped laser fibre with a wavelength of 780 nm (near infrared), and by incorporating 2PP, the absorption of two photons simultaneously at the voxel by the photoinitiator molecule should occur at 390 nm. Therefore, Irgacure D-2959 exhibiting excitation at 380 nm with a 0.1 % concentration, compliments the technique being used. The results of the experiment using this ink are depicted in **Table 7**.

5:95 pyrrole and ethanol ink	TSMPI-PPy
1 % mol Irgacure D-2959	-
2 % mol Irgacure D-2959	-
10 % mol Irgacure D-2959	?

Table 7. TSMPI-PPy production using Irgacure D-2959 5:95 pyrrole and ethanol ink. Yellow question mark depicts that black structures (potentially PPy) were observed into/on the TSMPI film, however, the TSMPI-PPy composites were produced unreliably, i.e. repeated experiments may or may not work and the black structures produced were not pronounced. The dash depicts that no TSMPI-PPy composites were produced i.e. no black structures were observed at all into/on the synthesised TSMPI film.

From **Table 7** the 5:95 pyrrole and ethanol ink with 10 % mol Irgacure D-2959 can demonstrate pyrrole polymerisation, as characterised by reproducing simple structures, demonstrated in **Figure 22**, into/on the synthesised TSMPI films, as portrayed in **Figure 23**.

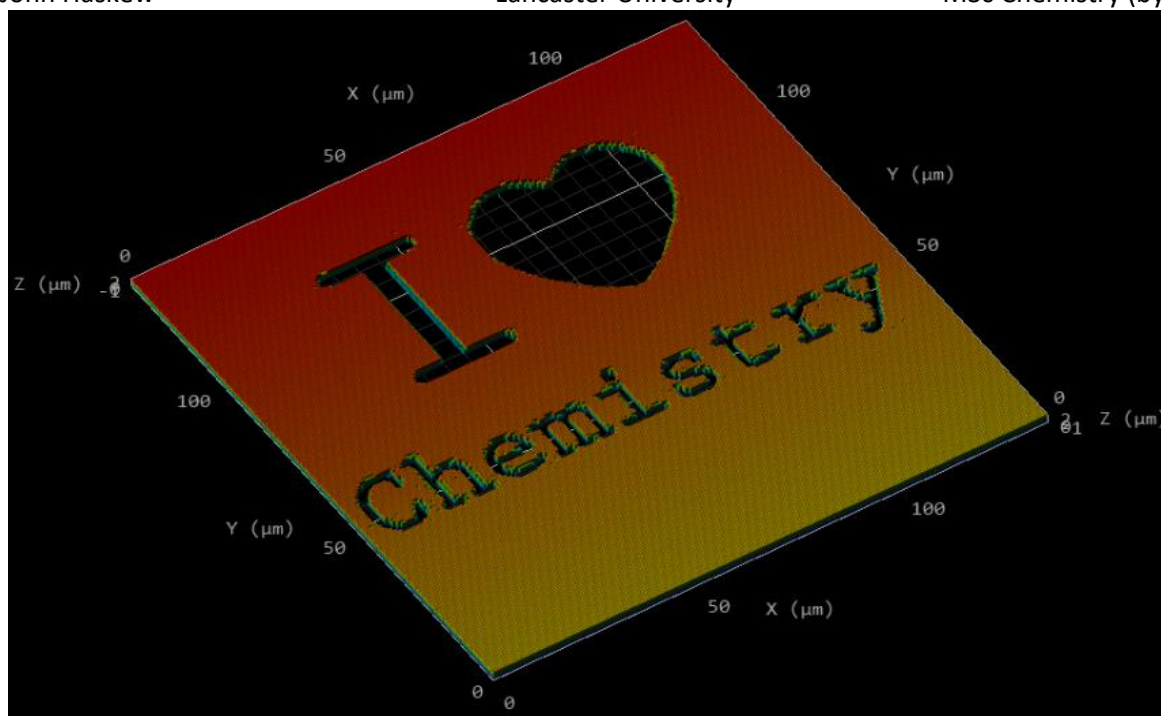


Figure 22. Picture from DeScribe software of a simple structure used to observe the initial 2PP of pyrrole into/on the TSMPI film. 130 μm (x and y-axis) and 1 μm (z-axis) square with "I <3 Chemistry etched into it.

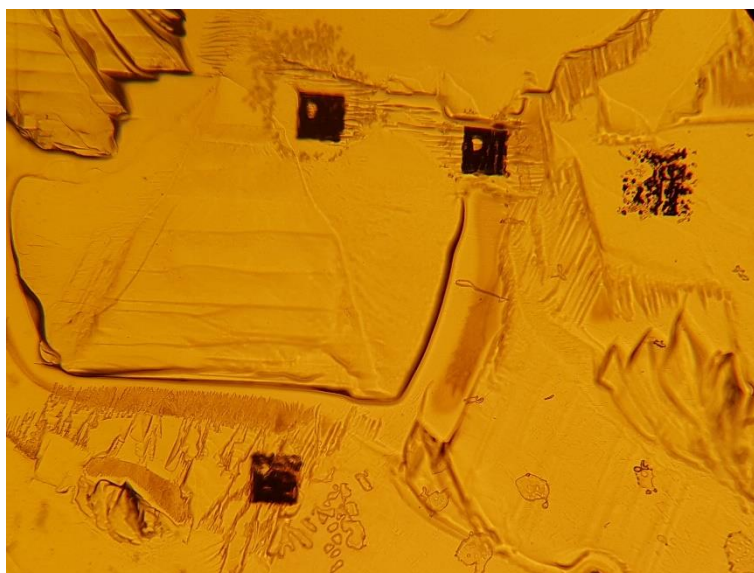


Figure 23. Picture of the TSMPI-PPy composite taken with an x10 optical microscope. The simple structures are observed, achieved via 2PP of pyrrole into/on the synthesised TSMPI films. Laser writing powers of 80 to 100 % were necessary to observe any polymerisation.

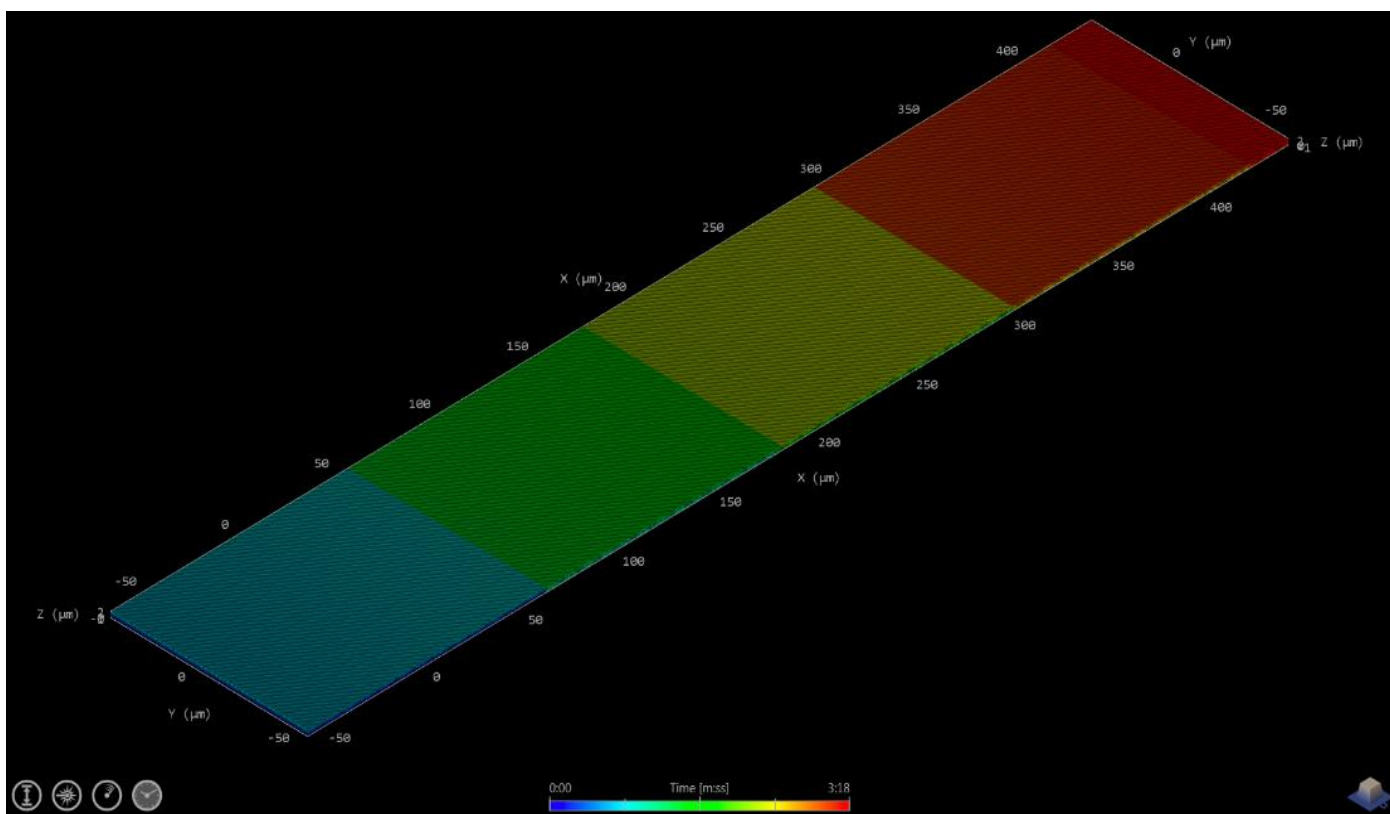
As seen from **Figure 23**, the presence of PPy is demonstrated into/on the synthesised TSMPI films by the black structures. The structures produced into/on the synthesised TSMPI films are recognisable to the design generated in **Figure 22**. However, at this stage, the structures are not very well-defined because “1 <3 Chemistry” is hardly visible, nor are these TSMPI-PPy composites easily reproduced. Thus, optimisation of this method was conducted to reliably produce TSMPI-PPy composites and with well-defined PPy structures.

With further inspection of the specific parameters to achieve 2PP of pyrrole using a Photonic Nanoscribe, the recommended optimum working distance was considered. Beforehand, the synthesised TSMPI films used were produced by slowly administering 500 μL of PAA via micropipette, which gave an average film thickness of 112 μm , mentioned previously. However, while utilising the x63 lens, the working distance range is 190 μm . Therefore, with the thickness of the glass cover slips (130 to 160 μm) accounted for, the total thickness of the samples in the initial tests were $\sim 242 \mu\text{m}$, $\sim 52 \mu\text{m}$ over the optimal working range for the technology.

Remembering the results gathered from GPC in **Figure 19**, how the M_n is an important property for determining TSMPIs possible polymer chain network entanglements, vital for its SMEs. The slow administration of 500 μL of PAA was not altered, as to prevent too much of a deviation from the average obtained M_n value at $13572 \text{ g mol}^{-1} (\pm 507.4)$. Therefore, after the slow administration of 500 μL of PAA via micropipette, a Dr Blade set at 60 μm (calibrated to compensate for the thickness of the glass substrate which was $\sim 1 \text{ mm}$ thick), was carefully dragged across the surface in each direction three times. As a result, synthesised TSMPI films with an average film thickness of 30 to 40 μm were produced from 500 μL of PAA. Hereby, with these new thinner TSMPI films, more success is to be achieved because it is within the optimum working range for the technology.

Initially, simple structures were fabricated for the purpose to observe the ability of 2PP of pyrrole using a Photonic Nanoscribe into/on the synthesised TSMPI films. As with the development of the method, new structural designs were also introduced, represented in **Figure 24** depicts the PPy lines first portrayed in **Figure 10** and **11**, essential for the proposed applications. The results of using thinner synthesised TSMPI films and the newly fabricated structural design (demonstrated in **Figure 24**) for 2PP of pyrrole into/on TSMPI films, are manifested in **Figure 25**.

a)



b)

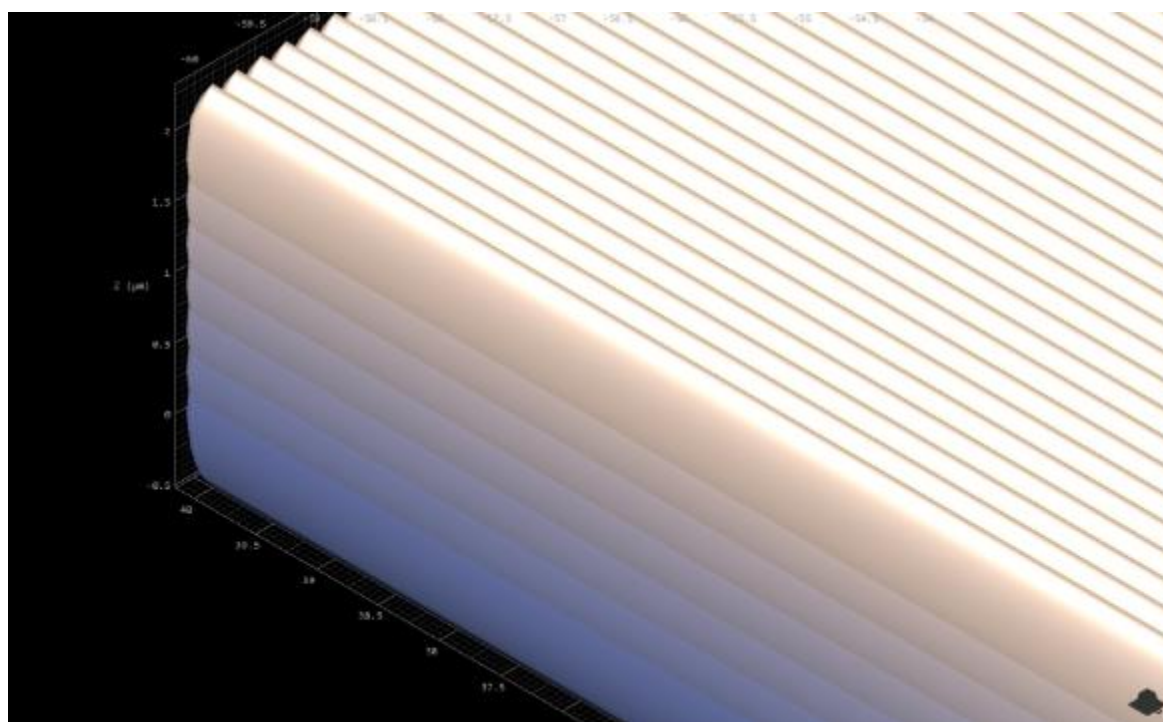


Figure 24. Pictures from DeScribe software of the new structures that would be used for subsequent 2PP of pyrrole into/on the TSMPI film. a) 500 μm (x-axis), 100 μm (y-axis) and 3 μm (z-axis) bar. b) Close inspection of the z-axis, portraying the stitching of each layer to connect them, because, it will remain a whole structure while penetrating 3 μm into the synthesised TSMPI film. This would prove important for electrical conductivity, as there should be no gaps in the CP.

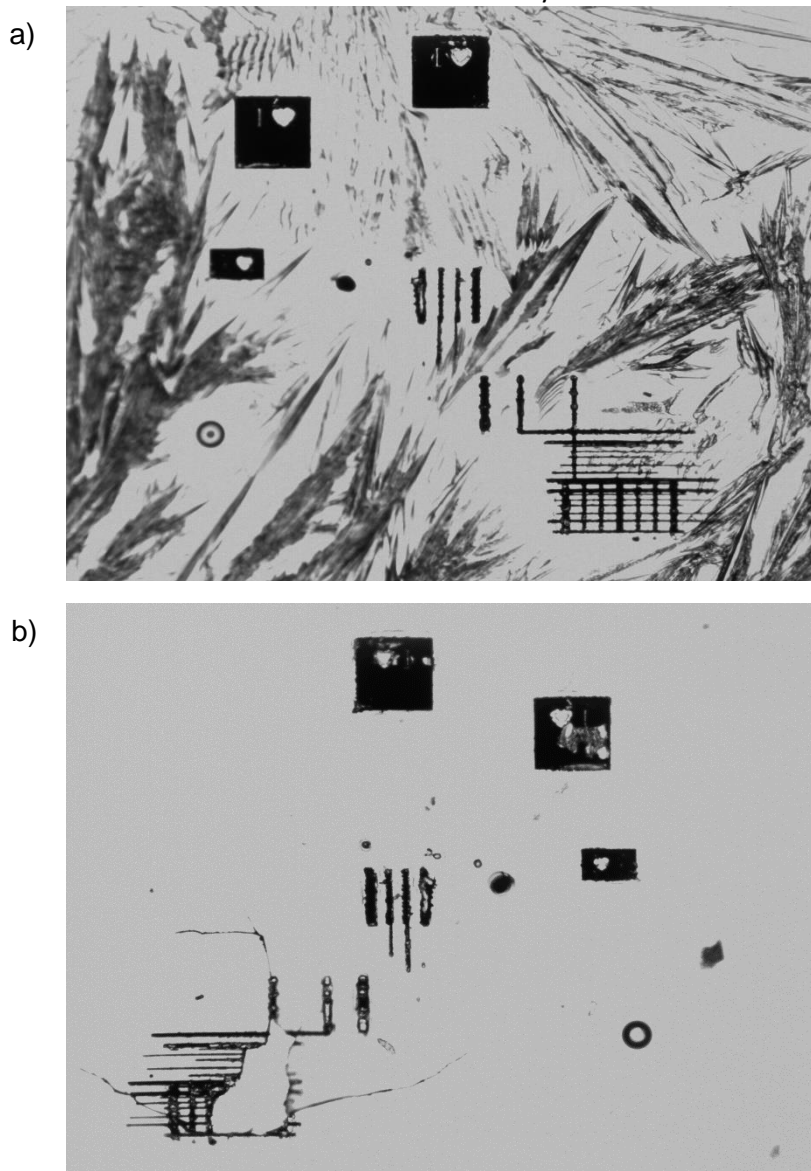


Figure 25. Picture of the TSMPI-PPy composite taken with LUCUM software and an x10Primo Star plan achromat ZEISS lens. a) TSMPI-PPy before ethanol washing. b) After ethanol washing which removes surface scarring, possibly being caused by the monomer on the TSMPI films surface.

The results shown in **Figure 25** represent an improvement over the initial tests depicted in **Figure 23**, by having an increased definition in the “I <3 Chemistry” structure, in addition, more PPy structures were also achieved, showing signs of the structural design generated in **Figure 24**. Furthermore, the fabrication of PPy into/on the synthesised TSMPI films were more reproducible, even with laser writing powers as low as 45 %.

The damage on the TSMPI-PPy composites shown in **Figure 25b)** occurred during the process of removing the material from the glass coverslip after ethanol washing, due to the reduced thickness, the TSMPI films were more delicate.

Although with the improvement of results, the method was further examined for potential avenues of improvement. As a result, different photoinitiators that excite closer to 390 nm were investigated (e.g. Darocur TPO). Like Irgacure D-2959, Darocur TPO is a highly efficient radical photoinitiator for UV curing of systems of unsaturated monomers. However, Darocur TPO at 0.1 % concentration in acetonitrile, exhibits an excitation spectrum upwards of 420 nm.³³ Hereby, utilising the same method previously discussed but with Darocur TPO as the photoinitiator in the 5:95 pyrrole and ethanol ink, could improve upon the results previously obtained. The experiment was conducted and the results are shown in **Table 8**.

5:95 pyrrole and ethanol ink	TSMPI-PPy
1 % mol Darocur TPO	-
2 % mol Darocur TPO	?
10 % mol Darocur TPO	✓

Table 8. TSMPI-PPy production using Darocur TPO 5:95 pyrrole and ethanol ink, and Dr Blading the administrated PAA to produce TSMPI films with an average film thickness of 30 to 40 μm . Green tick depicts that TSMPI-PPy composites were reliably reproduced with well-defined PPy structures, even at laser writing powers as low as 45 %. Yellow question mark depicts that TSMPI-PPy composites are produced but may require greater laser writing powers (e.g. 80 to 100 %). The dash depicts that no TSMPI-PPy composites were produced.

Thus, TSMPI-PPy composites are readily produced by 2PP of pyrrole using a Photonic Nanoscribe via 10 % mol Darocur TPO 5:95 pyrrole and ethanol ink, into/on synthesised TSMPI films with an average film thickness of 30 to 40 μm . The composites achieved via this method are reported for the first time and are portrayed in **Figure 26**.

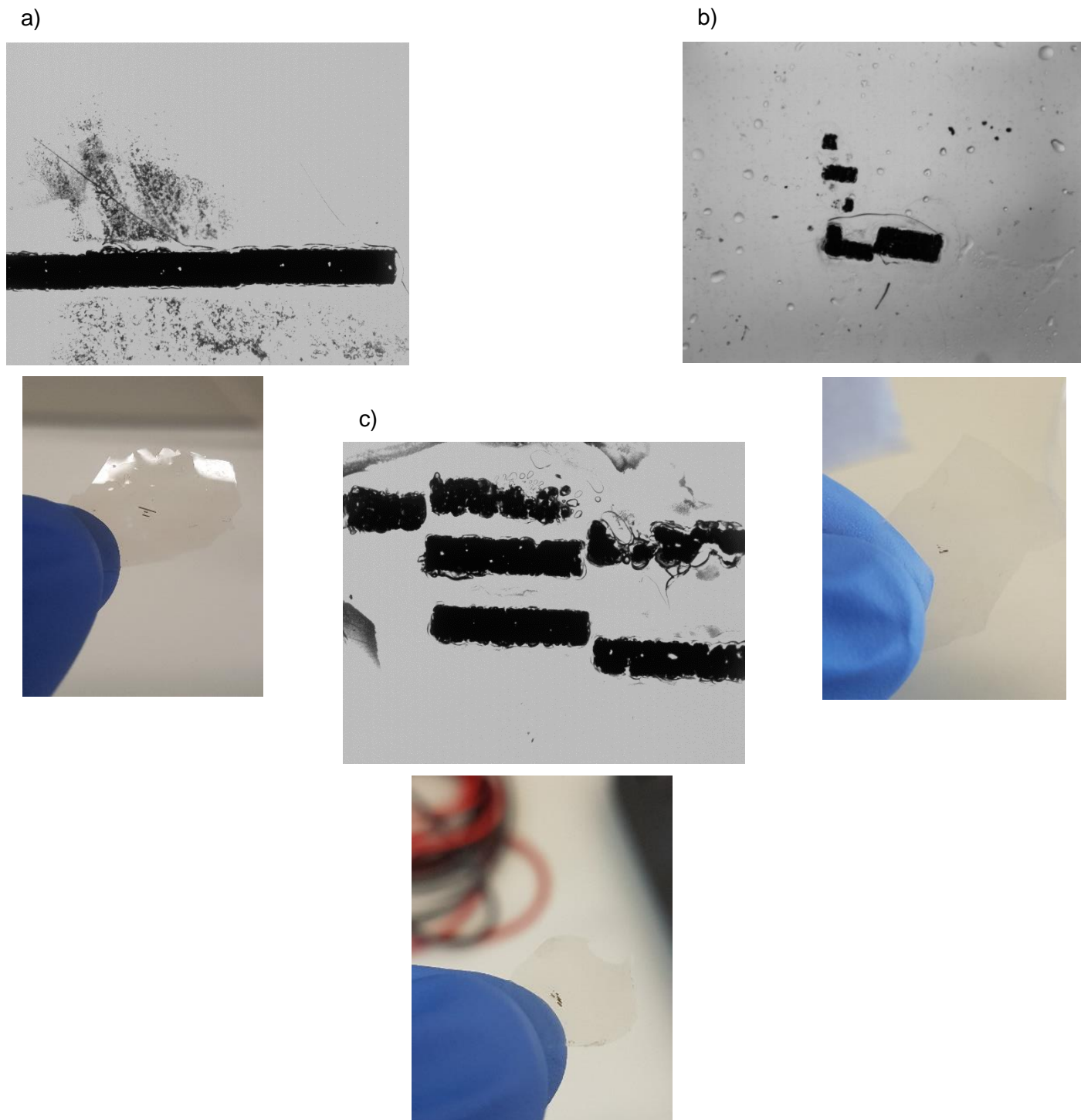
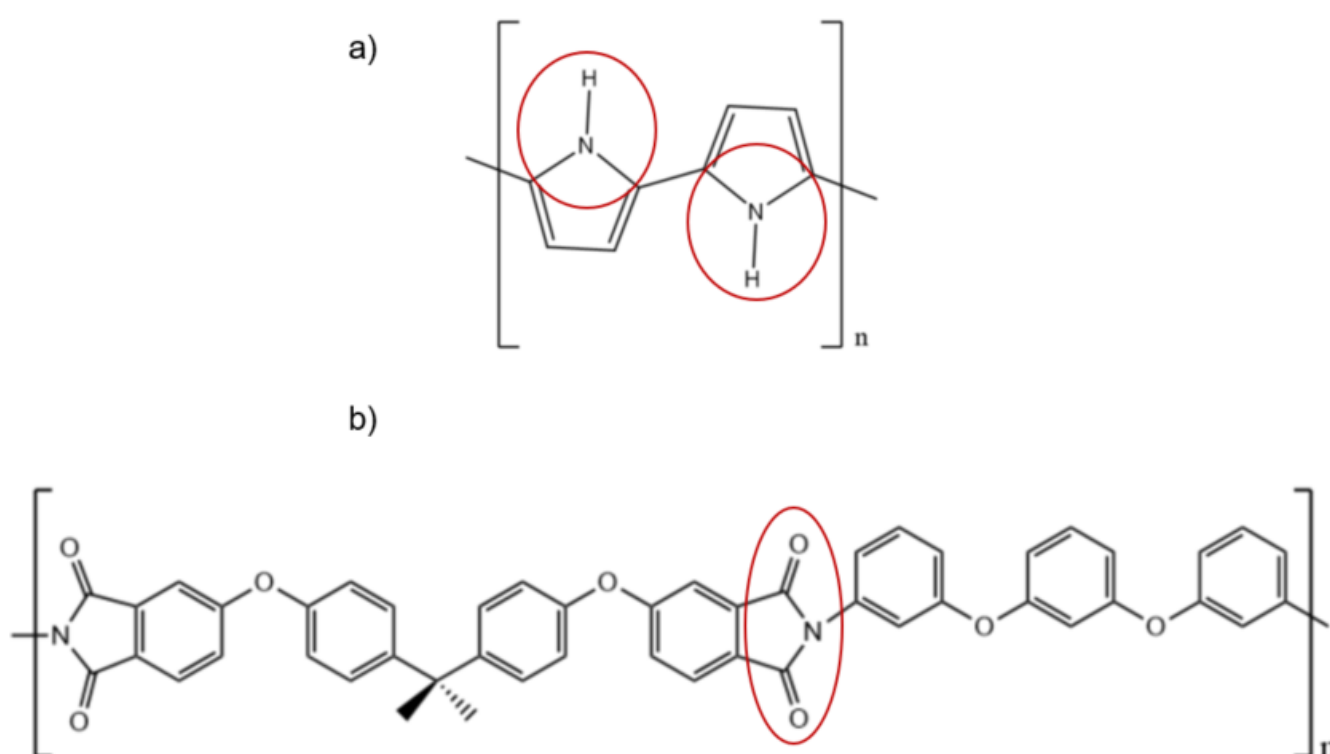


Figure 26. Pictures of the TSMPI-PPy composites. Pictures taken of TSMPI-PPy composites after a careful wash with ethanol, using LUCUM software and an x10Primo Star plan achromat ZEISS lens, and Samsung Galaxy S7 edge smartphone. a) TSMPI-PPy composite with PPy structures (long stitched bars) 3 to 4 mm in length. b) TSMPI-PPy composite with PPy structures (bars) 0.5 mm in length. c) TSMPI-PPy composites with PPy structures (bars) 0.5 mm to 1 mm in length.

3.4.2 Structural information

The black structures observed from 2PP of pyrrole using a Photonic Nanoscribe into/on synthesised TSMPI films could be assumed to be PPy, however, the FTIR spectra of the TSMPI-PPy composites were measured to characterise the functional groups present in the sample. This is beneficial because PPy possesses a functional group within its structure, depicted in **Scheme 2**, which the synthesised TSMPI films do not possess. Thus, if the dark structures were indeed PPy, peaks indicative of its characteristic functional group should be present, in addition to the signals from the TSMPI film.



Scheme 2. Chemical structure of PPy and TSMPI. a) PPy with its characteristic functional group being the secondary amine, circled red. b) TSMPI with its characteristic functional group being the imide ring, circled red. The discrete difference between both polymers should therefore be distinguishable via IR.

The FTIR spectrum of TSMPI-PPy compared to the synthesised TSMPI film is shown in **Figure 27**.

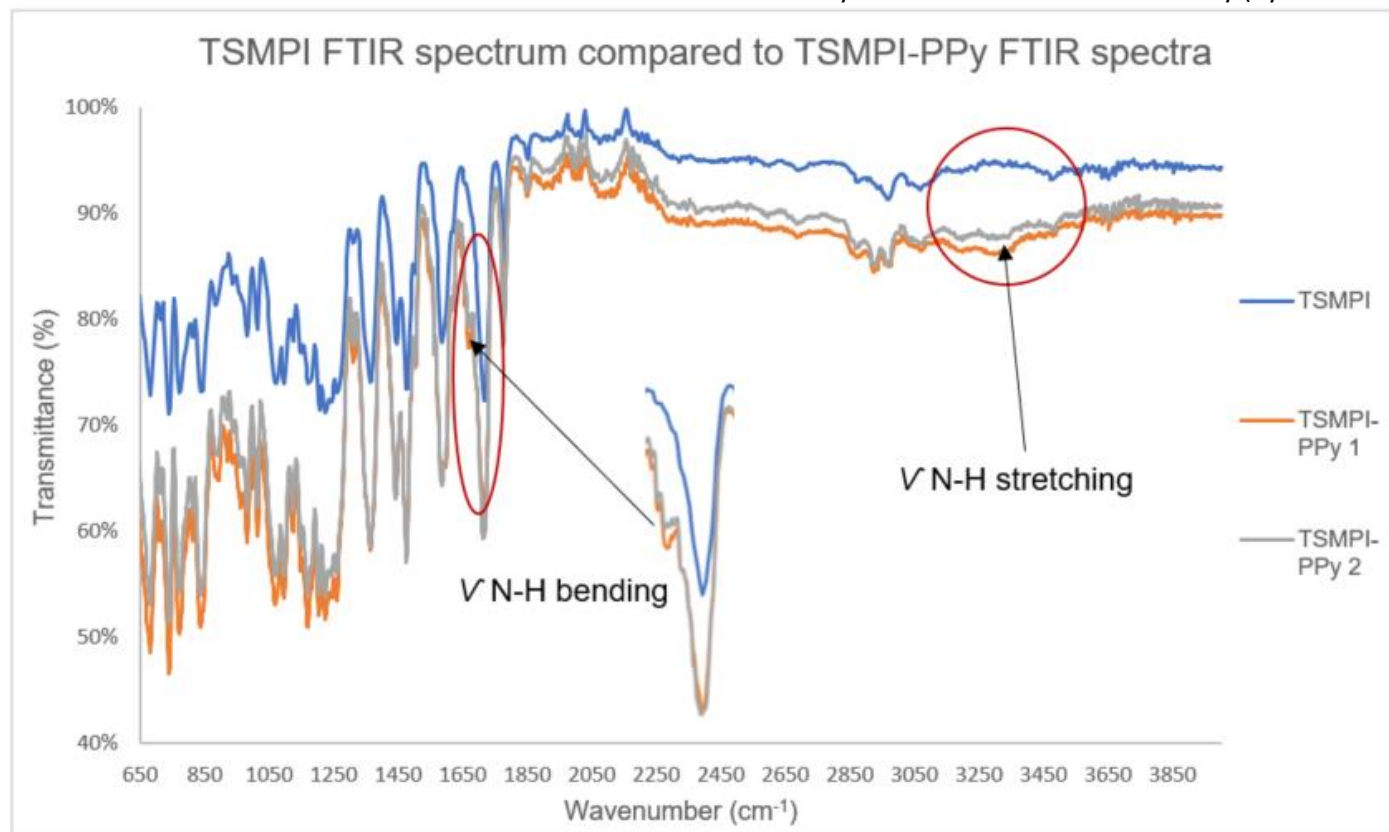


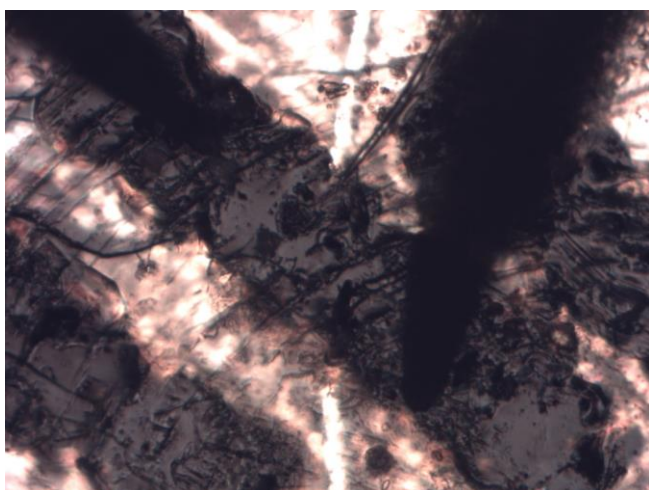
Figure 27. FTIR spectrum of the synthesised TSMPI film compared to TSMPI-PPy composite. By looking at the orange and grey lines, depicting TSMPI-PPy 1 and TSMPI-PPy 2 respectively. Noticeable differences are observed when compared to the synthesised TSMPI films FTIR spectrum (blue line), specifically, the peaks at 1670 cm⁻¹ (N-H secondary amine bending) and 3335 cm⁻¹ (N-H secondary amine stretching).

The results from the FTIR spectrum represented in **Figure 27**, demonstrates that there is an observable difference between the spectra of the synthesised TSMPI film and the TSMPI-PPy composite. Hereby, within the detection limits of IR and the appearance of the fabricated structures into/on the TSMPI films, suggest these black structures could likely be PPy, due to the presence of its characteristic functional groups being observed in the FTIR spectra that was not present beforehand. Thus, this information can be interpreted to be PPy, however, to definitively prove this, the composites electrical conductivity can be measured. By possessing electroconductive properties, PPy is ascertained because it is a well-known CP. Therefore, more conclusive results are obtained, while simultaneously providing proof of concept for the proposed applications described in **Figure 10** and **11**, towards our goal of achieving TRL 4.

3.4.3 Electrical conductivity

The electroconductive properties of polymers, such as PPy and polyaniline, arise due to their special structure, specifically, a backbone of contiguous sp^2 hybridised carbon centres. A valence electron on each centre would reside in a p_z orbital, which is orthogonal to the other three sigma-bonds.³⁴ All the p_z orbitals combine with each other which generates a molecule wide delocalised set of orbitals, the electrons in these delocalised orbitals have high mobility when the material is doped by oxidation.³⁴ The electroconductive properties of the TSMPI-PPy composites were first observed using a modified Micromanipulator miBot from Imina Technologies. This technology was incorporated to observe the difference in resistance (Ω) of the TSMPI-PPy composite and TSMPI film, by selectively measuring the resistance of the black structures found into/on the composites vs the TSMPI film. Like, an impedance metre being used to measure the resistance of electroactive substances, but on the microscale. The results from the modified Micromanipulator miBot of the TSMPI-PPy composite are represented in **Figure 28**.

a)



b)

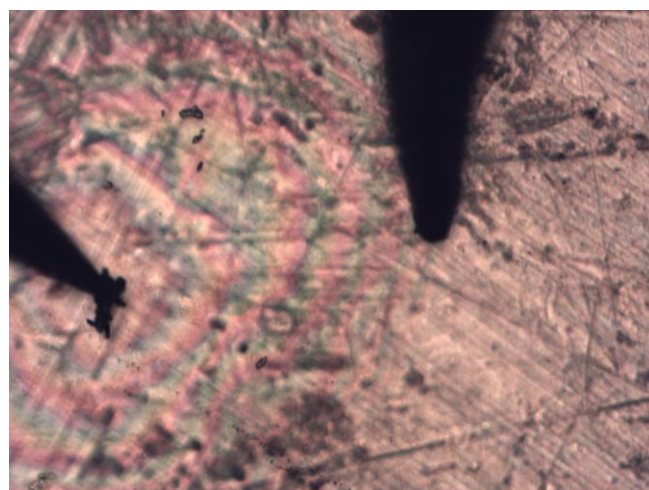


Figure 28. Pictures taken using an x10 optical microscope during electrical conductivity tests on the TSMPI-PPy composite and the synthesised TSMPI film. a) TSMPI-PPy composite with the micro-electric probes touching the observed black structures (14 to 18 μm gap between the micro-electric probes). b) The synthesised TSMPI film with the micro-electric probes touching the surface of the film (14 to 18 μm gap between the micro-electric probes).

When comparing the resistance values between **Figure 28a)** and **Figure 28b)** no difference was observed. The control for the experiment being the synthesised TSMPI film, possessed a resistance value like that of an air gap (1.3×10^{16} to $3.3 \times 10^{16} \Omega$). The TSMPI-PPy composites also possessed a resistance value like that of an air gap (1.3×10^{16} to $3.3 \times 10^{16} \Omega$). Therefore, these results suggest that the TSMPI-PPy composite does not conduct electricity. Furthermore, in **Figure 28b)** the image of the synthesised TSMPI film demonstrates a possible dielectric polarisation, represented by the striated coloured rings surrounding the micro-electric probes, which is indicative of an electrical insulator (typical property for PIs). However, in **Figure 28a)** the striated coloured rings are no longer present, which may suggest no dielectric polarisation is occurring and that the TSMPI-PPy composite is behaving differently to the synthesised TSMPI film.

Moreover, it is not yet conclusive whether these black structures are electroconductive, because the 2PP process fabricated the black structures within the TSMPI matrix. The experiment depicted in **Figure 28** could not accurately represent the electrical properties of these black structures, because it cannot measure them i.e. reach them in the TSMPI matrix as the micro-electric probes are only in contact with the surface.

3.5.1 Thermal properties

The thermal properties of the synthesised OCL-ODX was analysed by DSC, as shown in **Figure 29**. It is observed that the measured T_m was in good agreement when compared with the literature value. The literature value designates that the T_{trans} (through its T_m) was at ~ 40 °C. The obtained T_m for the synthesised OCL-ODX was ~ 7 °C higher than that of the literature value.

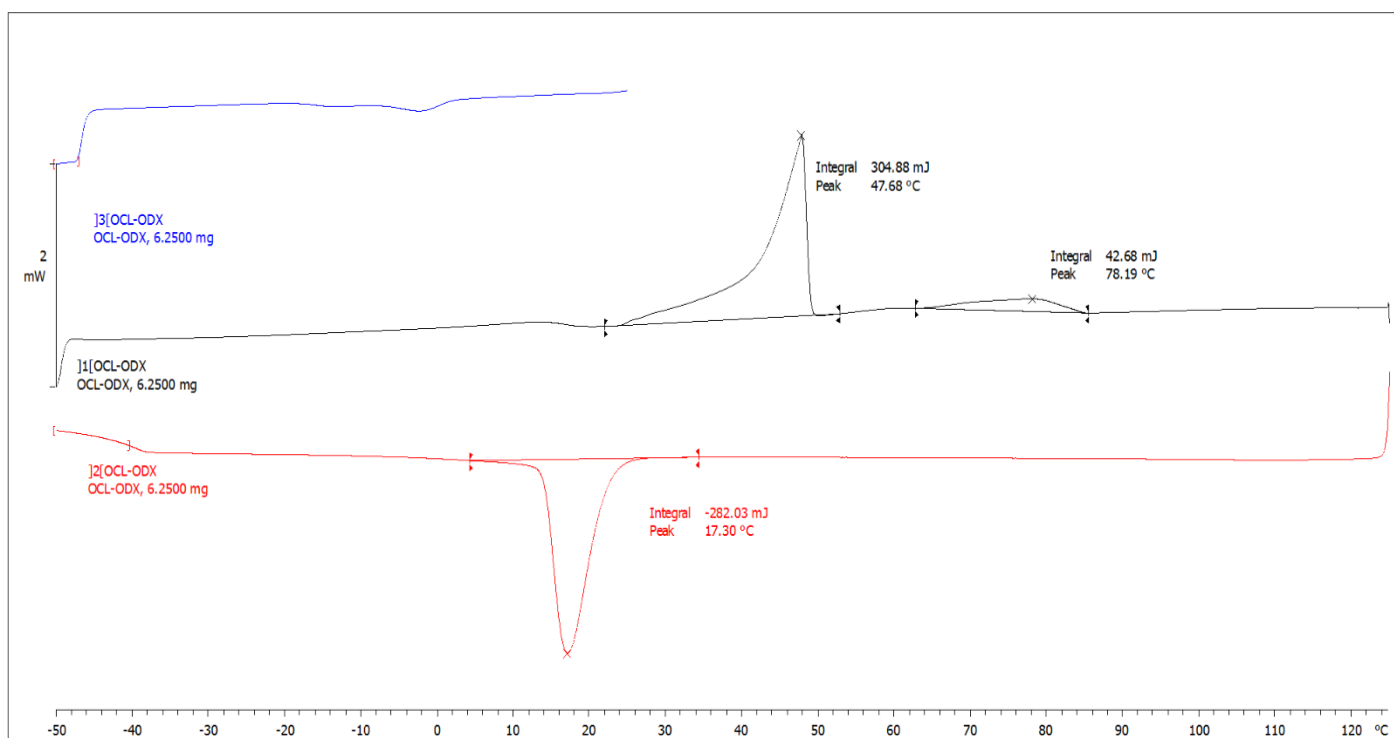


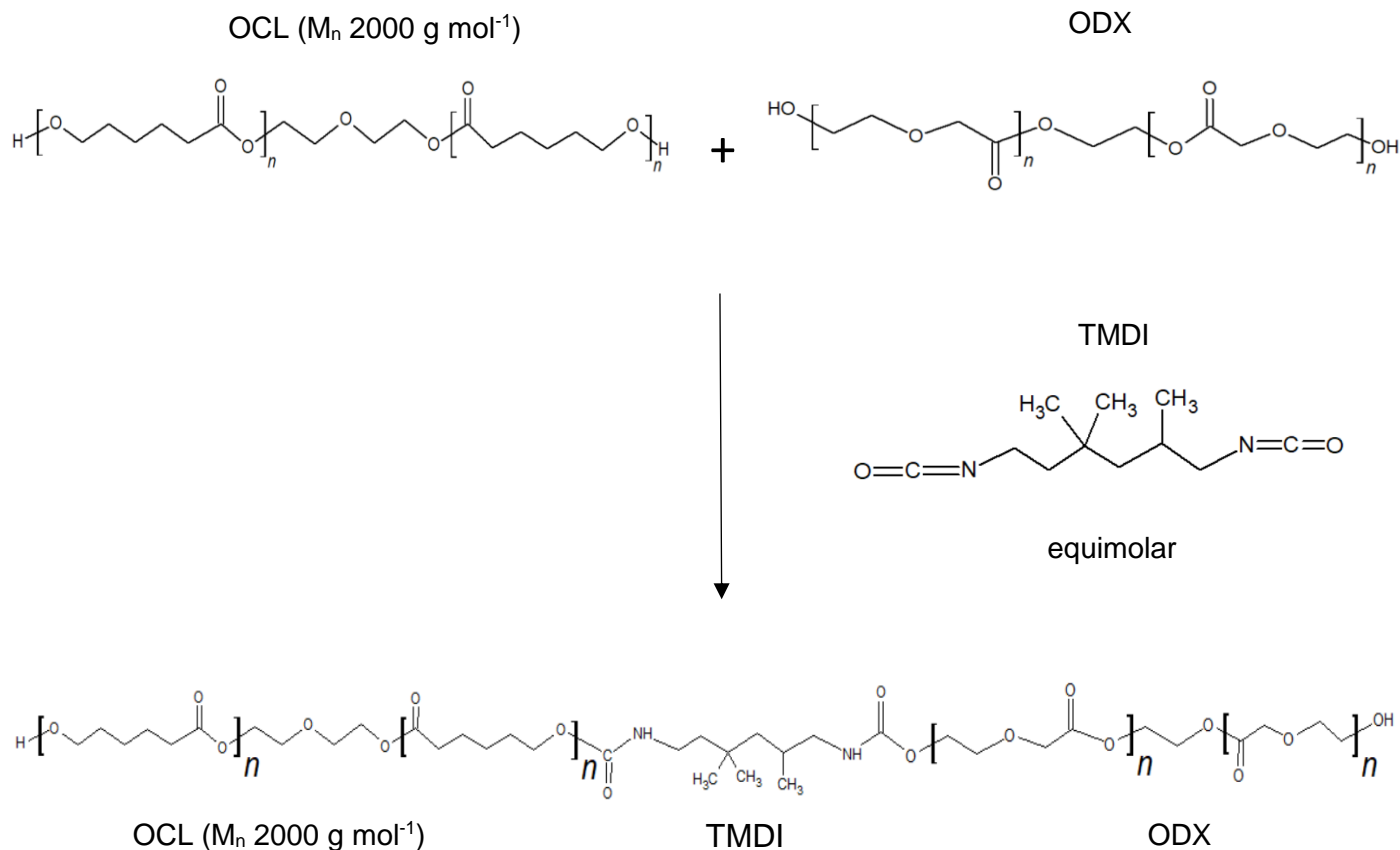
Figure 29. DSC results of the synthesised OCL-ODX. DSC range is -50 to 125 °C. The black line depicts the forward heating cycle at 2 °C min⁻¹. The first peak observed (at 47.68 °C) is indicative of the OCL segments T_m , the second peak observed (at 78.19 °C) is indicative of the ODX segments T_m . The red line depicts the reverse cooling cycle at 2 °C min⁻¹. The peak observed at 17.30 °C represents the crystallisation of the chain segments within the OCL-ODX sample, demonstrated by the peak occurring at a colder temperature i.e. before the first T_m peak begins. The blue line depicts a heating stage bringing the machine back to room temperature.

From **Figure 29** it is apparent the OCL and ODX segments are present within the OCL-ODX sample, because their characteristic T_m peaks are observed at 47 and 78 °C respectively. The literature values of similar polymers enabled the fabrication of the DSC working ranges used, in addition, the DSC results for OCL and ODX are manifested in the SI. By comparing the peaks in the OCL-ODX sample, the peak representative of OCL is noticeably more pronounced than the peak representative of ODX. This can be attributed to the ratios used to synthesise the polymer. ODX used for synthesis was at 67 % by weight of the OCL used.

The purpose for conducting DSC for the synthesised OCL-ODX was to evaluate its T_m properties, which is essential for the shape recovery process of the SMP. OCL was chosen as the precursor for the switching segments having a specific T_m value (47 °C), while crystallisable ODX with a higher T_m (78 °C) was chosen as the hard segment to provide the physical cross-links, as mentioned previously. Therefore, the SME occurs via OCL polymer chain segments melting (through its T_m), as a result, the polymer will subsequently become more flexible. However, the ODX polymer chain segments will maintain its rigidity, as a result, physical cross-links are possible between the polymer network chains. Thus, when cooling occurs when OCL-ODX is in its deformed state, the crystallisation of OCL polymer chain segments occur, “locking” the deformed shape. Upon reheating to 47 °C, the OCL polymer network chains melt, enabling flexibility and the strain energy stored in the deformed state is released, and thus, OCL-ODX can revert to its original shape. Remembering the proposed application in **Figure 11**, it is important that the SMEs occur at a suitable body temperature, ~ 40 °C. Hereby, from the results shown in **Figure 29**, the synthesised OCL-ODX T_m being 47 °C means that the OCL-ODX SMEs should occur at a temperature suitable for the human body.

3.5.2 Structural information

The reaction scheme for OCL-ODX via the polyaddition of OCL (M_n 2000 g mol^{-1}), ODX and TMDI is shown in **Scheme 3**.



Scheme 3. Reaction scheme for OCL-ODX. Polyaddition reaction of OCL-ODX from OCL, ODX and TMDI.

After the synthesis of OCL-ODX, its FTIR spectra was measured. In this case, to identify the formation of the copolymer which should arise from its characteristic functional groups. The representative FTIR spectrum of the synthesised OCL-ODX is shown in **Figure 30**.

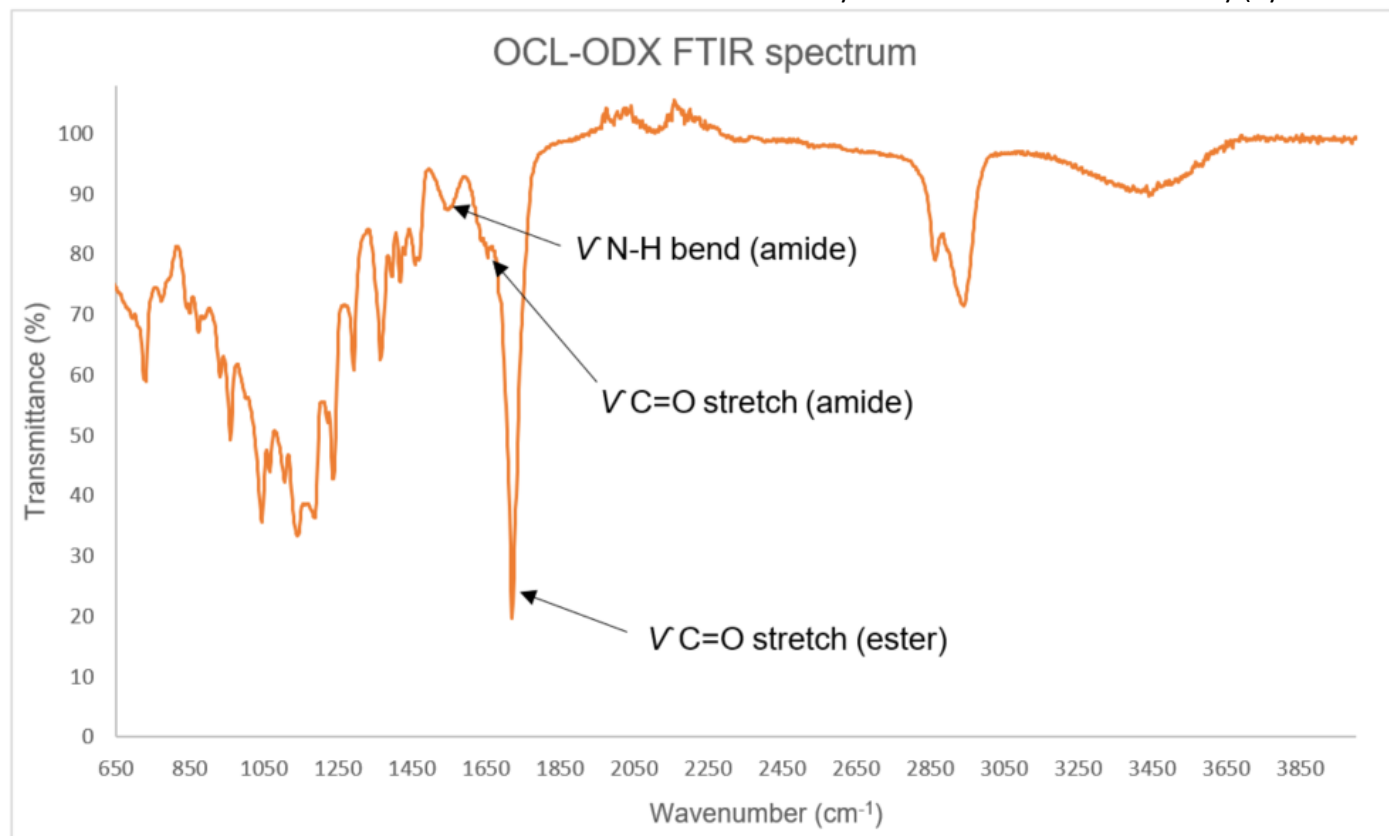


Figure 30. FTIR spectrum of the synthesised OCL-ODX. Peaks at 1550 cm⁻¹ (ν N-H amide bending), 1653 cm⁻¹ (ν C=O amide stretching) and 1720 cm⁻¹ (ν C=O ester stretching) confirm the characteristic functional groups expected in OCL-ODX.

Within the detection limit of IR, the results from **Figure 30** suggests the presence of the characteristic functional groups first portrayed in **Scheme 3**. The FTIR spectra for OCL and ODX are manifested in the SI.

To document the synthesised OCL-ODXs morphological structure, XRD was conducted and the results represented in **Figure 31**.

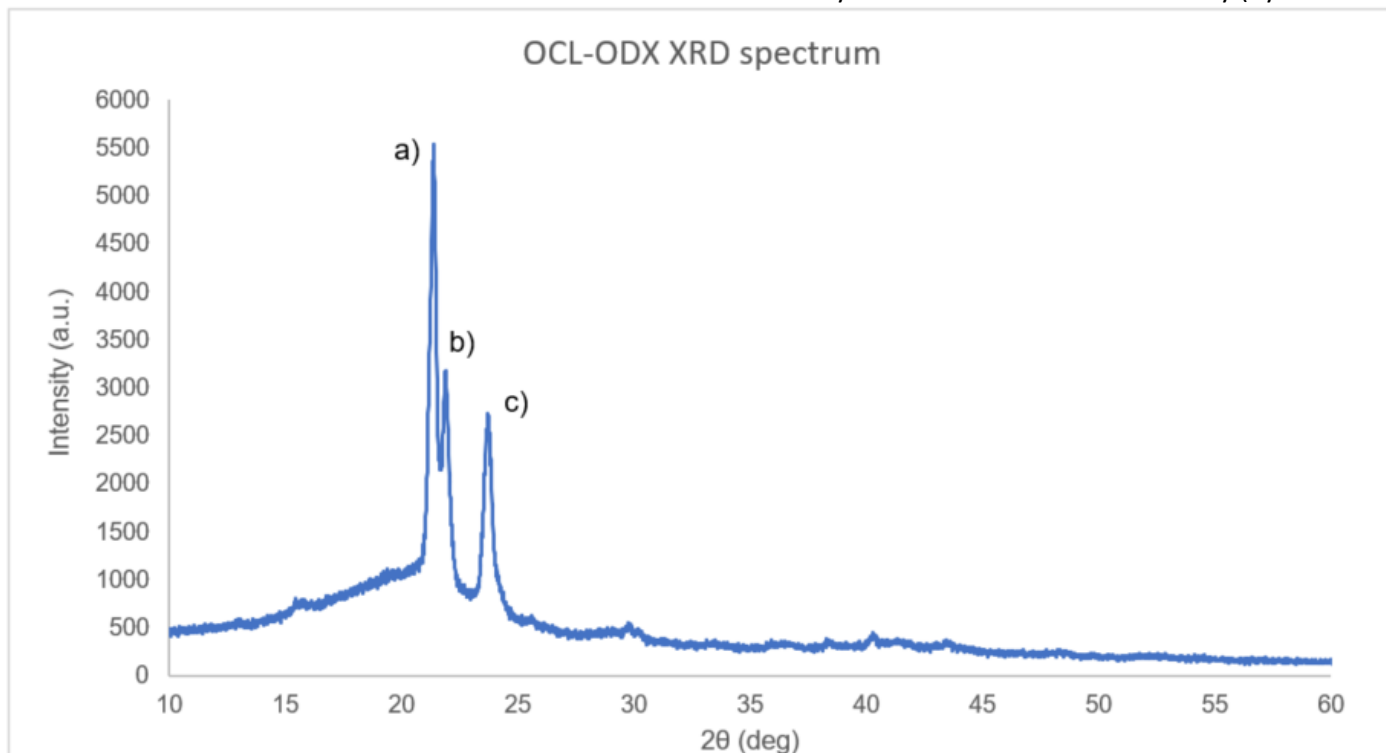


Figure 31. XRD spectrum of the synthesised OCL-ODX. A broad peak observed at 2θ 20° indicative of an amorphous polymer structure. a) Very sharp peak at 2θ 21° with intensity 5500 a.u. b) Very sharp peak at 2θ 22° with intensity 3000 a.u. c) Very sharp peak at 2θ 24° with intensity 2700 a.u. The addition of the sharp peaks amongst the broad peak indicates a semi-crystalline polymer structure.

The results from **Figure 31** suggest OCL-ODX is semi-crystalline in morphological structures. Furthermore, three sharp peaks are detected which suggest different regions within the sample. Comparing the peaks **Figure 31a)** and **Figure 31c)** to values obtained in the literature, suggest the OCL segments are responsible for these signals, because a 2θ 21° and a 2θ 24° were also represented.³⁵ Moreover, **Figure 31b)** could represent the ODX segments. This is supported when comparing their relative intensities and remembering the ratios used for synthesis, ODX used was at 67 % by weight of OCL used. Therefore, in **Figure 31b)** this peak is ~ 60 % that of **Figure 31a)** peak.

4 Future work

- Further characterisation of the synthesised OCL-ODX SMP, primarily to distinguish it as an SMP. The T_m values are known so the shape-memory and recovery process can be developed. Furthermore, completely characterise the SMEs of TSMPI and OCL-ODX SMP (including the composites TSMPI-PPy and OCL-ODX-PPy) via DMA to subsequently calculate R_r and R_f values.
- Produce OCL-ODX-PPy composites following a similar method depicted in chapter 3.4 for TSMPI-PPy.
- Continue the investigation into the electrical properties of the composites. Design new structures to be drawn into/on the SMPs that allow easier detection via the Micromanipulator miBot from Imina Technologies. Conductive tip AFM may yield insightful information on the electrical properties of the PPy structures fabricated into/on the SMPs. Increase the potential electrical conductivity of the PPy structures by adding dopants (e.g. camphor sulfonic acid).

5 Conclusion

The thesis focuses on innovating SMPs reported in the literature and attempts to improve the physical and mechanical properties of CPs, by manufacturing a composite with SMEs and electroconductive properties. Utilising the relatively new technique of 2PP using a Photonic Nanoscribe, TSMPI-PPy composites have been fabricated and is reported for the first time.

3 to 4 mm long stitched bars of PPy were fabricated within a TSMPI matrix, as a result, these composites possess SMEs responding to temperature, and the potential to conduct electricity.

Due to the unique combination of properties, attributed by the SMP and CP, technologically innovative applications, such as, negative switches for high thermal systems or biomedical devices rejuvenating damaged nerve cells are not unreasonable. The full potential of these materials has yet to be discovered, and with further investigation, could even replace expensive/out-dated materials, providing new and useful applications.

6 Bibliography

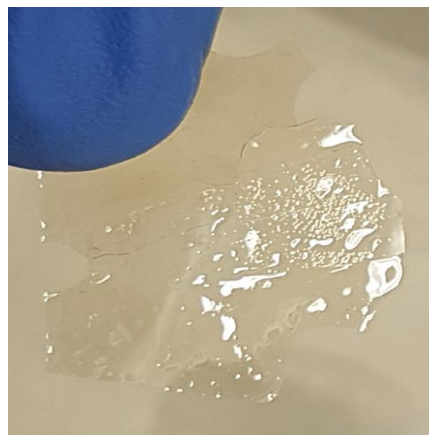
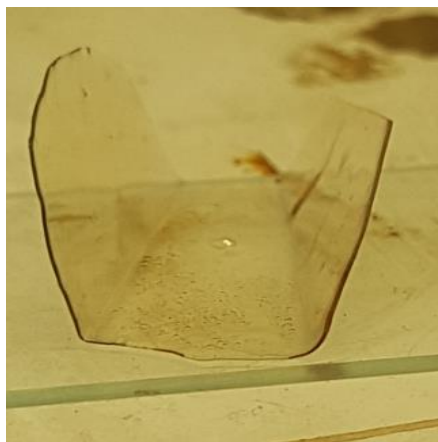
1. I. Bellin, S. Kelch, R. Langer, A. Lendlein, *Proc. of the National Acad. of Sci*, **2006**, 103 (48) 18043-18047.
2. J. Leng, X. Lan, Y. Liu and S. Du, *Prog. in Mater. Sci*, **2011**, 56, 1077-1085.
3. C. Lie, H. Qin and P.T. Mather, *J. Mater. Chem*, **2007**, 1543-1558.
4. L. B. Vernon et al, *Proc of manufac. art. of thermoplas. synth. resins*, **1941**.
5. J. Hu, Y. Zhu. H. Huang, J. Lu. *Prog. in Polymer Sci*, **2012**, 37, 1720-1722.
6. J. Hu, Y. Zhu. H. Huang, J. Lu. *Prog. in Polymer Sci* **2012**, 37, 1723-1729.
7. C. Liu, H. Quin and P.T. Mather, *J. Mater.Chem*, **2007**, 17, 1543-1558.
8. E. Havens, E. A. Snyder, T. H. Tong, *Smart Struc. and Mater*, **2005**.
9. H. Luo, Z. Li, G. Yi, X. Zu, H. Wang, Y. Wang, H. Huang, J. Hu, Z. Liang, B. Zhong, *Mater. Letters*, 134, **2004**, 172-175.
10. M. Ma, L. Guo, D. G. Anderson, R. Langer, *Sci*, **2013**, 339, 186-189.
11. Y. Li, H. Chen, D. Liu, W. Wang, Y. Liu and S. Zhou, *Applied Mater. & Interfaces*, **2015**, 7, 12988-12999.
12. J. Leng, X. Lan, Y. Liu and S. Du, *Prog. in Mater. Sci*, **2011**, 56, 1081-1087.
13. J. Hu, Y. Zhu. H. Huang, J. Lu. *Prog. in Polymer Sci*, **2012**, 37, 1730-1763.
14. J. Leng, X. Lan, Y. Liu and S. Du, *Prog. in Mater. Sci*, **2011**, 56, 1081-1088-1092.
15. D.A. Skoog, F.J. Holler, S.R. Crouch, *Principles of Instru. anal. (6th ed.)*, **2007**, 169–173.
16. W. Paudler, *Nuc Magn. Res. Allyn and Bacon Chem. Series*, **1974**, 9–11.
17. R.H. Garrett, C.M. Grisham, *Biochem, (5th ed.)*, **1974**, 108.
18. H. Lobo, J.V. Bonilla, *Handbook of plast. anal. New York: Marcel Dekker, INC*, **2003**.
19. J.L. Hu, *Shape memory polymers and textiles, In: Characterization techniques for shape memory polymers, CRC Press LLC*, **2007**, 92–104.
20. P.T. Mather, H.G. Jeon, A. Romo-Uribe, T.S. Haddad, J.D. Lichtenhan, *Mechanical relaxation and microstructure of poly(norbornyl-poss) copolymers, Macromol*, **1999**, 32, 203-1194.
21. F. Yang, E. Wornyo, K. Gall, W.P. King, *Nanoscale indent formation in shape memory polymers using a heated probe tip. Nanotechnology*, **2007**, 18, 285302, 1–2, 8.
22. M. Deubel, M. Wegener, S. Linden, G. von Freymann, and S. John, *3D-2D-3D photonic crystal heterostructures fabricated by direct laser writing, Opt. Lett.* **2006**, 31, 805-807.
23. L. Huang, R.S. Dyer, R.J. Lago, A.A. Stolov, J. Li, *Mechanical properties of polyimide coated optical fibers at elevated temperatures, Proc. SPIE 9702, Optical Fibers and Sensors for Medical Diagnostics and Treatment Applications XVI*, **2016**.
24. X. Xiao, X. Qiu, D. Kong, W. Zhang, Y. Liuc and J. Leng, *Soft Matter*, **2016**, 12, 2894.

25. J. March, *Advanced Org. Chem, Reactions, Mechanisms, and Structure 3rd ed.* **1985**.
26. A. Lendlein, P. Neuenchwander, U. W. Suter, *Macromol. Chem.* **2000**, *Phys. 201*, 1067.
27. H. Grablowitz and A. Lendlein, *J. Mater. Chem*, **2007**, *17*, 4050–4056.
28. A. Lendlein and R. Langer, *Sci.* **2000**, *296*, 1673-1676.
29. Horizon 2020 Work Programme. *19. General Annexes Revised.* **2014**, 4995.
30. N. S. Ilicheva, N. K. Kitaeva, V. R. Dufлот and V. I. Kabanova, *ISRN. Poly. Sci.* **2012**, 2012, 1-7.
31. Tools for NMR spectroscopists, <https://www.nmrdb.org/13c/index.shtml?v=v2.95.0>, (accessed August 2018).
32. Ciba IRGACURE 2959, <http://www.xtgchem.cn/upload/20110629045632.PDF>, (accessed August 2018).
33. Ciba Darocur TPO, http://www.mufong.com.tw/ciba/ciba_photo_tds/tds_darocur_tpo.pdf, (accessed August 2018).
34. G. Inzelt, *Conducting Polymers: A new Era in Electrochemistry*, Springer Science and Business Media, Berlin, Germany, **2008**.
35. R. Balu, T. S. S. Kumar, M. Ramalingam and S. Ramakrishna, *J. Biomater. Tissue Eng.* **2011**, *Vol 1, No. 1*.

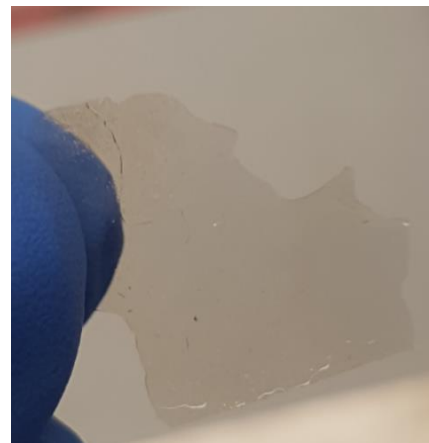
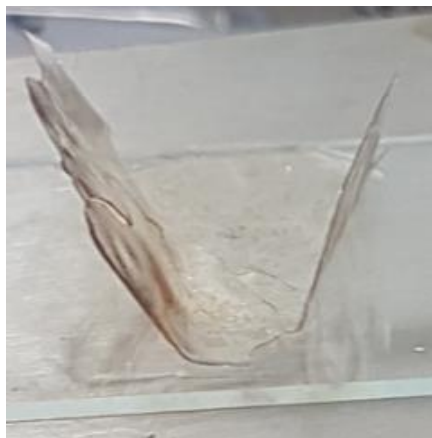
Appendix I

SI

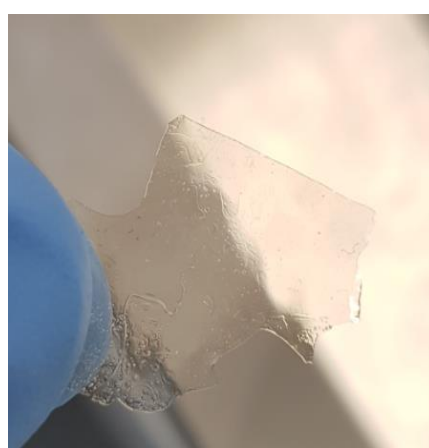
a)



b)

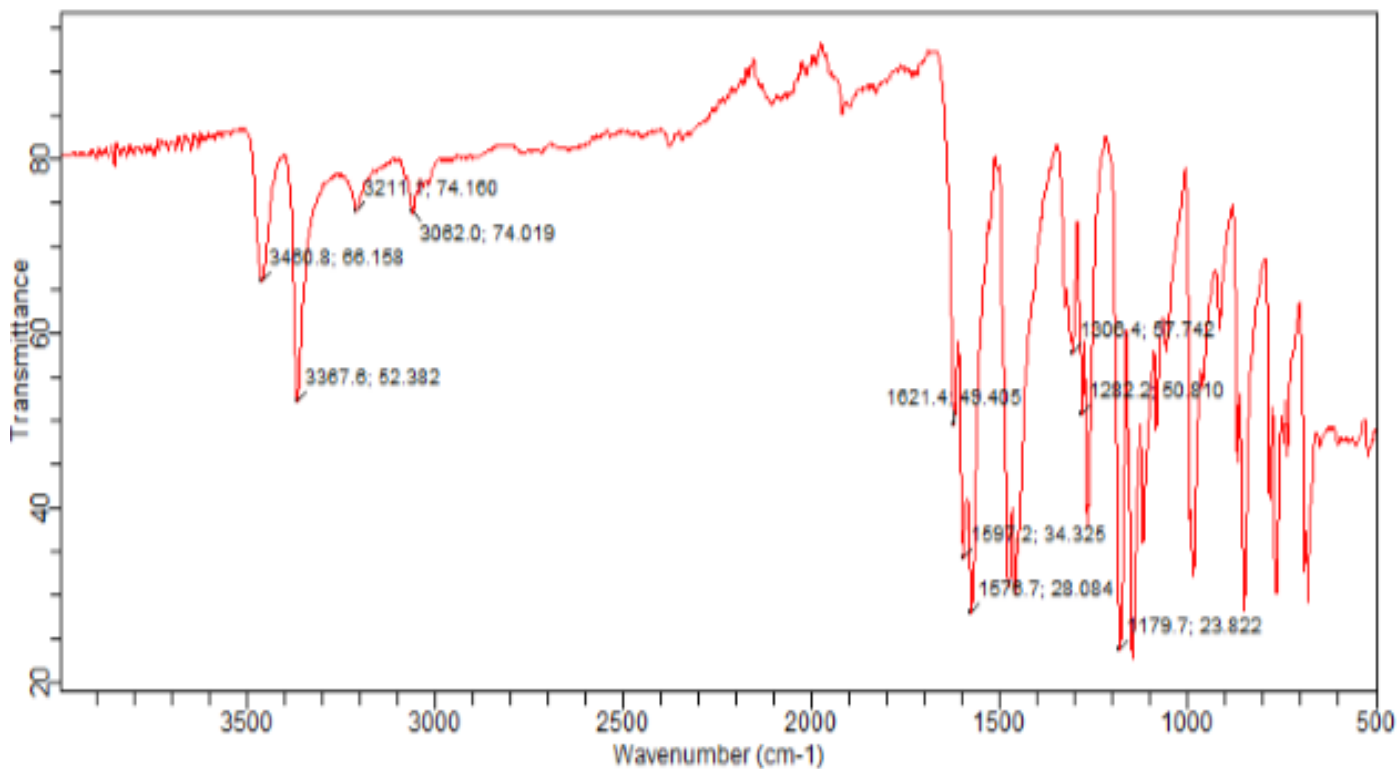


c)

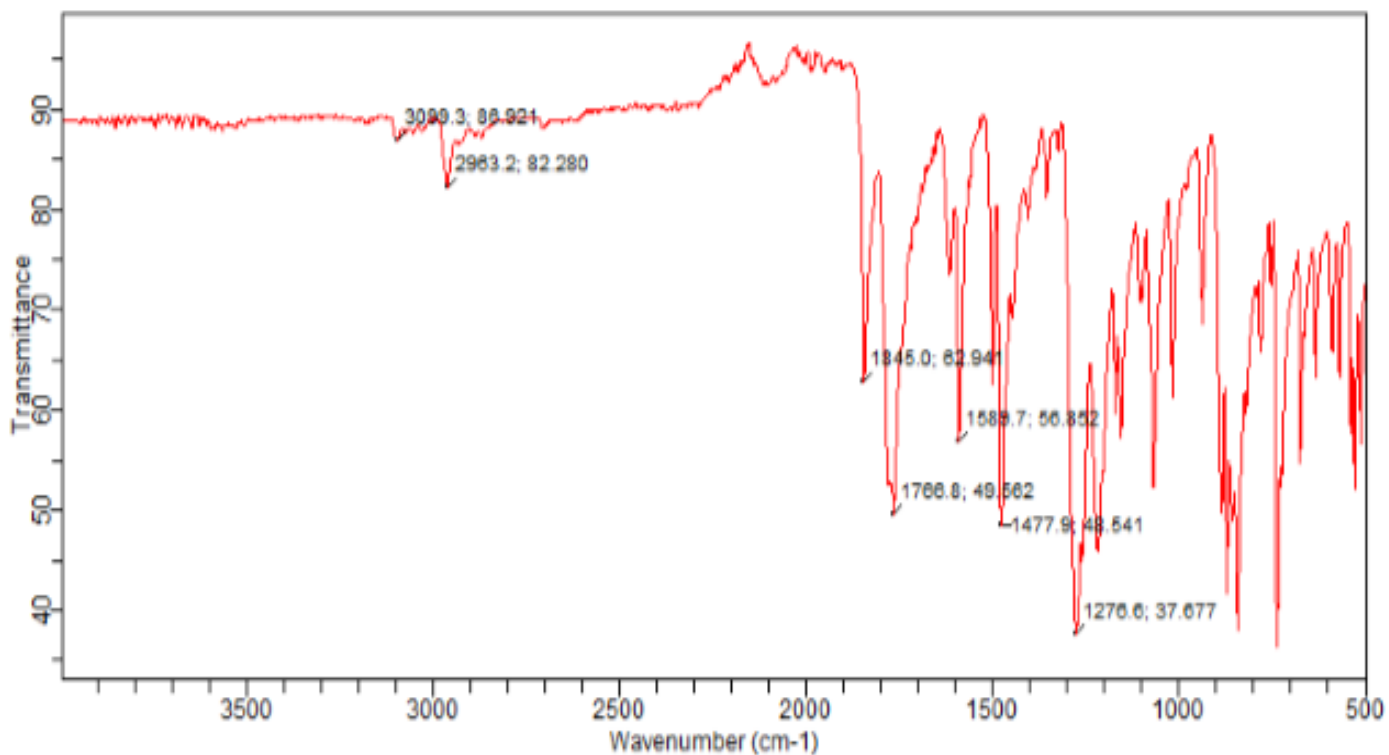


a) First cycle of the shape-recovery of a synthesised TSMPI film. b) Second cycle of the shape-recovery. c) Third cycle of the shape recovery.

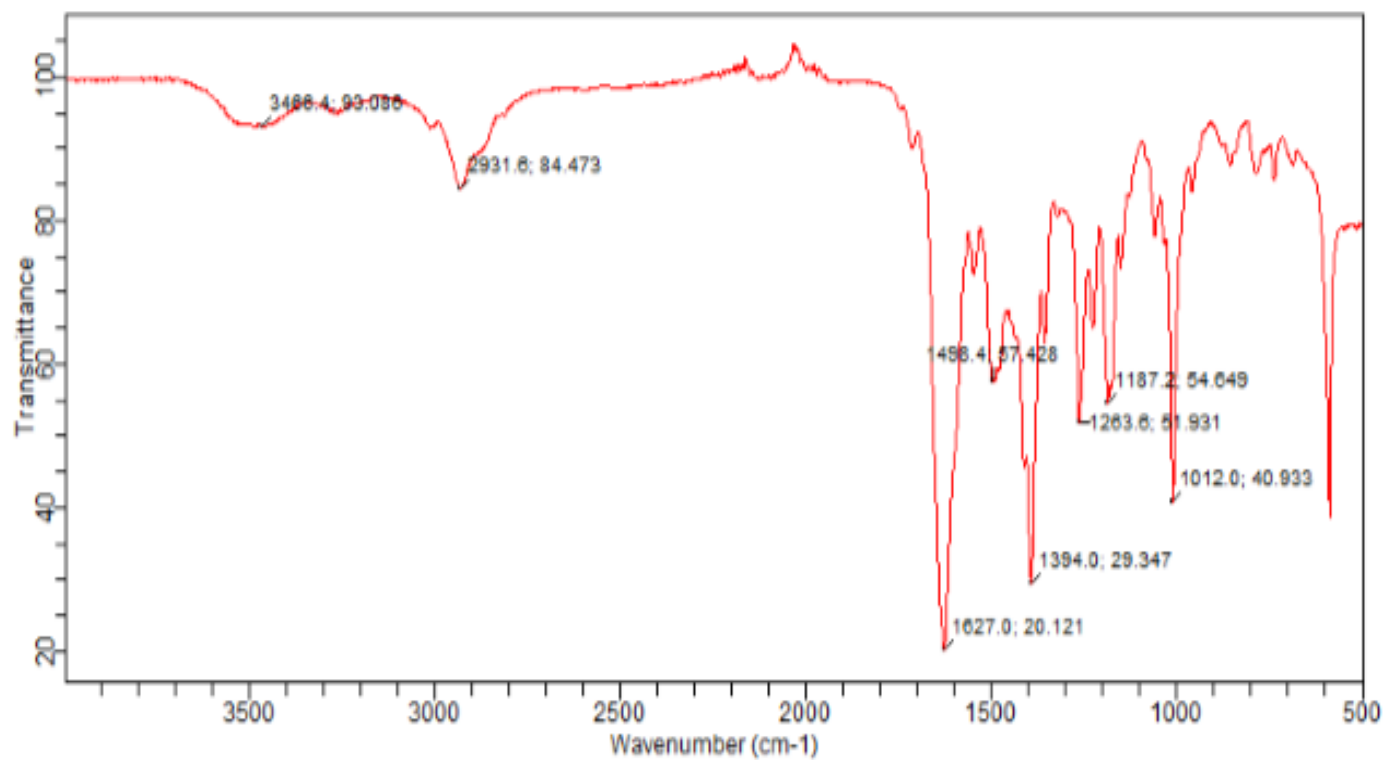
a)



b)

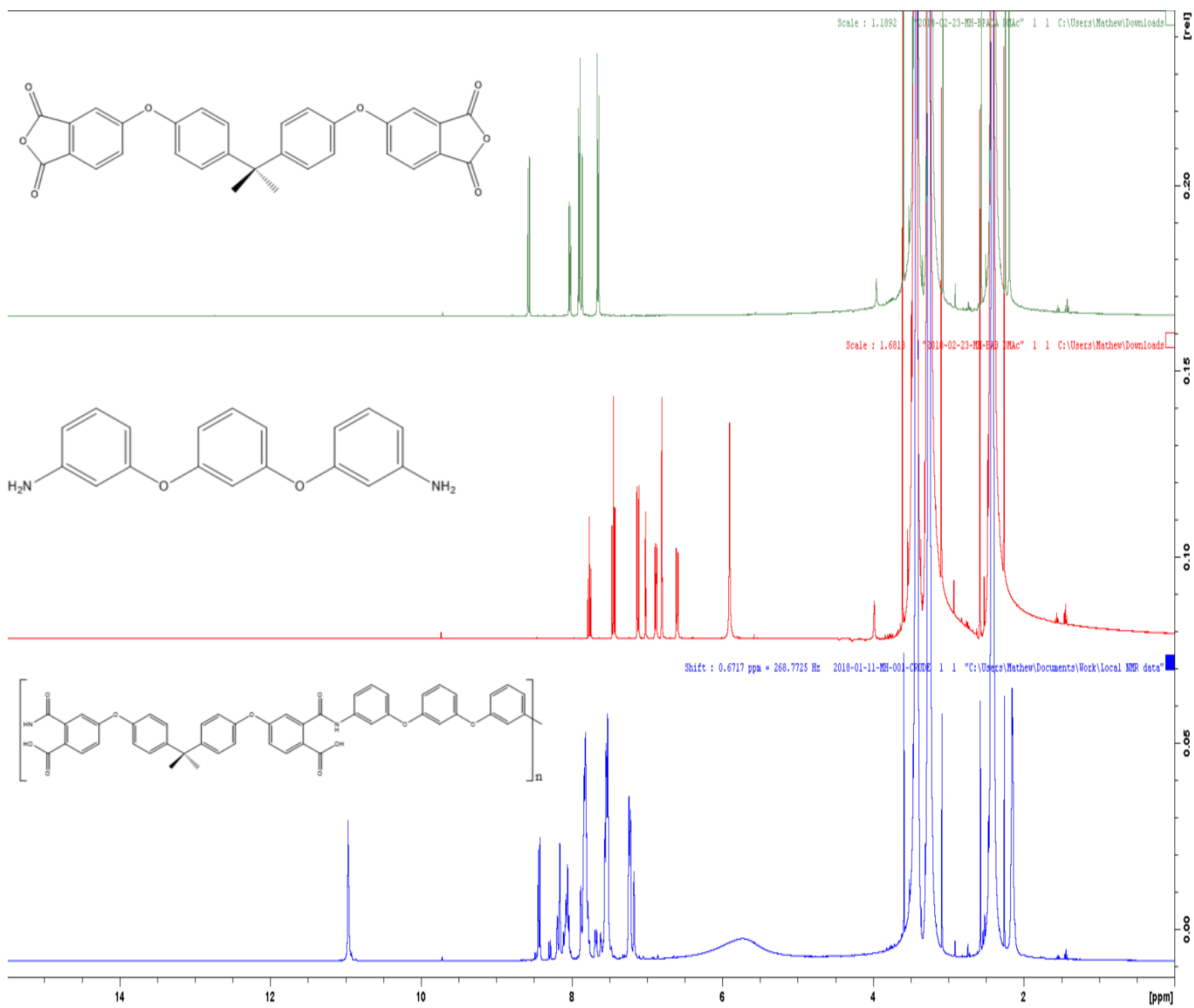


c)

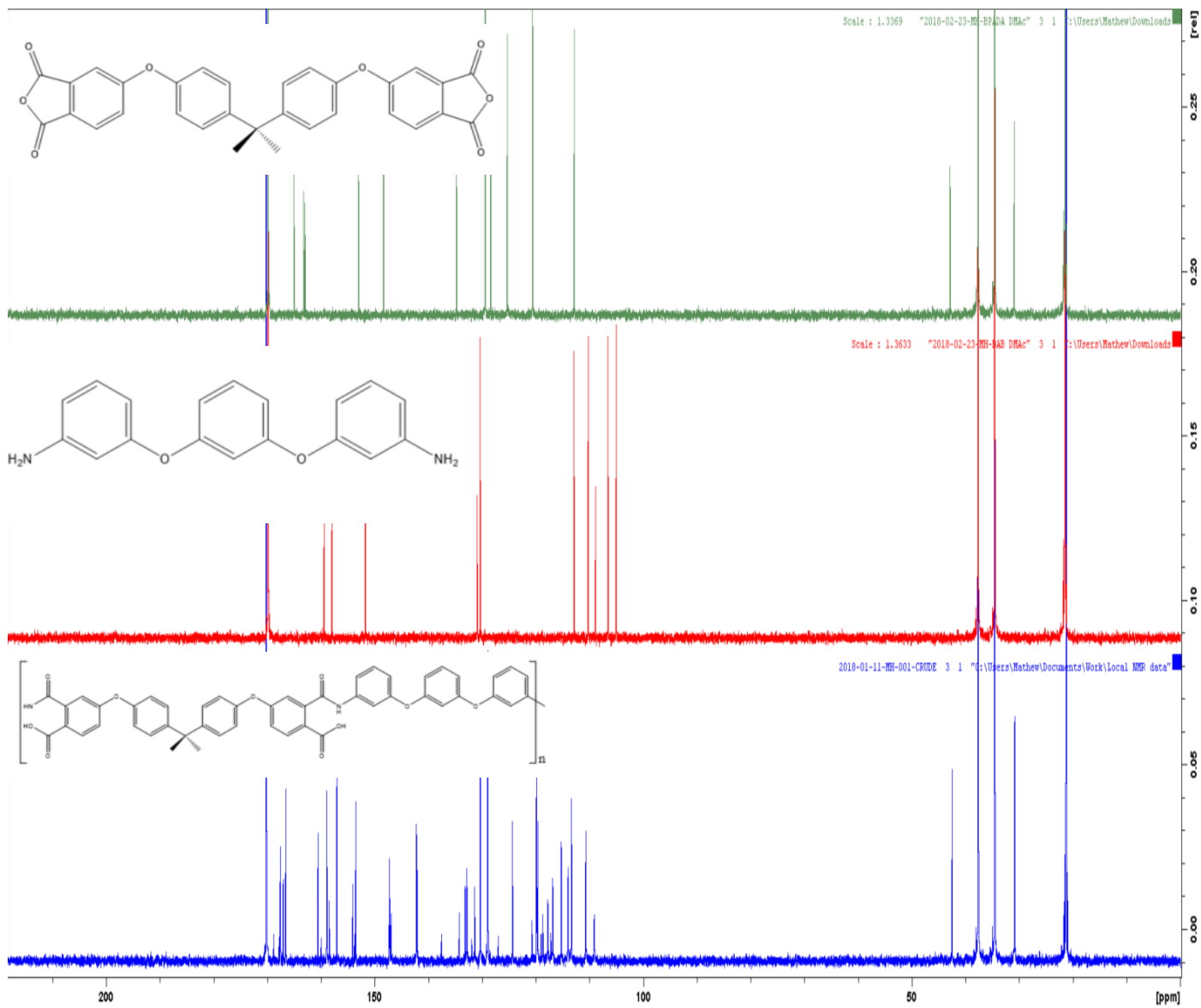


a) BAB FTIR spectrum. b) BPADA FTIR spectrum. c) PAA FTIR spectrum.

a)

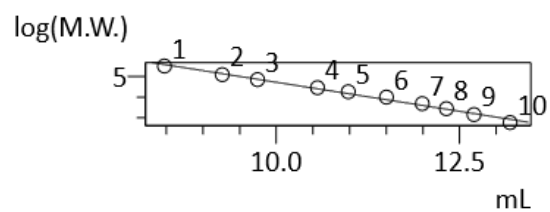


b)



a) ^1H NMR of BPADA, BAB and PAA in DMSO- d_6 . b) ^{13}C NMR of BPADA, BAB and PAA in DMSO- d_6 .

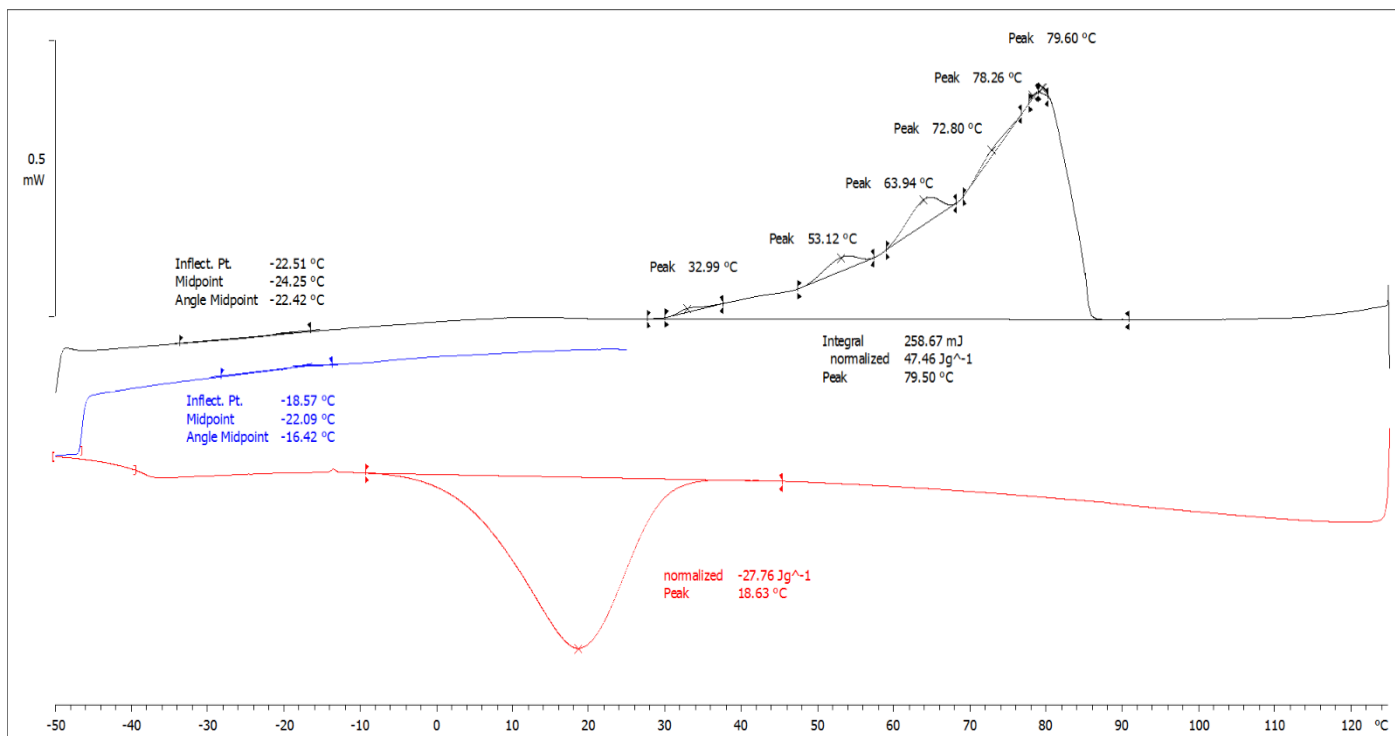
$$R^2=0.9897018$$



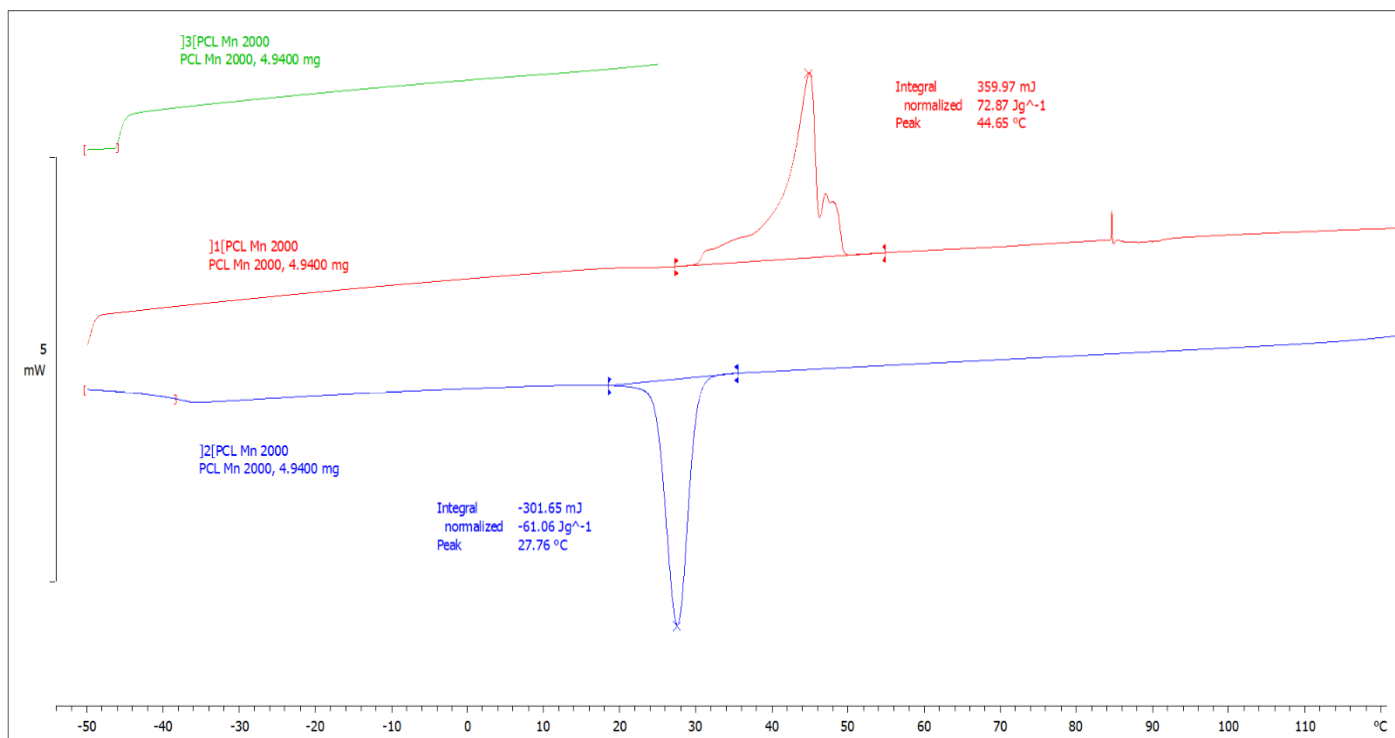
#	Time (min)	Molecular Weight
1	8.476	325600
2	9.267	124300
3	9.746	69650
4	10.562	29150
5	10.985	18340
6	11.507	9960
7	11.995	4830
8	12.321	2780
9	12.698	1390
10	13.193	580

Calibration curve analysis (using PS standards) used for calculating GPC results.

a)

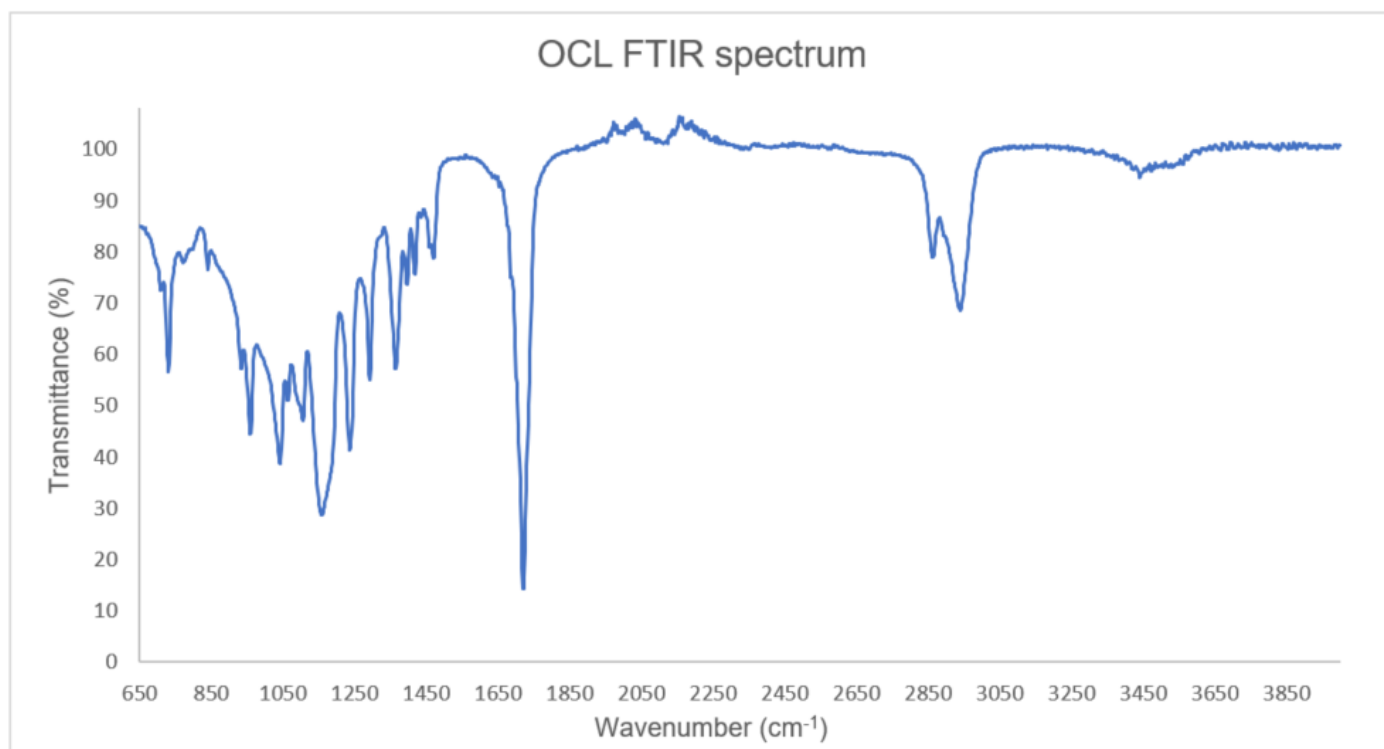


b)

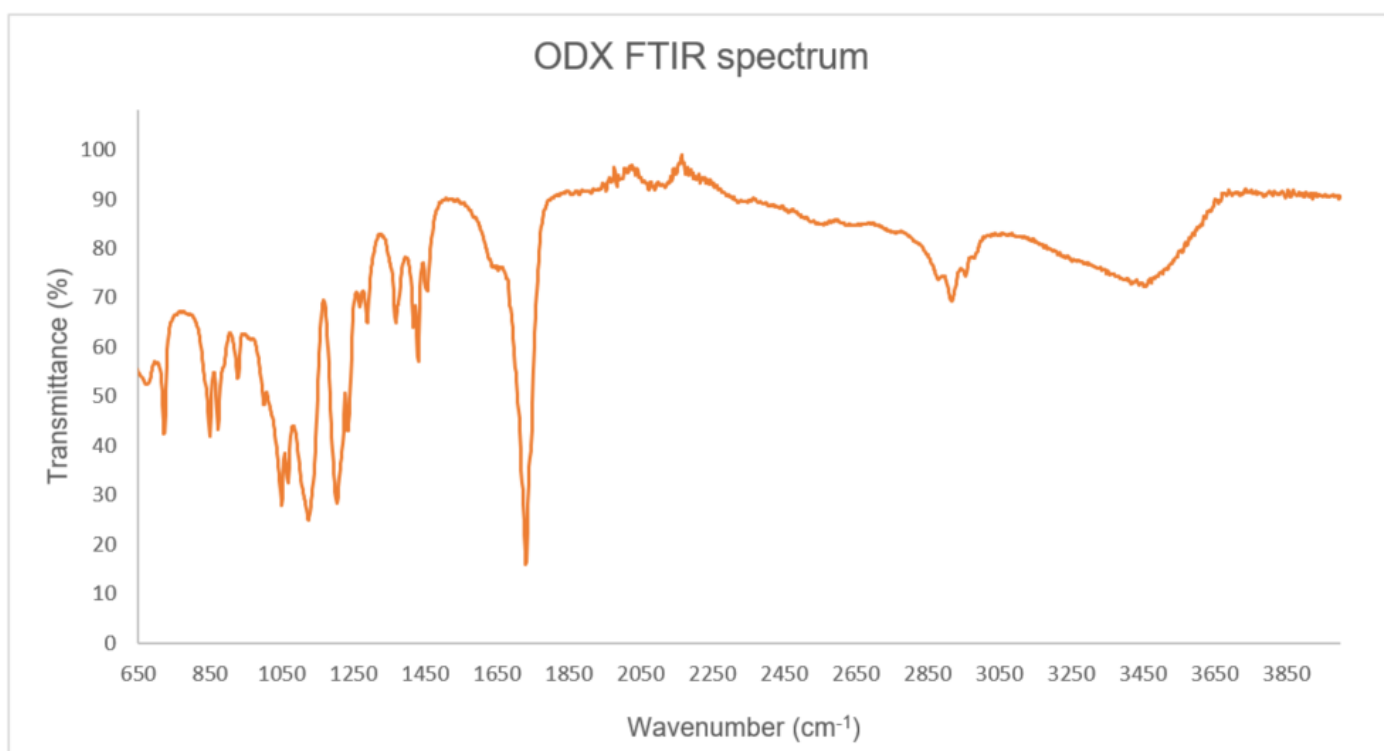


a) DSC results for ODX. b) DSC results for OCL.

a)



b)



a) OCL FTIR spectrum. b) ODX FTIR spectrum.

Appendix II**Record of a risk assessment**

Task:
The synthesis of TSMPI and carrying out its characterization, and printing PPy structures into the SMP

Department	Chemistry	Assessment ID	
Assessor	Mathew John Haskew	Date of assessment	20/02/18
Authorised by	Dr John George Hardy	Review date	

Step 1 List significant hazards	Step 2 who might be harmed	Step 3 determine appropriate controls	Step 4 make it happen
The chemicals to be used in the experiment are: skin and eye irritant, harmful if ingested or inhaled, cause damage to eyes, respiratory system and organs, mutagenic, cancerogenic, flammable, and toxic. In addition, harmful to the environment.	Person carrying out task most at risk and other people present in the laboratory.	<p>Eliminate: Some solvents for mixture stability testing may be substituted.</p> <p>Reduce: Possible to reduce amount of sample for NMR tests.</p> <p>Isolate: All work carried out inside fume-hood.</p> <p>Control: Keep work safely within fume-hood.</p> <p>PPE: Lab coat, goggles, gloves, appropriate clothing and footwear, and longhair tied up.</p> <p>Discipline: Ensure an understanding of the procedure before carrying out experiment.</p>	<ul style="list-style-type: none"> • Procedure – All procedures to be followed by those involved with task. • Training – People involved with task to be given appropriate training ensuring that the appropriate conduct is maintained throughout the task. • Supervision – No supervision is generally needed if competent with the tasks.

Appendix III**COSHH Worksheet CB-1-001****Experiment reference 1**

Assessors and persons authorising work with hazardous substances must be familiar with;

- the list of prohibited substances
- University guidance relating to specific hazards
- University guidance relating to the use of personal protective equipment

See the University's Manual of Safety for details

Carried out by: Mathew John Haskew	Authorised by: Dr John George Hardy
Date of assessment: 20th February 2018	
Task <i>Synthesis and characterisation of TSMPI and the composite TSMPI- (electroconductive polymer e.g. PPy). Transparent shape-memory polyimide (TSMPI) and polypyrrole (PPy).</i>	

Step 1: Hazard Identification

Use the following table to summarise the chemical hazards associated with the task. This information can be found in the Safety Data Sheet which your chemical supplier is legally obliged to provide to you.

Substance	Risk Phrases	Exposure route and consequence	Workplace exposure limits [from safety data sheets]
<i>Pyrrrole</i>	H226 - Flammable liquid and vapour. H301 - Toxic if swallowed. H318 - Causes serious eye damage. H332 - Harmful if inhaled.	Flammable liquids Acute toxicity, Oral Serious eye damage Acute toxicity, Inhalation	N/A
<i>N, N-Dimethylacetamide (DMAc)</i>	H312 + H332 - Harmful in contact with skin or if inhaled H319 - Causes serious eye irritation. H360D - May damage the unborn child.	Acute toxicity, Inhalation and acute toxicity, Dermal Eye irritation Reproductive toxicity	10 ppm (rapidly absorbed through skin)
<i>1,3-Bis(3-aminophenoxy) benzene (BAB)</i>	H302 - Harmful if swallowed. H315 - Causes skin irritation. H319 - Causes serious eye irritation. H335 - May cause respiratory irritation.	Acute toxicity, Oral Skin irritation Eye irritation Specific target organ toxicity - single exposure	N/A
<i>4,4'-(4,4'-Isopropylidenediphenoxy) bis (phthalic anhydride) (BPADA)</i>	H315 - Causes skin irritation. H319 - Causes serious eye irritation. H334 - May cause allergy or asthma symptoms or breathing difficulties if inhaled. H335 - May cause	Skin irritation Eye irritation Respiratory sensitization Specific target organ toxicity - single exposure	N/A

	respiratory irritation.		
Aniline	<p>H301 + H311 + H331 - Toxic if swallowed, in contact with skin or if inhaled.</p> <p>H317 - May cause an allergic skin reaction.</p> <p>H318 - Causes serious eye damage.</p> <p>H341 - Suspected of causing genetic defects.</p> <p>H351 - Suspected of causing cancer.</p> <p>H372 - Causes damage to organs (Blood) through prolonged or repeated exposure.</p> <p>H410 - Very toxic to aquatic life with long lasting effects</p>	<p>Acute toxicity, Oral, acute toxicity, Inhalation, and Acute toxicity, Dermal</p> <p>Skin sensitisation</p> <p>Serious eye damage</p> <p>Germ cell mutagenicity</p> <p>Carcinogenicity</p> <p>Specific target organ toxicity - repeated exposure and specific target organ toxicity - repeated exposure (blood)</p> <p>Acute aquatic toxicity and chronic aquatic toxicity</p>	5 ppm (through skin)
3,4-Ethylenedioxythiophene (EDOT)	<p>H302 - Harmful if swallowed.</p> <p>H311 - Toxic in contact with skin.</p> <p>H319 - Causes serious eye irritation.</p>	<p>Acute toxicity, Oral</p> <p>Acute toxicity, Dermal</p> <p>Eye irritation</p>	N/A
Methanol	<p>H225 - Highly flammable liquid and vapour.</p> <p>H301 + H311 + H331 - Toxic if swallowed, in contact with skin or if inhaled</p> <p>H370 - Causes damage to organs.</p>	<p>Flammable liquids</p> <p>Acute toxicity, Oral, acute toxicity, Inhalation, and acute toxicity, Dermal</p> <p>Specific target organ toxicity - single exposure</p>	Europe indicative occupational exposure limits before systematic toxicity: 200 ppm 260 mg/m³ (through skin)

Ethanol	H225 - Highly flammable liquid and vapour. H319 - Causes serious eye irritation.	Flammable liquids Eye irritation	1,000 ppm 1,920 mg/m ³ (through skin)
2-Hydroxy-4'-(2-hydroxyethoxy)-2-methylpropiophenone (Irgacure D-2959)	N/A	Inhalation - May be harmful if inhaled, may cause respiratory tract irritation Ingestion - may be harmful if swallowed Skin - may be harmful if absorbed through skin, may cause skin irritation Eyes - may cause eye irritation.	N/A
2,4,6-Trimethylbenzoyl-diphenyl-phosphineoxide (Darocur TPO)	H317- Skin sensitisation (Category 1) H361 - Reproductive toxicity (Category 2) H411 - Chronic aquatic toxicity (Category 2)	May cause an allergic skin reaction Suspected of damaging fertility or the unborn child Toxic to aquatic life with long lasting effects	N/A
Dimethyl sulfoxide-d6 (DMSO-d6)	H227 - Combustible liquid H320 - Causes eye irritation	May be harmful if inhaled May cause respiratory tract irritation May be harmful if absorbed through skin May cause skin irritation May be harmful if swallowed	LD50 oral rat 14500 mg/kg LD50 dermal rabbit > 5000 mg/kg LC50 inhalation rat (ppm) 40250 ppm 4h ATE (oral) 14500.000 mg/kg body weight
N, N-Dimethylacetamide (DMAc) (Within the crude product sample for NMR spectroscopy)	H312 + H332 - Harmful in contact with skin or if inhaled H319 - Causes serious eye irritation. H360D - May damage the unborn child.	Acute toxicity, Inhalation and acute toxicity, Dermal Eye irritation Reproductive toxicity	10 ppm (rapidly absorbed through skin)

<i>N, N-Dimethylformamide (DMF)</i>	H312 + H332 - Harmful in contact with skin or if inhaled H319 - Causes serious eye irritation. H360D - May damage the unborn child. H226 – Flammable liquid and vapour	Acute toxicity, Inhalation and acute toxicity, Dermal Eye irritation Reproductive toxicity Flammable	AGW (Germany) Long term value: 15 mg/m³, 5ppm
Do any substances listed require health surveillance or workplace monitoring? <i>Guidance can be found in the University's Manual of Safety</i>			
Substance		Details of surveillance required	
N/A		N/A	

Step 2: List those people who may be at risk of exposure

The following groups of people may be exposed to substances hazardous to health during normal operations;

- x Undergraduate students
- x Postgraduate students
- x Postdoctoral researcher
- x Technical support staff
- x Academic staff
- x Room occupants not carrying out the task
- Other (specify)

Describe the level, type and duration of exposures likely to occur during routine operations¹ (you must include the handling and disposal of any wastes generated during the work);

Work to be carried out in fume-hoods – plausible for a leakage and fume inhalation and skin contact possible, exposure would be very minimal and brief in this case. Minimise exposure with appropriate PPE, and competency with experimental procedures. All un-chlorinated aqueous waste should be disposed of into un-chlorinated aqueous waste containers stored within fume hoods in the lab, and any chlorinated waste in chlorinated waste containers. Polyimide films can be disposed of in yellow solid waste bins, glass disposed of in the green glass bins.

Describe foreseeable accidental exposure scenarios (e.g. spillage on bench).

Spillage on floor or in fume hood due to container breakage, equipment malfunction or in the unlikely event of inappropriate handling.

The following groups of people may be exposed to substances hazardous to health during foreseeable accident scenarios;

- x Undergraduate students
- x Post graduate students
- x Post-doctoral researcher
- x Technical support staff
- x Academic staff
- x Room occupants not carrying out the task
- Other (specify)

Flammable or explosive substances: Pyrrole, Methanol and Ethanol

Keep isolated and contained in fume-hood in the event of fire the fume hood will dispense fire control parameters. For very minor spillages can clean up with blue roll and dispose tissue in contaminated yellow bins. For major spillages inform supervisor and consider the use of a spill-kit (if trained how to do so).

Uncontrolled access to the work area: N/A

Do the substances used or produced require the work area to be designated as a 'Hazardous Area' as per the University's Code of Practice on access to hazardous areas for Facilities personnel or contractors.

¹ A separate COSHH assessment may be necessary to cover maintenance operations

Step 3: Determine appropriate controls

Regulation 7 of COSHH stipulates that exposure to substances harmful to health MUST be prevented, or where this is not reasonably practicable, adequately controlled.

Provide a statement against each item of the following hierarchy of control giving details of the controls you will adopt or a justification as to why no controls in this category are being implemented.

Your controls must address the routine aspects of the work (including waste handling and disposal) and must reduce the risk of any accidental exposures listed in step 2.

<p>Eliminate Can the hazardous substance be eliminated from the task for example by the substitution of a non-hazardous or less-hazardous alternative? (give a justification if not)</p> <p>DMAc, BAB, BPADA are essential for the experimental procedure and cannot be substituted. All other solvents, such as pyrrole, can be substituted if necessary as their purpose was to carry out the stability of the polyimide films. However, they must remain as monomers to then later be polymerised using a photo-initiator when nanoscribing a circuit into the films allowing conductivity.</p> <p>Methanol is used to clean FT-IR machine, inexpensive and only a small amount required, therefore no need to eliminate methanol usage.</p> <p>NMR machines with Gauss value 5, therefore, remove any jewellery to eliminate the chances of jewellery being pulled from person etc.</p>
<p>Reduce Can the hazard be reduced? –e.g. smaller quantities, use of a less hazardous form of the substance, greater dilution, lower frequency use, shorter exposure times.</p> <p>Exposure can be reduced by reducing the volume used for each solvent e.g. testing stability of polyimide films in 1.5 mL Eppendorf tubes. PPE will also be employed (see below).</p> <p>Exposure to materials can be reduced by reducing the mass per NMR sample.</p>
<p>Isolate: Containment Can the operator be isolated from the hazard? – e.g. use of glove box, hazardous substance always contained.</p> <p>Carry out all work inside fume-hood, only polyimide film can be handled outside of fume-hood as currently no hazards are reported on it.</p>
<p>Control: General ventilation to Local Exhaust Ventilation (single point extract close to source to ventilated partial containment) Can engineered controls be used such as fume cupboards, LEV, pumping of liquids?</p> <p>Fume-hood will be used when conducting all procedures to prevent exposure to vapours and possible contact with skin.</p>
<p>PPE This must meet the relevant standards, be maintained in good condition and operators must be trained in its use and given adequate means of storage.</p>

Gloves, eye protection, closed toe footwear, lab coat.

Further guidance is available in the COSHH section of the University's Manual of Safety

Lab coat and safety glasses will be used always in the laboratory, gloves will be worn when handling chemicals. Long hair will be tied back, and appropriate clothing and sturdy closed-toe footwear will be worn.

Discipline

Such as signs and instructions.

Act sensibly and responsibly and maintain awareness and competency throughout experiment and ensure appropriate practice when cleaning up and carrying out experiments.

Special precautions to be adopted in the event of a spillage;

Immediate actions	If a spillage is minor, it will be sufficient to mop up with blue paper roll and dispose of as contaminated waste. If the spillage is larger, the supervisor will be informed, and their advice followed, a spill kit may need to be used. Dropped/ or broken glass to be disposed of correctly in the green glass bin. Any injury e.g. puncture wound from broken glass, seek immediate assistance by informing person in lab or contacting first aider from the list designated in the lab. It is important not to continue with the experiment as the wound may become contaminated and lead to further issues.
Clean-up procedure	Any contaminated waste must be placed into the appropriate contaminated chemical waste containment areas to be disposed of accordingly.

Step 4: Complete a COSHH Summary Sheet and develop a Safe System of Work

Summarise the salient points of the assessment on a COSHH Summary sheet and append this to the front of any Operating Procedures which relate to the task.

REMEMBER:

A COSHH assessment will not protect you; it is the adoption of the control measures arising from the assessment into a 'Safe System of Work' which will keep you and your colleagues safe.

Please consider each of the following three elements of a Safe System of Work;

Procedures	<p>Do you have a written procedure? (If not how are hazard control measures to be communicated to those undertaking the task).</p> <p>Are the hazards associated with the task clearly described in the procedure?</p> <p>Are the control measures generated by your COSHH assessment clearly identified in the procedure?</p>
Training and Instruction	<p>Have all those undertaking the task received an appropriate level of training in relation to any hazards and their control?</p> <p>Are suitable warning signs and notices displayed?</p>
Supervision	<p>Has an appropriate level of supervision been discussed and agreed?</p> <p>B – Approval and advice required from supervisor prior to work starting</p>

Appendix IV

Record of a risk assessment

Task:
Synthesis of pDO, α , ω -dihydroxy-telechelic oligo(p-dioxanone) (ODX) and OCL-ODX and carrying out its characterization

Department	Chemistry	Assessment ID	
Assessor	Mathew John Haskew	Date of assessment	06/03/18
Authorised by	Dr John George Hardy	Review date	

Step 1 List significant hazards	Step 2 who might be harmed	Step 3 determine appropriate controls	Step 4 make it happen
The chemicals to be used in the experiment are: skin and eye irritant, harmful if ingested or inhaled, cause damage to eyes, respiratory system and organs, mutagenic, cancerogenic, flammable, and toxic. In addition, harmful to the environment.	Person carrying out task most at risk and other people present in the laboratory.	<p>Eliminate: Take care of NMR machines (Gauss 5).</p> <p>Reduce: Possible to reduce amount of sample for NMR tests.</p> <p>Isolate: All work carried out inside fume-hood.</p> <p>Control: Keep work safely within fume-hood.</p> <p>PPE: Lab coat, goggles, gloves, appropriate clothing and footwear, and longhair tied up.</p> <p>Discipline: Ensure an understanding of the procedure before carrying out experiment.</p>	<ul style="list-style-type: none"> • Procedure – All procedures to be followed by those involved with task. • Training – People involved with task to be given appropriate training ensuring that the appropriate conduct is maintained throughout the task. • Supervision – No supervision is generally needed if competent with the tasks.

Appendix V**COSHH Worksheet CB-1-001****Experiment reference 1**

Assessors and persons authorising work with hazardous substances must be familiar with;

- the list of prohibited substances
- University guidance relating to specific hazards
- University guidance relating to the use of personal protective equipment

See the University's Manual of Safety for details

Carried out by: Mathew John Haskew	Authorised by: Dr John George Hardy
Date of assessment: 6 th March 2018	
Task <i>Synthesis and analysis of OCL-ODX. Crystallisable oligo(p-dioxanone) diol (ODX) and oligo(ϵ-caprolactone) diol (OCL) and polypyrrole (PPy)</i>	

Step 1: Hazard Identification

Use the following table to summarise the chemical hazards associated with the task. This information can be found in the Safety Data Sheet which your chemical supplier is legally obliged to provide to you.

Substance	Risk Phrases	Exposure route and consequence	Workplace exposure limits [from safety data sheets]
<i>Di-n-butyltin oxide (DBTO)</i>	H300 – Acute toxicity 2. H411 - Toxic to aquatic life with long lasting effects. H319 - Causes serious eye irritation.	Fatal if swallowed Hazardous to the environment Serious eye damage	Short term value: 0.2 mg/m ³ Long term value: 0.1 mg/m ³
<i>Hydrobromic acid (62%) (HBr)</i>	H280 - Gases under pressure (Compressed gas). H314 - Skin corrosion (Category 1A). H335 - Specific target organ toxicity - single exposure (Category 3), Respiratory system.	Contains gas under pressure; may explode if heated Causes severe skin burns and eye damage May cause respiratory irritation.	2 ppm, 6.7 mg/m ³
<i>n-Hexane</i>	H304 – May be fatal if swallowed and enters airways. H225 – Highly flammable liquid and vapour. H315 - Causes skin irritation. H362f – Suspected of damaging fertility. H373 – May cause damage to the peripheral nervous system, the lung, the kidneys, the liver, the reproductive system and the brain through prolonged or	Ingestion and Inhalation Flammable Irritant through skin Damage to fertility Health hazard respiratory Hazardous to the environment	Long term value: 72 mg/m ³ , 20 ppm

	<p>repeated exposure. H336 - May cause drowsiness or dizziness. H411 – Toxic to aquatic life with long lasting effects.</p>		
<i>Ethylene glycol (EG)</i>	H302 – Harmful if swallowed.	Harmful via ingestion	N/A
<i>2-(2-Methoxyethoxy) acetic acid</i>	H314 - Causes severe skin burns and eye damage.	Burning via eyes and skin	
<i>1,2- dichloroethane</i>	<p>H225- Flammable liquids (Category 2)</p> <p>H302 - Acute toxicity, Oral (Category 4)</p> <p>H331 - Acute toxicity, Inhalation (Category 3)</p> <p>H319 – Eye irritation (Category 2)</p> <p>H315 - Skin irritation (Category 2)</p> <p>H335 - Specific target organ toxicity - single exposure (Category 3), Respiratory system</p> <p>H350 - Carcinogenicity (Category 1B)</p>	<p>Highly flammable liquid and vapour</p> <p>Harmful if swallowed</p> <p>Toxic if inhaled</p> <p>Causes serious eye irritation</p> <p>Causes skin irritation</p> <p>May cause respiratory irritation</p> <p>May cause cancer</p>	
<i>Methanol</i>	<p>H225 - Highly flammable liquid and vapour. H301 + H311 + H331 - Toxic if swallowed, in</p>	<p>Flammable liquids</p> <p>Acute toxicity, Oral, acute toxicity, Inhalation, and acute toxicity, Dermal</p>	<p>Europe indicative occupational exposure limits before systematic</p>

	contact with skin or if inhaled H370 - Causes damage to organs.	Specific target organ toxicity - single exposure	toxicity: 200 ppm 260 mg/m³ (through skin)
<i>Sodium bicarbonate</i>	N/A	N/A	Acute toxicity - LD50 Oral – Rat – 4220 mg/kg Human – skin – mild skin irritation 3 d
1,6-Diisocyanato-2,2,4-trimethylhexane (TMDI)	H315 – Skin irritation (Category 2) H319 – Eye irritation (Category 2) H331 – Acute toxicity, inhalation (Category 3) H334 - Respiratory sensitisation (Category 1) H335 - Specific target organ toxicity - single exposure (Category 3), Respiratory system H413 - Chronic aquatic toxicity (Category 4)	Causes skin irritation Causes serious eye irritation Toxic if inhaled May cause allergy or asthma symptoms or breathing difficulties if inhaled May cause respiratory irritation. May cause long lasting harmful effects to aquatic life.	
Do any substances listed require health surveillance or workplace monitoring? <i>Guidance can be found in the University's Manual of Safety</i>			
Substance		Details of surveillance required	
N/A		N/A	

Step 2: List those people who may be at risk of exposure

<p>The following groups of people may be exposed to substances hazardous to health during normal operations;</p> <ul style="list-style-type: none"> x Undergraduate students x Postgraduate students x Postdoctoral researcher x Technical support staff x Academic staff x Room occupants not carrying out the task Other (specify)
<p>Describe the level, type and duration of exposures likely to occur during routine operations² (you must include the handling and disposal of any wastes generated during the work);</p> <p>Work to be carried out in fume-hoods – plausible for a leakage and fume inhalation and skin contact possible, exposure would be very minimal and brief in this case. Minimise exposure with appropriate PPE, and competency with experimental procedures. All un-chlorinated aqueous waste should be disposed of into un-chlorinated aqueous waste containers stored within fume hoods in the lab, and any chlorinated waste in chlorinated waste containers. Polyimide films can be disposed of in yellow solid waste bins, glass disposed of in the green glass bins.</p>
<p>Describe foreseeable accidental exposure scenarios (e.g. spillage on bench).</p> <p>Spillage on floor or in fume hood due to container breakage, equipment malfunction or in the unlikely event of inappropriate handling.</p>
<p>The following groups of people may be exposed to substances hazardous to health during foreseeable accident scenarios;</p> <ul style="list-style-type: none"> x Undergraduate students x Post graduate students x Post-doctoral researcher x Technical support staff x Academic staff x Room occupants not carrying out the task Other (specify)

Flammable or explosive substances: Pyrrole, Methanol and Ethanol

Keep isolated and contained in fume-hood in the event of fire the fume hood will dispense fire control parameters. For very minor spillages can clean up with blue roll and dispose tissue in contaminated yellow bins. For major spillages inform supervisor and consider the use of a spill-kit (if trained how to do so).

Uncontrolled access to the work area: N/A

Do the substances used or produced require the work area to be designated as a 'Hazardous Area' as per the University's Code of Practice on access to hazardous areas for Facilities personnel or contractors.

² A separate COSHH assessment may be necessary to cover maintenance operations

Step 3: Determine appropriate controls

Regulation 7 of COSHH stipulates that exposure to substances harmful to health MUST be prevented, or where this is not reasonably practicable, adequately controlled.

Provide a statement against each item of the following hierarchy of control giving details of the controls you will adopt or a justification as to why no controls in this category are being implemented.

Your controls must address the routine aspects of the work (including waste handling and disposal) and must reduce the risk of any accidental exposures listed in step 2.

<p>Eliminate Can the hazardous substance be eliminated from the task for example by the substitution of a non-hazardous or less-hazardous alternative? (give a justification if not)</p> <p>Methanol is used to clean FT-IR machine, inexpensive and only a small amount required, therefore no need to eliminate methanol usage.</p> <p>NMR machines with Gauss value 5, therefore, remove any jewellery to eliminate the chances of jewellery being pulled from person etc.</p>
<p>Reduce Can the hazard be reduced? –e.g. smaller quantities, use of a less hazardous form of the substance, greater dilution, lower frequency use, shorter exposure times.</p> <p>Exposure to materials can be reduced by reducing the mass per NMR sample.</p>
<p>Isolate: Containment Can the operator be isolated from the hazard? – e.g. use of glove box, hazardous substance always contained.</p> <p>Carry out all work inside fume-hood.</p>
<p>Control: General ventilation to Local Exhaust Ventilation (single point extract close to source to ventilated partial containment) Can engineered controls be used such as fume cupboards, LEV, pumping of liquids?</p> <p>Fume-hood will be used when conducting all procedures to prevent exposure to vapours and possible contact with skin.</p>
<p>PPE This must meet the relevant standards, be maintained in good condition and operators must be trained in its use and given adequate means of storage.</p> <p>Gloves, eye protection, closed toe footwear, lab coat.</p> <p>Further guidance is available in the COSHH section of the University's Manual of Safety</p> <p>Lab coat and safety glasses will be used always in the laboratory, gloves will be worn when handling chemicals. Long hair will be tied back, and appropriate clothing and sturdy closed-toe footwear will be worn.</p>
<p>Discipline Such as signs and instructions.</p> <p>Act sensibly and responsibly and maintain awareness and competency throughout experiment and ensure appropriate practice when cleaning up and carrying out experiments.</p>

Special precautions to be adopted in the event of a spillage;

Immediate actions	If a spillage is minor, it will be sufficient to mop up with blue paper roll and dispose of as contaminated waste. If the spillage is larger, the supervisor will be informed, and their advice followed, a spill kit may need to be used. Dropped/ or broken glass to be disposed of correctly in the green glass bin. Any injury e.g. puncture wound from broken glass, seek immediate assistance by informing person in lab or contacting first aider from the list designated in the lab. It is important not to continue with the experiment as the wound may become contaminated and lead to further issues.
Clean-up procedure	Any contaminated waste must be placed into the appropriate contaminated chemical waste containment areas to be disposed of accordingly.

Step 4: Complete a COSHH Summary Sheet and develop a Safe System of Work

Summarise the salient points of the assessment on a COSHH Summary sheet and append this to the front of any Operating Procedures which relate to the task.

REMEMBER:

A COSHH assessment will not protect you; it is the adoption of the control measures arising from the assessment into a 'Safe System of Work' which will keep you and your colleagues safe.

Please consider each of the following three elements of a Safe System of Work;

Procedures	<p>Do you have a written procedure? (If not how are hazard control measures to be communicated to those undertaking the task).</p> <p>Are the hazards associated with the task clearly described in the procedure?</p> <p>Are the control measures generated by your COSHH assessment clearly identified in the procedure?</p>
Training and Instruction	<p>Have all those undertaking the task received an appropriate level of training in relation to any hazards and their control?</p> <p>Are suitable warning signs and notices displayed?</p>
Supervision	<p>Has an appropriate level of supervision been discussed and agreed?</p> <p>B – Approval and advice required from supervisor prior to work starting</p>

